GAS PATH ANALYSIS AS A TOOL FOR THE PREDICTIVE MAINTENANCE OF THE HONEYWELL 331-500 AUXILIARY POWER UNIT

Keith Ward

TU Delft

18th November 2018

Gas Path Analysis as a Tool for the Predictive Maintenance of the Honeywell 331-500 Auxiliary Power Unit

by

Keith Ward

in partial fulfilment of the requirements for the degree of

Master of Science in Mechanical Engineering

Delft University of Technology

To be defended publicly on Wednesday November 28, 2018 at 10:30 AM.

Student number:	4614933	
Project duration:	March 2018 – November 2018	
Thesis committee:	Prof. dr. ir. S. Klein,	P&E, TU Delft | Chair
	Dr. ir. R. Pecnik,	P&E, TU Delft
	Ir. S. Smit,	P&E, TU Delft
	Dr. ir. W.P.J. Visser,	LR, TU Delft

An electronic version of this thesis is available at `http://repository.tudelft.nl/`.

This thesis is confidential and cannot be made public until December 1, 2023.

TU Delft

Abstract

This study examines Gas Path Analysis (GPA) as a method for the predictive maintenance of the Honeywell 331-500 Auxiliary Power Unit (APU). The 331-500 is used on the Boeing 777 and is susceptible to a sudden failure during operation due to the release of a first stage turbine blade. Investigations found the failure mechanisms of the blade release to be hot corrosion and thermal fatigue. Prolonged operation and the ingestion of environmental contaminants cause corrosion and a loss of material of the first stage Nozzle Guide Vane (NGV) which leads to a reduction in turbine performance. To counter this loss in performance, the APU controller increases the fuel flow, hence Turbine Inlet Temperature (TIT), which leads to under-platform crack growth of the first stage rotor and the eventual release of a blade.

A thermodynamic model of the 331-500 is created and validated using the Gas Turbine Simulation Program. Test cell data is used to characterise the APU at its design point before historical failure data comprising on-wing APU performance is analysed to assess the condition of the turbine. GPA, in the form of adaptive modelling, is used to adjust the turbine efficiency to match the model with the performance data thereby determining the deterioration of the machine.

Analysis highlights a relationship between the gradient of turbine efficiency, the ratio of the controller- to model-calculated TIT, and the condition of the first stage NGV. A larger gradient and TIT ratio indicate significant material loss in the NGV and that the turbine is heavily deteriorated. From the analysis, a rule functioning as a threshold on both the turbine efficiency gradient and the TIT ratio is formulated and is capable of predicting the historical first stage turbine blade failures up to 600-250 cycles before failure. This rule may then be used for the monitoring of current and future 331-500s in operation with the aim of preventing failure.

Acknowledgements

I would like to thank Prof. Sikke Klein, Dr. Rene Pecnik, and Ir. Stephan Smit for their technical supervision over the course of this thesis. I enjoyed our discussions on tackling this project and I appreciated your proofreading of this report.

I would also like to thank Mr. Niels van Hofwegen at EPCOR for providing the opportunity to pursue this project. Sincere thanks also to Mr. Kaj Rook and Mr. Olivier Ouwehand for providing technical information on the Honeywell 331-500. I wish the very best of success to EPCOR and the *Prognos for APU* team in the coming years and beyond.

I wish to extend my sincere gratitude to the friends who I have met during my studies here in Delft and with whom I have made countless, comical memories. Oliver, Magnus, Munna, Sean, David, Jelle and Stefan: it was a great chapter and I'm already looking forward to the next one.

Keith Ward
November 2018

Table of Contents

List of Figures

List of Tables

List of Symbols

β	Variable for gradient descent
β_o	Initial value of variable for gradient descent
$\dot{m}_b$	Load compressor air flow rate
$\dot{m}_c$	Compressor air flow rate
$\dot{m}_f$	Fuel flow rate
$\dot{m}_t$	Turbine gas flow rate
$\dot{Q}_{cc}$	Combustion chamber heat addition
$\dot{W}_c$	Compressor load
$\dot{W}_{gen}$	Generator load
$\dot{W}_{lc}$	Load compressor load
$\dot{W}_{load}$	Total shaft load
$\dot{W}_t$	Turbine work
η_c	Compressor isentropic efficiency
η_{lc}	Load compressor isentropic efficiency
η_t	Turbine isentropic efficiency
γ	Specific heat ratio for a gas
$\hat{\beta}$	Non-dimensionalised variable for gradient descent
$\overline{c}$	Vector of gas turbine condition parameters
$\overline{o}$	Vector of gas turbine operation parameters
$\overline{p}$	Vector of gas turbine performance parameters
ϕ	Learning rate
a	Cost function weight

A_f	Turbine throat area
A_{NGV}	Condition of first stage nozzle guide vane
G	Influence coefficient matrix
g	Non-linear function representing the aero-thermodynamic performance of a gas turbine
G'	Fault coefficient matrix
h_{01}	Compressor inlet enthalpy
h_{04}	Exhaust gas enthalpy
h_i	Inlet enthalpy for a compression, expansion, or choked process
h_o	Outlet enthalpy for a compression, expansion, or choked process
J	Cost function
LHV_f	Lower heating value of fuel
N_c	Corrected rotational speed
O	Distance between two adjacent turbine stator vanes
P_{01}	Compressor inlet pressure
P_{02}	Compressor outlet temperature
P_{03}	Turbine inlet pressure
P_{04}	Exhaust gas pressure
P_b	Load compressor outlet pressure
P_i	Inlet pressure for a compression, expansion, or choked process
P_o	Outlet pressure for a compression, expansion, or choked process
PR_c	Compressor pressure ratio
PR_{lc}	Load compressor pressure ratio

R	Correlation coefficient
T_{01}	Compressor inlet temperature
T_{02}	Compressor outlet temperature
T_{03}	Turbine inlet temperature
T_{04}	Exhaust gas temperature
T_b	Load compressor outlet temperature
T_i	Inlet temperature for a compression, expansion, or choked process
T_o	Outlet temperature for a compression, expansion, or choked process
TIT_{apuc}	Controller-calculated turbine inlet temperature
W	Corrected air flow

List of Abbreviations

AOG	Aircraft on Ground
APU	Auxiliary Power Unit
APUC	Auxiliary Power Unit Controller
BBM	Black Box Model
COV	Coefficient of Variance
EGT	Exhaust Gas Temperature
EPCOR	European Pneumatic Component Overhaul and Repair
FAR	Fuel-to-air Ratio
FCM	Fault Coefficient Matrix
GGE	Global Greenhouse Gas Emissions
GPA	Gas Path Analysis
GSP	Gas Turbine Simulation Program
ICM	Influence Coefficient Matrix
MES	Main Engine Start
MRO	Maintenance, Repair and Overhaul
NGV	Nozzle Guide Vane
OEM	Original Equipment Manufacturer
PR	Pressure Ratio
T1	Turbine First Stage
TIT	Turbine Inlet Temperature
WBM	White Box Model
500TM	331-500 Thermodynamic Model

1 Introduction

Maintenance is an expensive part of aircraft operation. In 2015, total civil aircraft Maintenance, Repair and Overhaul (MRO) costs amounted to $50 billion with the value expected to exceed $65 billion by 2020 [1]. For a typical civil airliner, 37% of its direct operating costs are a result of engine and aircraft maintenance [2]. The Boeing 777, a moderate aircraft in terms of maintenance expenses, has a cost of $1300 per flight hour dedicated to MRO services. It is in the interest of both aircraft operators and Original Equipment Manufacturers (OEMS) to lower these costs.

In the coming decades, the aviation industry is expected to invest heavily in lowering its carbon footprint with the industry currently accounting for approximately 2% of Global Greenhouse Emissions (GGE). By 2050, the Intergovernmental Panel on Climate Change forecasts that GGE due to civil aviation could grow by a further 300-700% [3]. Improvements in engine fuel consumption, aircraft design, and logistical operations are ways to reduce this however, this will require major financial investment by airliners and OEMs in the industry. A reduction in MRO costs will provide the aviation industry with more capital to invest in these developments. Opportunities for reducing these costs include the use of predictive maintenance tools for scheduling MRO services on an aircraft's components. One such component of relevance is the Auxiliary Power Unit (APU).

Almost every modern civil aircraft in operation today is fitted with an APU. Its function is to provide electrical and air flow requirements to the aircraft. Like all machines operating at high temperatures, the APU is prone to corrosion, fatigue, and creep and will eventually fail rendering the aircraft inoperable until replacement. The cause of failure varies but it is usually due to deterioration in the hot section of the machine. If this failure could be predicted, the aircraft operator would have enhanced flexibility in scheduling the maintenance of the APU thereby avoiding any unscheduled removals and reducing Aircraft on Ground (AOG) time.

The aim of this work is to develop a tool for condition monitoring and predictive maintenance of the Honeywell 331-500 APU that is used on the Boeing 777. The focus will be on first stage turbine (T1) blade failure which is a result of extended deterioration of the hot section of the APU. Gas Path Analysis (GPA) will be used as a method of monitoring the real-time performance of the APU and assessing the deterioration of the machine's main components. Historical failure data is analysed to determine trends in the deterioration data that indicate

when T1 blade failure is likely to occur and by monitoring 331-500 APUs in operation, future failures may be predicted.

This work has been completed in collaboration with European Pneumatic Component Overhaul and Repair (EPCOR) B.V. in Schiphol, Netherlands. The following subsections outline an APU in more detail and provide background information on EPCOR.

1.1 The Auxiliary Power Unit

An APU is a single-shaft, constant-speed, gas turbine. As shown in Figure 1.1, it is located inside the tail of the aircraft and its function is to supply both bleed air and electrical power. Bleed air is used to start the aircraft's main engines and meet cabin air demand while electrical power is used for flight controls. In the absence of ground power units and air starters, the APU may be the only power source of the aircraft. Additionally, in the unlikely event of in-flight engine shutdown or failure, the APU can supply both electrical power and air flow.

The main sections of a typical APU are shown below in Figure 1.2. The turbine, compressor and combustion chamber form the power section of the machine. The turbine drives both a load compressor and, via a gearbox, an electrical generator which both provide the air and electrical supply to the aircraft.

The main reason for choosing the Honeywell 331-500 APU for this study is because, in the event of a severe failure such as T1 blade failure, it is the most expensive to repair. As it is the largest APU that EPCOR repairs, its components are more costly to purchase new and/or repair after failure. Additionally, the 331-500 is the APU with the most frequent repairs at the EPCOR workshop and the one with the most available data, both from the test cell and on-wing. The specifics of the machine will be discussed in section 5.

Figure 1.1: The tail of the Boeing 737-300 showing the APU and its exhaust outlet [4].

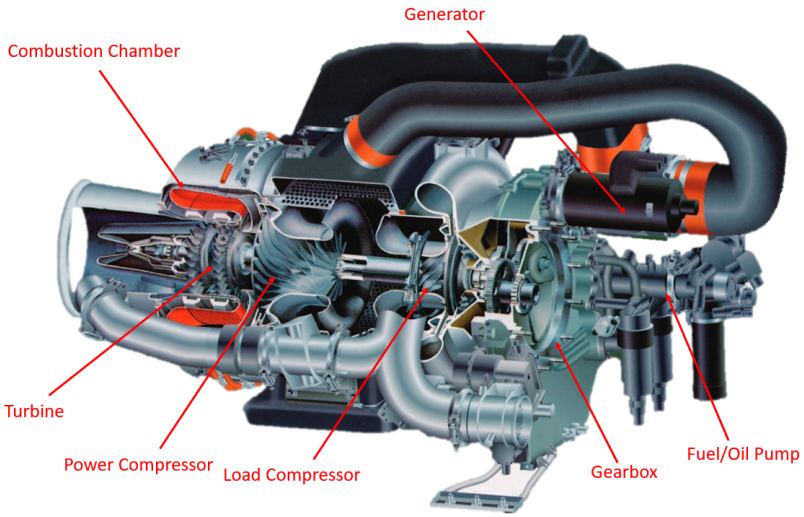

Figure 1.2: Cutaway diagram of a typical APU showing the main components of the machine [5].

1.2 Maintenance, Repair and Overhaul Services at EPCOR

EPCOR is a MRO service provider for aircraft components and APUs. Founded in 1999, it became entirely a subsidiary of Royal Dutch Airlines (KLM) in 2005. Initially providing MRO services to aircraft components (valves, pumps, compressors), it extended its operations to APUs in 2007. The shop floor at EPCOR is shown in Figure 1.3.

Figure 1.3: Shop floor at EPCOR where APUs and aircraft components undergo repair and overhaul.

When an aircraft operator wishes to avail of the MRO services of a repair shop, such as EPCOR, a cost is agreed by both parties. This cost is usually defined such that the aircraft operator pays the MRO provider an amount based on how long the APU ran since its previous repair rather than paying for the actual repair costs. In other words, the longer the time between two successive repairs of an APU, the more revenue it generates for the MRO provider. Subtracting the repair costs from the revenue leaves the MRO provider with a profit or, in the case of a costly repair or short run time, a loss. As based on discussions with APU engineers at EPCOR, the cost breakdown of a typical APU repair is shown in Figure 1.4 below.

As shown, 80% of a typical APU repair cost is associated with material costs for the machine while labour costs account for the remainder. Of those material costs, 80% (or 64% of the total repair cost) is due to purchasing new parts from the OEM rather than repairing the damaged ones. The main reason for this is that certain parts of the APU are too severely damaged to be repaired by the MRO provider. In the case of a damaged impeller or turbine disc, the MRO provider will typically not have access to either the high-precision equipment or expertise to repair or manufacture these components. This is particularly evident in the event of a failure along the APU gas path, such as in a T1 blade failure. In this scenario, the power section of the machine suffers extensive damage leading to unrepairable compressor and turbine stages which in turn balloon the total material costs. If these failures could be avoided, both the

material and the total cost for an APU repair would be reduced. Therefore, it is in the interest of the MRO service provider to remove the APU for repair before severe deterioration occurs while also not removing the machine too early and reducing the total revenue.

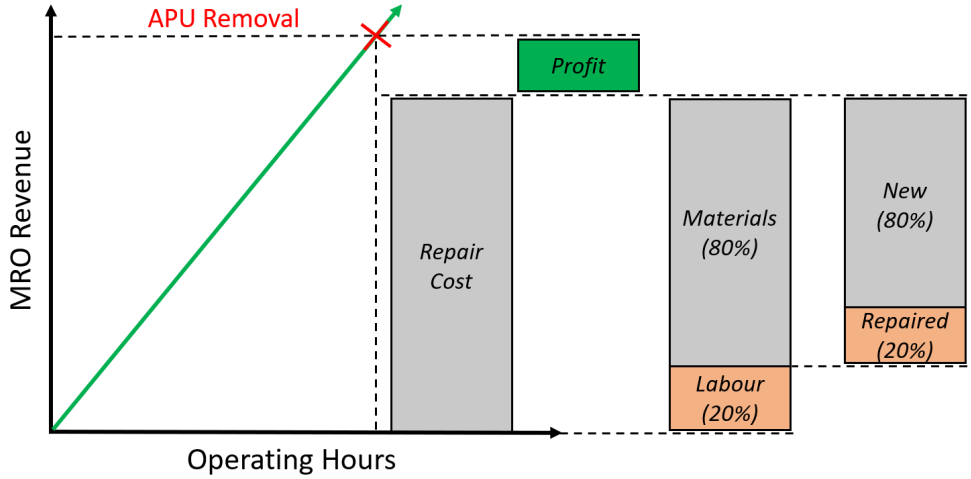

Figure 1.4: Breakdown of the cost of a typical APU repair.

1.3 Available Data Streams

The application of GPA relies on the input of various data streams. As this report will refer to these data streams throughout, they are briefly defined and discussed here.

Trendsheet

Since December 2007, EPCOR have continuously stored the data of each APU shop visit in a database known as the *Trendsheet*. Useful data such as the failure cause, number of cycles since the previous repair, and the level of repair are recorded as well as less technical information such as the cost of the repair. As will be discussed later, this data may be used for ranking various APU failures in terms of cost and number of occurrences as a means of accurately comparing the cost impact of each failure.

Test Cell Data

Prior to the completion of every APU repair at EPCOR, aircraft regulations require that the machine undergoes a performance test under various conditions that represent the load requirements of the APU. Through the use of multiple sensors, performance parameters such as the Exhaust Gas Temperature (EGT), fuel flow, generator power and load compressor outlet conditions are measured throughout the test. These parameters are measured for load

conditions such as idle and Main Engine Start (MES), a high power condition. As detailed later in section 5, this test cell data is used to determine the design point performance of the Honeywell 331-500 APU. The preparation of a 331-500 for testing at EPCOR is shown below in Figure 1.5.

Figure 1.5: The preparation of a Honeywell 331-50 APU for testing at EPCOR.

On-wing Data

In September 2017, EPCOR launched *Prognos for APU*, an online tool for tracking various measured performance parameters and non-technical data of an on-wing APU. When an aircraft operator is using the online tool, sensor data from the APU is sent via the aircraft condition monitoring system to a database operated by EPCOR. The data is then cleaned and uploaded to *Prognos for APU* for visualisation.

During each cycle of a power condition, such as MES, on-wing measurements are taken from the APU. These measurements consist of both snapshots during the cycle and the average value of each measurement over the cycle. A screenshot of typical performance tracking for an APU on *Prognos for APU* is shown below in Figure 1.6. The upper chart tracks the time and number of cycles since the APUs previous repair while the lower chart tracks the average EGT for every MES cycle. In September 2017, this APU was removed for repair resulting in a

pause in on-wing data until February 2018.

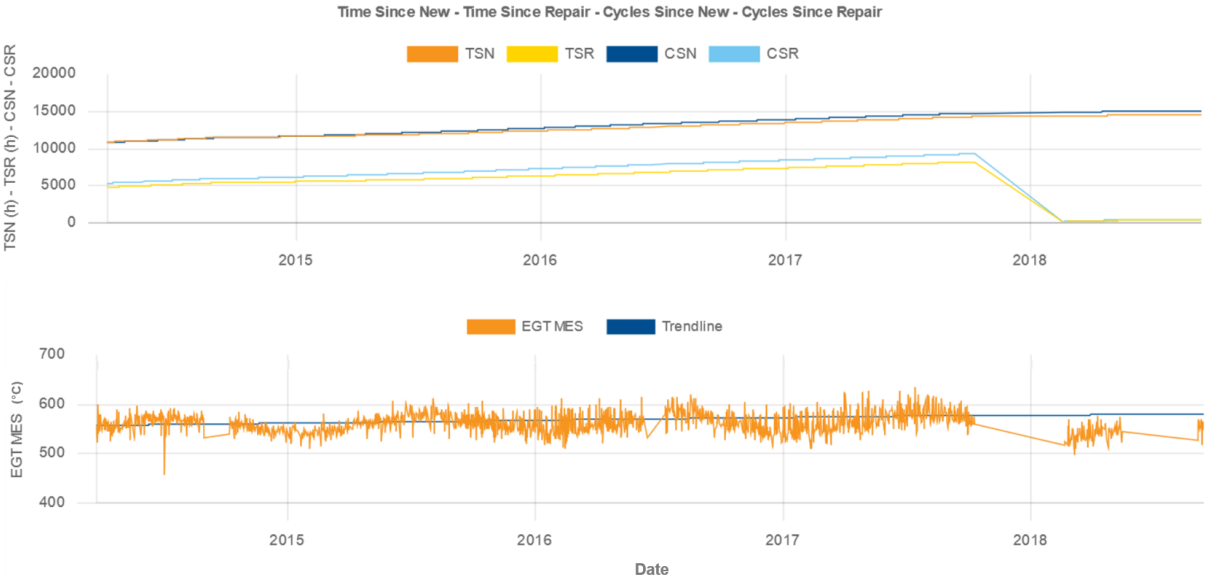

Figure 1.6: Typical performance tracking of an APU on the *Prognos for APU* system. The upper graph tracks the time and number of cycles since both the previous repair and the first cycle (new) of the APU while the lower chart tracks the EGT of the machine.

Inspection Data

During a typical APU repair at EPCOR, the machine passes through several stations located across the shop floor. Each station represents a stage in the repair process including disassembly, cleaning, part inspection, assembly and testing. The level of damage of each component is assessed and photos are taken for future records. Many photos from the disassembly and inspection of 331-500 APUs will be shown throughout this report.

2 Deterioration in Auxiliary Power Units

All operating APUs will eventually fail as a result of a variety of mechanisms (corrosion, fatigue, creep etc). These failure mechanisms affect each component of the engine differently and may be due to a variety of causes such as foreign object damage, harsh environmental conditions or simply extended operation (high time). Rather than implementing a predictive maintenance tool to monitor the condition of the entire Honeywell 331-500 APU, it was decided to identify a single failure and analyse the mechanisms that lead to its occurrence. This process is discussed below.

2.1 331-500 Failure Investigation

The criteria for identifying a single failure for this study is based on the financial cost it incurs to EPCOR. Firstly, a list of 331-500 repairs was extracted from the aforementioned *Trendsheet* with the cause for the APU removal and its number of occurrences noted. Some of these repairs occur as a result of a scheduled removal of the APU, due to high time or life-limited parts, or as a result of an unscheduled removal, such as a failure. To correctly compare each repair, an average cost per repair C is calculated for each. Since the financial data of both EPCOR and its customers may not be disclosed, C is normalised to that of high time repairs, the most common cause for 331-500 removal. Each repair is then ranked in terms of its cost per repair, as shown in Table 2.1.

Table 2.1: Ranking of the top fifteen 331-500 repairs by cost per repair C when normalised to that of high time repairs.

Removal Cause	**No. of Occurrences**	***C***
T1 Blade Failure	22	1.81
High Time	74	1.00
Thrust/Ball Bearing Failure	32	0.71
Electric Starter Clutch Failure	8	0.68
Hot Section Deterioration	64	0.66
Anti-rotation Pin Failure	8	0.66
High-speed Pinion Gear Bearing Failure	10	0.66
Air Turbine Starter Clutch Failure	17	0.64
Foreign Object Damage	27	0.63
Compressor Carbon Seal Failure	26	0.54
Generator Failure	9	0.53
Tube Oil-in/Oil-out Failure	22	0.48
Turbine Carbon Seal Failure	22	0.41
Maintenance Error	10	0.32
Re-certification Test	52	0.04

Being 81% more expensive than a high time repair, it is clear that T1 blade failure is the most costly failure for the 331-500. Further investigation shows that although only making up 4.4% of all 331-500 failures since December 2007, it accounts for 12.4% of the total cost. Comparing that to the percentage of total occurrences and total costs of the two most common causes of 331-500 removal, high time and hot section deterioration, the results are 13.5%/21.8% and 12.7%/13.1% respectively. This is presented in Table 2.2 below.

The repair data shows that the occurrence of T1 blade failure drastically increased since the start of 2016. During the period from January 2016 to January 2018, 50% of the total cases of T1 blade failure have occurred since December 2007. The reason for this is unclear and has yet to be investigated. The percentage of total occurrences and total costs for the three removal causes mentioned above is recalculated for this specific period and summarised in Table 2.3. Here the results are even more extreme with T1 blade failure occurrences making up just 8.5% of total failures but accounting for 19.5% of the total cost.

Table 2.2: Percentage of total occurrences and total cost as a result of repairs caused by T1 blade failure, high time, and hot section deterioration between December 2007 and January 2018.

Removal Reason	% Occurrence	% Cost
T1 Blade Failure	4.4	12.4
High Time	13.5	21.8
Hot Section Deterioration	12.7	13.1

Table 2.3: Percentage of total occurrences and total cost as a result of repairs caused by T1 blade failure, high time, and hot section deterioration between January 2016 and January 2018.

Removal Reason	% Occurrence	% Cost
T1 Blade Failure	8.5	19.5
High Time	23.1	29.2
Hot Section Deterioration	5.1	7.8

From the above, it is clear that T1 blade failures result in a large financial expense on MRO operations at EPCOR. The reason for this is that the failure leads to a large section of the 331-500 to be irreparable meaning most components must be purchased as new from Honeywell.

2.2 Failure Mechanisms of First Stage Turbine Blade Failure

The main failure mechanisms of T1 blade failure are hot corrosion and thermal fatigue. During APU operation, the machine undergoes a series of MES cycles with each cycle consisting of a startup, steady state and shutdown phase. Over the course of these three phases, the turbine blades are subjected to a thermal fatigue cycle. In addition to this, corrosion due to large temperatures and flue gas contaminants degrade the material of the first stage Nozzle Guide Vanes (NGVs) and blades. The potential causes and their effects on T1 blade failure are summarised below in Figure 2.1.

Thermal barrier coatings, along with blade cooling holes in the first stage NGVs and rotor blades, are utilised to reduce the blade metal temperatures and mitigate the effects of corrosion and fatigue. However, after an extensive amount of cycles, the effectiveness of these measures are reduced. Thermal barrier coatings wear off and, depending on the region in which the APU operates in, ingestion of environmental dust and contaminants such as sulphur will lead to the accelerated corrosion of the blade platform and shank. Additionally, the continual ingestion of environmental dust will result in the obstruction of blade cooling

passages which leads to an increase in the blade metal temperatures thereby strengthening the effects of corrosion and fatigue. As shown in Figure 2.3, this leads to elevated temperatures at the blade shanks which intensifies corrosion and fatigue crack growth in the region. In addition to this, poor performance by the fuel atomiser can lead to hot streaking across the NGVs which results in material loss (Figure 2.2). This in turn affects the turbine flow characteristics and will lead to poor turbine performance. To counter this loss in performance, the fuel flow will increase thereby leading to a higher TIT and further fatiguing of the blade shank. A combination of these self-reinforcing effects will result in under-platform crack growth and the subsequent release of a first stage blade.

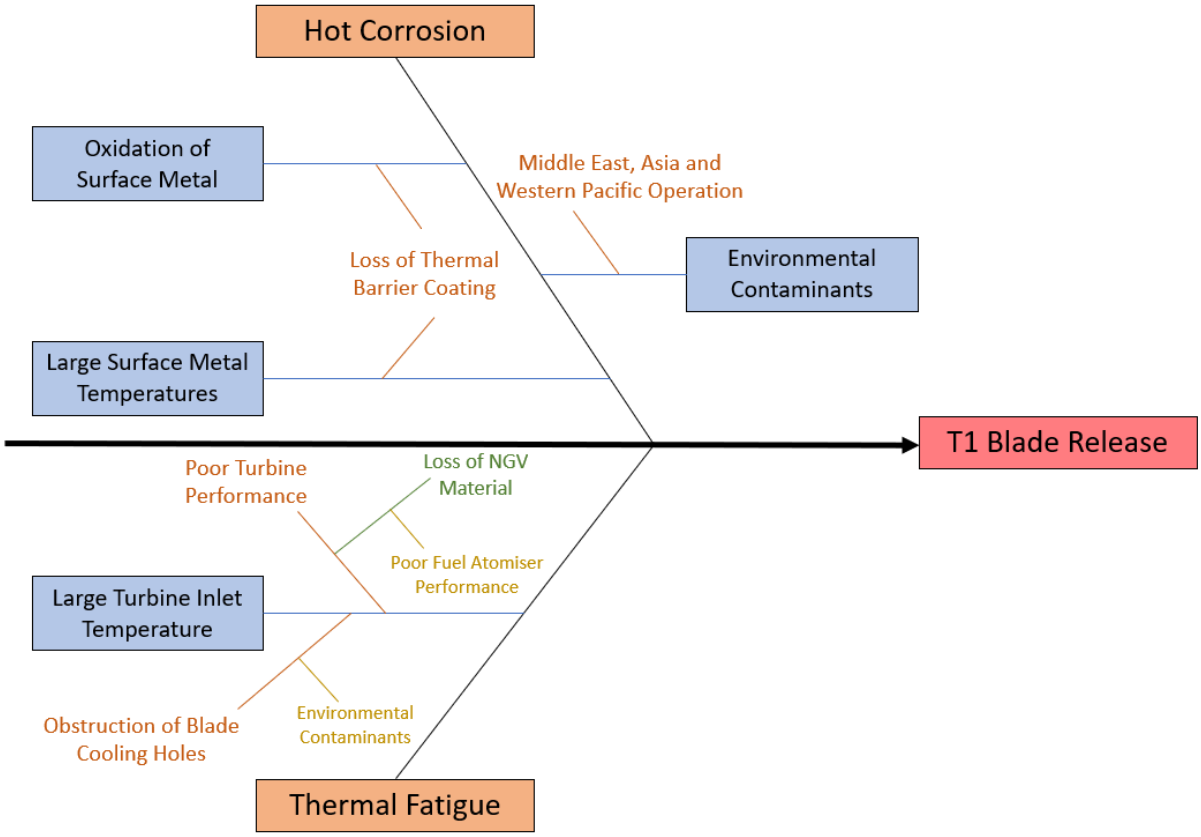

Figure 2.1: Cause-and-effect diagram of the potential factors that lead to a first stage turbine blade release on the Honeywell 331-500.

Figure 2.2: The first stage NGV assembly of the turbine of a 331-500 showing extensive corrosion and damage.

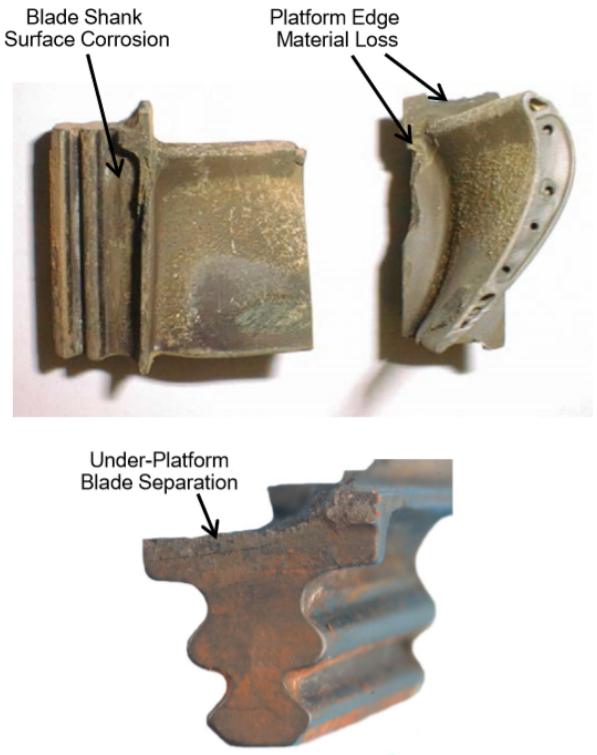

Figure 2.3: First stage turbine blades after extensive under-platform corrosion and crack growth [6].

Since the 331-500 runs at 39000 RPM, a release of a turbine blade during operation will lead to extreme downstream damage of the APU with high-speed material flowing through the second and third stages of the turbine. Additionally, upstream components such as both compressors are also damaged due to the subsequent shaft imbalance as a result of a T1 blade

release. This imbalance causes blade tip/casing rub and accelerated wear of the compressor impellers. Photos of various components after T1 blade failure are shown below in Figures 2.4 to 2.7.

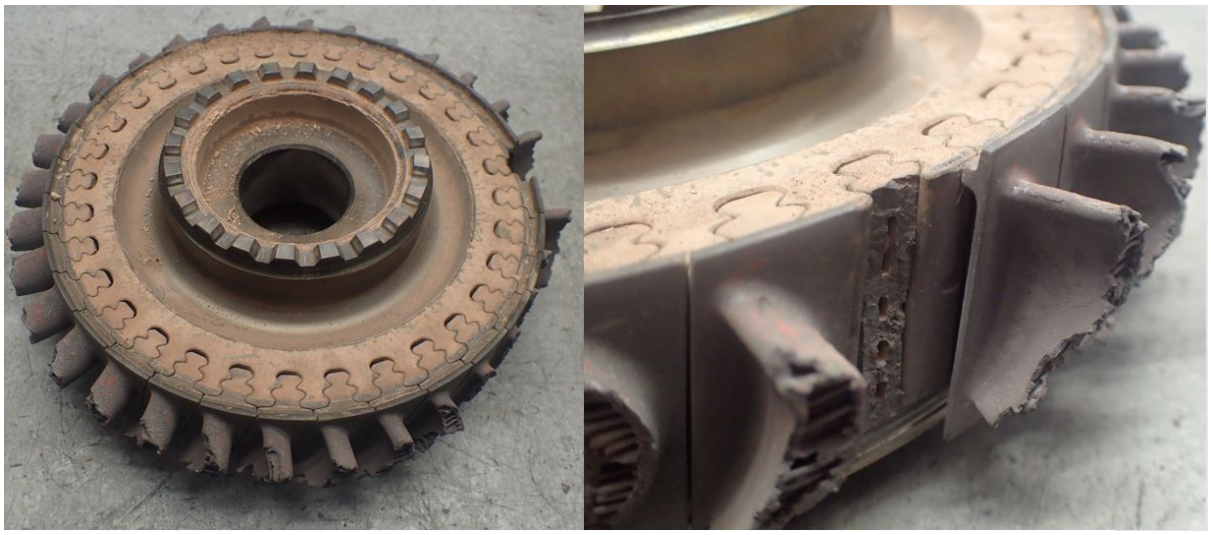

Figure 2.4: First stage turbine rotor of a 331-500 after T1 blade failure showing extensive impact damage.

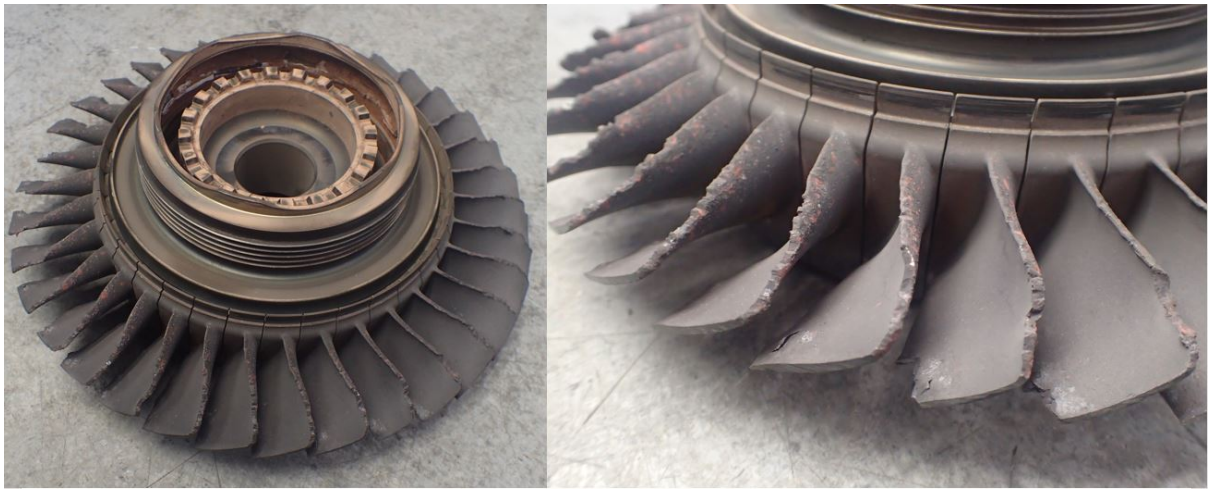

Figure 2.5: Second stage turbine rotor of a 331-500 after T1 blade failure showing extensive impact damage.

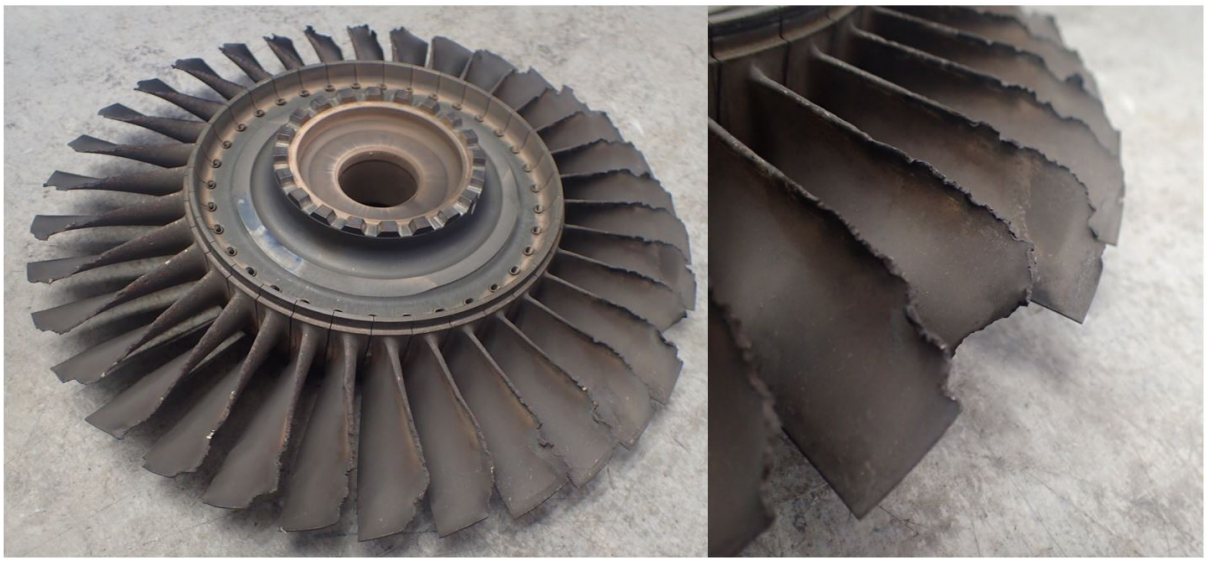

Figure 2.6: Third stage turbine rotor of a 331-500 after T1 blade failure showing extensive impact damage.

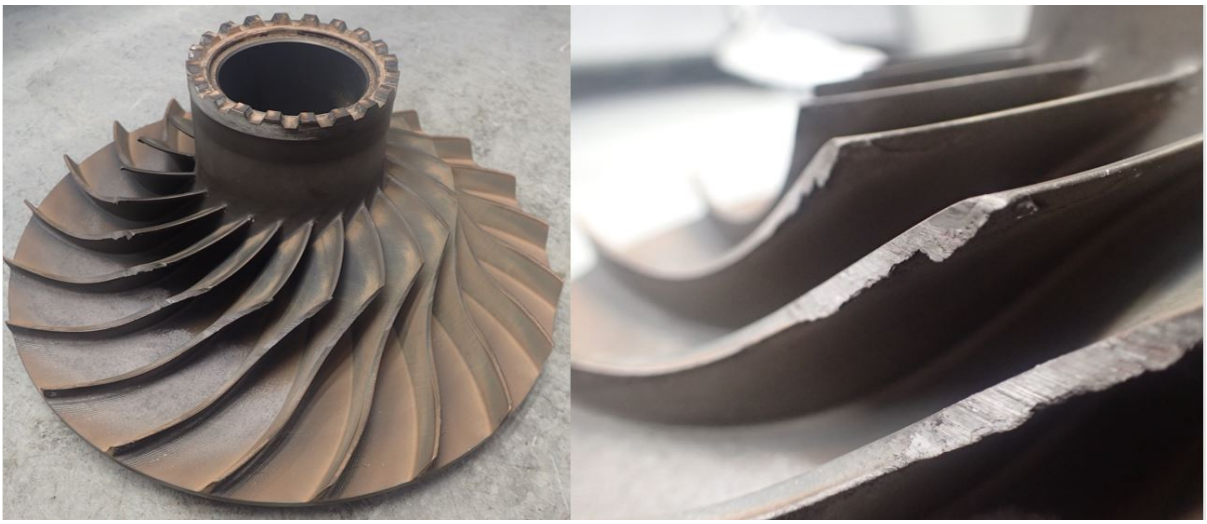

Figure 2.7: Second stage compressor impeller of the 331-500 after T1 blade failure showing heavy abrasion of the contours.

The above images highlight the severity of a T1 blade failure on the 331-500. Typically, T1 blade failure occurs with little or no warning and leads to the sudden shutdown of the APU. Aircraft operator's have 10 days to replace the APU before the aircraft is grounded and it's revenue generation is stalled. Therefore, it is in the interest of both the MRO service provider and their customers to reduce the number of unscheduled APU removals. This is the reason why T1 blade failure has been chosen for this study.

3 Review of Current Gas Path Analysis Methods

GPA has been used as a method for gas turbine diagnostics since the early 1970s [7]. The underlying principle to the method is to relate the deterioration in the performance of the machine (temperatures and pressures) to the deterioration in the condition of the main components along the gas path (efficiencies and mass flows). This is done by making use of the aero-thermodynamic relations that exist between the conditional and performance parameters of the machine. Any deviation in the condition of a gas turbine component, which may not be directly measurable, will have a corresponding deviation in performance, which is easier to measure. These deviations are from a known reference state which is usually that of a healthy engine i.e. as shipped by the OEM or directly after repair. At this state, the performance and condition parameters of the gas turbine are known and any deviation from these reference values is considered to be a result of deterioration. Therefore, GPA may be used to identify and isolate a faulty component of a gas turbine whose deterioration may not be easily visible in the raw measurement data.

Several versions of GPA exist and many incorporate statistical and machine learning methods to improve the overall accuracy. The most notable ones will be discussed below and the method used for this study will be outlined.

3.1 Linear GPA

Excluding measurement uncertainty, a gas turbine may be described as followed [7]:

$$\overline{p} = g\left(\overline{c}, \overline{o}\right) \tag{1}$$

Where $\overline{p}$ is a vector of measured performance parameters, $\overline{c}$ is a vector of calculated condition parameters and $\overline{o}$ represents operating condition parameters such as ambient conditions and power requirements. g is a non-linear function that represents the aero-thermodynamic equations mentioned above and relates the gas turbine performance, condition, and operation parameters to each other. To simplify, these relations may be linearised about a single operating point with the assumption that both the deviation from this operating point and the deterioration of the gas turbine is small. This results in the following system of equations:

$$\Delta\overline{p} = G\Delta\overline{c} \tag{2}$$

Where G is known as a the Influence Coefficient Matrix (ICM). Rearranging this equation for c, the conditional parameters of the gas turbine, results in the following:

$$\Delta\overline{c} = G'\Delta\overline{p} \tag{3}$$

Where G', the inverse of the ICM, is known as the Fault Coefficient Matrix (FCM) and can only be determined if the number of performance parameters is equal to the number of measurements i.e. if G is a square matrix and invertible. A visual representation of this linearisation is shown in Figure 3.1 below.

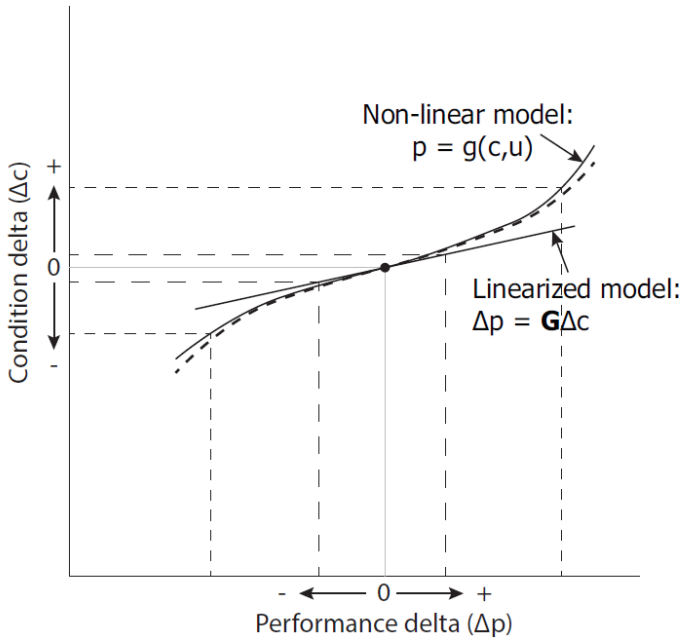

Figure 3.1: Effect of linearising the non-linear performance of a gas turbine about a single operating point [8].

In reality, sensor noise and inlet effects lead to significant variance in the measured performance of a gas turbine. Additionally, after extensive operation of a gas turbine, significant deterioration of the hot section of the machine will occur leading to large deviations in performance from the operating point to which the aero-thermodynamic relations are linearised about. As this study focuses on extensive deterioration of the 331-500 APU, the underlying assumption of linear GPA will therefore be invalid and non-linear effects must be considered.

3.2 Non-linear GPA

Fundamentally, non-linear GPA is the same as linear GPA in that it relates performance deterioration to component deterioration. However, at larger deviations from the operating point of the reference engine, non-linear GPA is more accurate. One such method of non-linear GPA is known as *adaptive modelling* [9]. In this method, the deviation in performance between an unhealthy and healthy engine is reduced by adjusting, or adapting, the conditional parameters of the gas turbine's components until the healthy performance matches that of the unhealthy engine. The amount by which the conditional parameters are adapted is the deterioration in the engine. For example, at a certain operating point, a healthy reference engine may have a measured EGT of 1000K whereas an unhealthy one may have an EGT of 1100K. To calculate the deterioration in the unhealthy engine's components, such as the the turbine, various conditional parameters of the healthy engine are adapted until the EGT matches that of the unhealthy one. In the case of the turbine, the adapted conditional parameter may be the turbine efficiency. The subsequent difference in the turbine efficiency ,$\Delta\eta_t$, is that component's deterioration. This is shown in (4) below, where $\eta_{t,ref}$ is the efficiency of the reference engine and $\eta_{t,det}$ is that of the deteriorated machine.

$$\Delta\eta_t = \mid \eta_{t,ref} - \eta_{t,det} \mid \tag{4}$$

Adaptive modelling differs from alternative, empirical GPA methods as it is primarily a physics-based approach. Rather than making use of data-driven optimisation methods, such as genetic algorithms and neural networks, it requires a thermodynamic model of the gas turbine to be built and the adapting to measured performance data results in deterioration data for the machine. This deterioration data may be analysed to identify trends or other measures that may prove useful for the monitoring of gas turbines in operation. Furthermore, any observed deterioration should be explained through the known failure mechanisms of the components of a gas turbine.

To adapt the conditional parameters of a GPA model, the model must be capable of adjusting the parameters in such a way as to reduce the deviation between the healthy and unhealthy performance. Various ways of achieving this include a Newton-Raphson iterative scheme as is done on the Gas Turbine Simulation Program (GSP) [10]. Another method is to define an error function as the summation of the squares of the various calculated and measured performance deltas and then minimise that function [11]. As the minimisation of the error function may involve adapting several parameters, a stable method should be chosen for

minimisation. One suitable method is known as gradient descent which is primarily used today in training machine learning models for data science applications. Since gradient descent is stable and relatively simple to implement, it is chosen as the minimisation method to be used with adaptive modelling. Further information on gradient descent is discussed below.

3.3 Gradient Descent

As mentioned above, one example of the application of GPA is to adapt the turbine efficiency of a gas turbine model until the EGT is equal in value to that of the corresponding measurement on the real engine. This is the simplest case, where the error in the model's EGT prediction is minimised by the varying of a single variable. It may also be the case that the compressor efficiency of a gas turbine is an unknown variable. As with the turbine efficiency and the EGT, the compressor efficiency is also adapted until the error between another measurement and its model-predicted value are minimised, such as the compressor outlet temperature. However, as the compressor efficiency will also have an effect on the EGT, it too will affect the final value of the turbine efficiency. Therefore, a certain compressor efficiency that minimises the error in the compressor outlet temperature may not necessarily result in a minimised error in the EGT. In this multivariable case, the adapting of both variables must be done such as the minimise the **total error** of the model. This process is outlined in detail below.

3.3.1 Cost Function

Firstly, a function is defined as the summation of the deltas between the predicted and measured performance parameters in the model. As the deltas may be positive or negative, each one is also squared. To account for the difference in magnitude of the calculated performance parameters, each value is scaled with its corresponding measured value. This is to enable different parameters to be used in the function, such as pressures and temperatures. This function, referred to as the cost function, is defined in (5) below. The unknown variables that are adapted to minimise the cost function are represented in a vector as defined in (6).

$$J = \sum_{i=1}^{n} a_i \left(1 - \frac{J_{i,c}}{J_{i,m}}\right)^2 \tag{5}$$

$$\overline{\beta} = \begin{bmatrix} \beta_1 & \beta_2 & \dots & \beta_n \end{bmatrix} \tag{6}$$

Where the subscripts c and m denote the calculated and measured values of each performance parameter and n is the number of terms in the cost function. a is defined as the weights used to prioritise certain terms over others.

3.3.2 Cost Function Gradient

To determine the direction and magnitude by which to vary the unknown variables to minimise the cost function, the gradient of the function with respect to each variable is computed. In trivial cases, an analytical solution for the cost function derivative will exist but in reality it is usually more complex and computed numerically.

First, a sensible initial value (β_o) is assigned to each of the unknown variables and the cost function is computed as above. Each variable is then increased by a small delta and the cost function computed thereby enabling the individual gradients to be determined. As shown in (7) below, these gradients are defined as a vector of partial derivatives of the cost function with respect to each variable. The numerical definition of the partial derivative is defined directly after in (8).

$$\frac{\partial J}{\partial \overline{\beta}} = \left[\frac{\partial J}{\partial \beta_1} \quad \frac{\partial J}{\partial \beta_2} \quad \dots \quad \frac{\partial J}{\partial \beta_n} \right] \tag{7}$$

$$\frac{\partial J}{\partial \beta} = \frac{\Delta J}{\Delta \beta} \approx \frac{J(\beta + \Delta\beta) - J(\beta)}{\Delta \beta} \tag{8}$$

As was the case with the cost function parameters, the unknown variables should be scaled such that $\Delta\beta$ reflects the same relative increment to all variables. One such way of doing this is to non-dimensionalise each variable with its initial value as is defined in (9) below. In this case, a common delta may be used for all variables during the partial derivative vector calculation. The updated vector of unknown variables is defined in (10).

$$\hat{\beta} = \frac{\beta}{\beta_o} \tag{9}$$

$$\hat{\overline{\beta}} = \left[\hat{\beta}_1 \quad \hat{\beta}_2 \quad \dots \quad \hat{\beta}_n \right] \tag{10}$$

Once the gradient vector is computed, the vector of variables is updated from the initial values as determined by the size and sign of the individual gradients. However, the gradient vector can be such that it is either too weak to significantly vary the variables, leading to a long run time, or too strong such that it is unstable and unable to find a solution. To account

for this, a factor known as the learning rate (ϕ) is applied to the gradient vector. The learning rate's value is model-specific and depends on the number of unknown variables, the number of terms in the cost function, and their sensitivity. It is usually determined by trial and error.

The updating of the vector of variables is shown below in (11). This process is known as gradient descent and continues until the cost function is minimised.

$$\overline{\beta}_{new} = \overline{\beta}_{old} - \phi \frac{\partial J}{\partial \overline{\beta}_{old}} \tag{11}$$

3.3.3 Limitations of Gradient Descent

The process of adjusting a set of unknown variables to minimise some dependent function becomes increasingly more complex with the addition of more unknown variables. In the case of a gas turbine, where the unknown variables tend to be component efficiencies or pressure ratios, extreme and non-physical values may be required to minimise the cost function and thus match calculated and measured parameters. The matching of these parameters may also cause energy or mass balances to not be satisfied [12].

In addition to this, it may be the case that multiple unknowns exist but there are only a handful of measurements available for matching. This will be a problem, particularly if any of the measurements are sensitive to more than one variable. This occurs in the case where the compressor and turbine efficiency of a gas turbine are unknown and the only available measurement is the EGT. Both the compressor and turbine efficiency will affect the EGT with the turbine efficiency being the most sensitive of the two. To account for this, more measurements, such as the compressor outlet temperature, are required to adapt both variables in a stable manner. As a general rule, the number of unknown variables should equal the number of terms in the cost function with each term being dependent on only one variable [12]. In the case of multiple cost function terms, weights can be applied to each term to prioritise certain measurements over others. This can be useful when one variable is particularly more sensitive to altering the cost function than the other or more confidence is given to one measurement over another.

These limitations of adaptive modelling and gradient descent will become apparent in the application of these methods and will be discussed further in the recommendations section of this report.

4 Thermodynamic Model of a Single-shaft Gas Turbine

A schematic of a simple, single-shaft gas turbine with labelled states is shown below in Figure 4.1. At *State 1*, air at ambient conditions enters the compressor and is compressed to the conditions at *State 2*. After combustion, the temperature and pressure of the gas are raised to that of *State 3* before being expanded in a turbine to *State 4*. This schematic is representative to the power section of an APU with the mechanical load from the load compressor and generator combined as a total shaft load $\dot{W}_{load}$. The performance of the gas turbine below is simulated using a thermodynamic model while the specifics of the Honeywell 331-500 APU are added later in section 5. The following subsections will detail the fundamentals of this thermodynamic model including assumptions, equations, fluid properties and calculation processes.

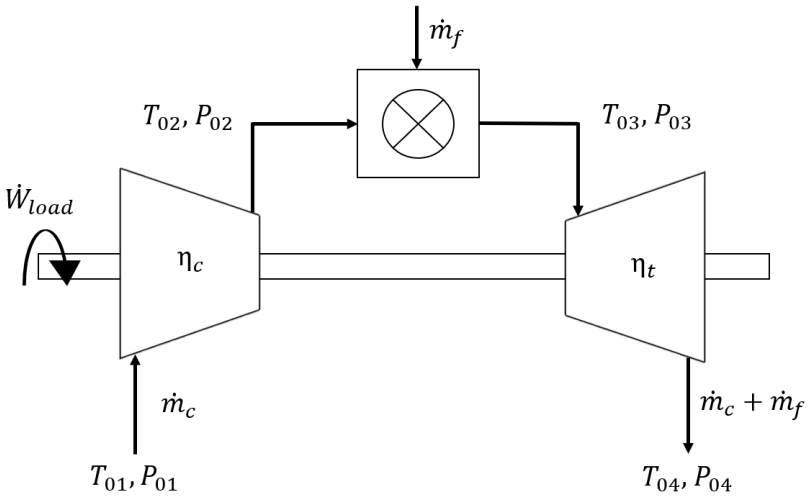

Figure 4.1: Schematic of the main components along the gas path of a single-shaft gas turbine.

4.1 Assumptions

Before outlining the equations used in the thermodynamic model, the assumptions made are outlined as follows:

- The gas turbine is analysed as a zero-dimensional (0-D) model. The internal workings of each component are not considered i.e. number of stages, combustion chamber length etc.

- The compressor and turbine outlet conditions are calculated based on the isentropic relations for the compression/expansion of a gas.
- The inlet of the turbine is choked during both on- and off-design operation.
- The ambient temperature and pressure are equal to that of the compressor inlet i.e. no heat pick-up or pressure loss.
- The turbine exit pressure is equal to that of ambient pressure.
- The mechanical efficiency of the shaft and bearings is 100%.
- Chemical equilibrium is not accounted for in the combustion process. The heat addition is treated as an enthalpy rise in the working fluid.
- The combustion chamber operates with an efficiency of 100% and with no pressure loss.
- The effects of relative humidity are considered to be small and not accounted for in the model [13].

4.2 Thermodynamic Equations

The equations used for the compression, combustion, choking and expansion processes of the gas turbine components are defined below in Figures 4.2 and 4.3. During the compression and expansion processes, the specific heat ratio (γ) of the gas will change with the varying pressure and temperature. To account for this, the compression and expansion processes are discretised into n pressure deltas with the specific heat ratio recalculated for each delta in the gas temperature and pressure. The two resulting equations are included in the figures below.

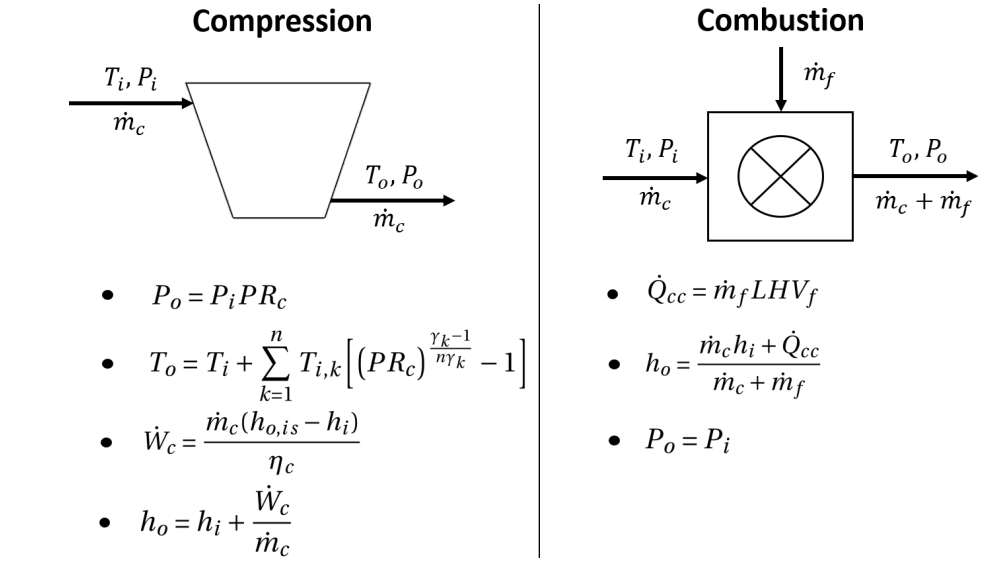

Figure 4.2: Equations used for the compression and combustion processes of the thermodynamic model.

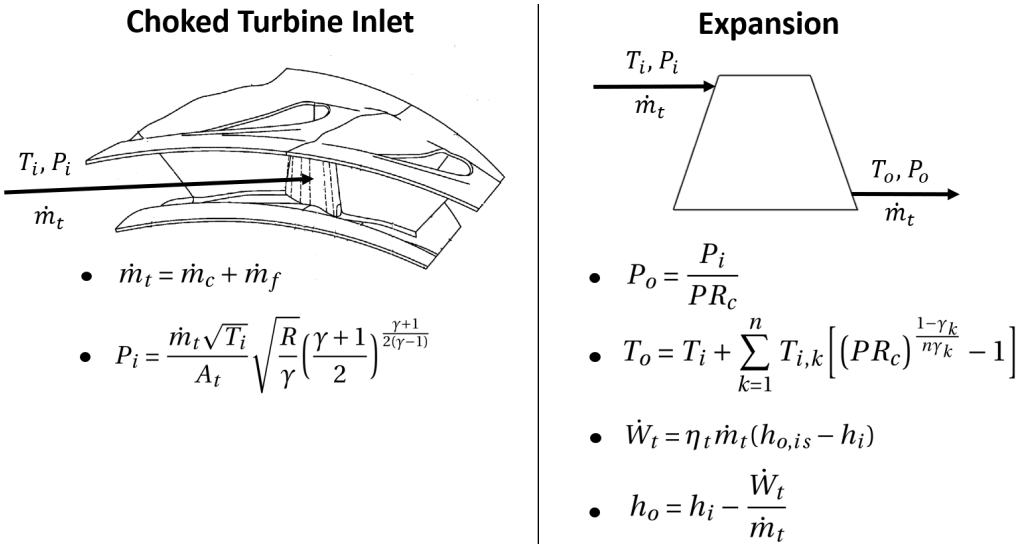

Figure 4.3: Equations used for the choking and expansion processes of the thermodynamic model.

4.3 Choked Turbine Inlet

The turbine inlet is assumed to be choked meaning, for a given air and fuel flow, the throat area determines the Pressure Ratio (PR) of the machine. The throat area of a turbine is defined as the minimum flow area of the first stage stator, or NGV assembly. Between two stator vanes, a line is drawn perpendicular to the trailing edge of one vane until it intersects the adjacent vane, as shown in Figure 4.4. The length of this line is the turbine throat. In two dimensions,

this line forms a plane that intersects both the shroud and the base of the vane and the area of this plane is defined as the throat area between two vanes. Finally, the summation of this area for each set of vanes across the circumference of the first stage stator is the throat area of the turbine.

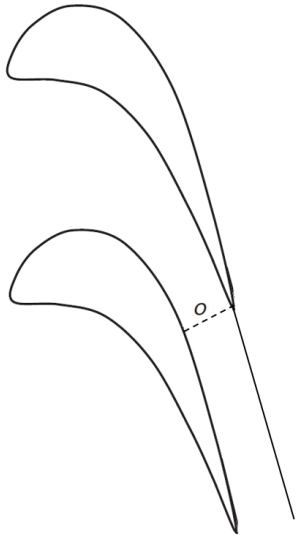

Figure 4.4: Definition of the throat as the distance *O* between two adjacent turbine stator vanes [14].

4.4 Air and Flue Gas Data

Both the air and flue gas data are taken from RefProp. The required fluid properties for the APU model are the enthalpies and specific heat ratios at various pressures and temperatures. Standard air is used for the air properties while the flue gas composition is determined from the reaction in (12) below. The reference state for both the flue gas and air data is chosen as 500 K at 1 bar. This is to ensure that the H_2O component of the flue gas is in a gaseous state and the latent heat of vaporisation is not included in enthalpy calculations. Lastly, the fuel used for the combustion chamber of the 331-500 is Jet-A1 with a lower heating value of 43.2 MJ/kg.

$$\frac{1}{6}C_{12}H_{24} + 15\Big(0.8N_2 + 0.2O_2\Big) \longrightarrow 2CO_2 + 2H_2O + 12N_2 \tag{12}$$

4.5 Calculation Process

The calculation process of the thermodynamic model varies between on- and off-design operation. Here, the general process for both is outlined with the specific APU behaviour added later in the following section.

4.5.1 On-design

At the design point of a gas turbine, the input parameters (ambient conditions, mass/fuel flows, shaft load requirements and component efficiencies) are assumed to be known. As the turbine is choked, the PR is determined by the turbine throat area and mass flow although some iteration is required. The process is outlined below in Figure 4.5.

Each block represents a component/process of the gas turbine while the arrows represent the flow of inputs and outputs of each block. The calculation process starts at the top with the inputs for the compressor calculations: the ambient conditions, compressor mass flow, efficiency, and initial choice for the PR. The process then proceeds from top to bottom through each calculation block until the equation for the choked turbine inlet results in an updated (new) compressor PR. The initial (old) value for the PR is then updated with this new value. After, the calculation loops back to the compressor calculations until the difference between the new and old PR is within a chosen tolerance. Lastly, the turbine calculations are completed to determine the EGT and net work on the shaft.

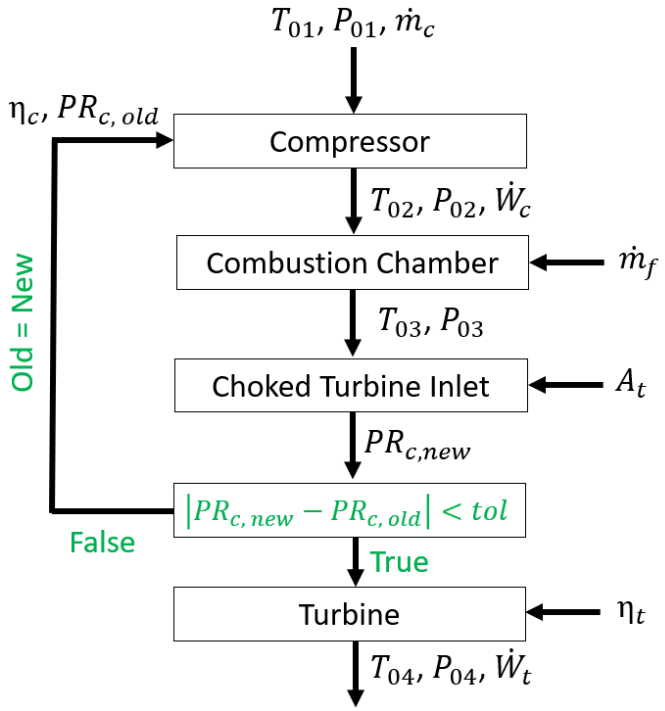

Figure 4.5: Calculation process for the on-design operation of a single-shaft gas turbine with a choked turbine inlet.

4.5.2 Off-design

During off-design operation, the variance in ambient conditions, shaft load and fuel flow lead to a corresponding variance in compressor mass flow, PR and efficiency. The relationship between the compressor parameters and the ambient/operating conditions is quantified in a compressor map. Again, the turbine is assumed to be choked and its efficiency is constant (unless deterioration is considered). The process, outlined in Figure 4.6 below, is almost identical to on-design operation except for the addition of the compressor map calculations to update the compressor efficiency and mass flow.

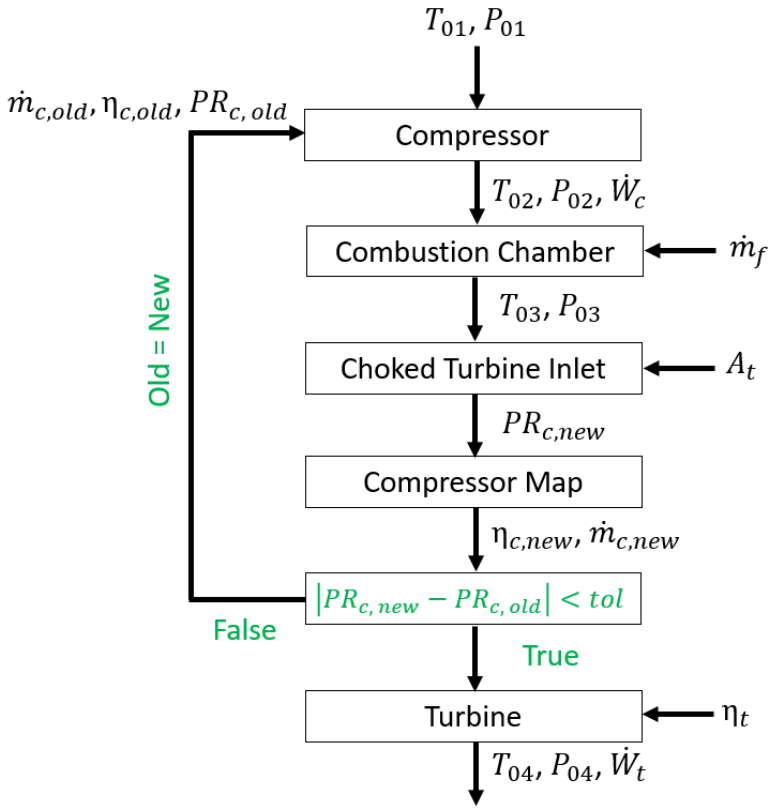

Figure 4.6: Calculation process for the off-design operation of a single-shaft gas turbine with a choked turbine inlet.

4.6 Model Validation

Before applying GPA to the thermodynamic model, and analysing deterioration, the model is validated. This is done by building and running an almost identical model using GSP and comparing results. The thermodynamic model itself is written in the MATLAB environment.

Arbitrary design point parameters for the thermodynamic model are described below in Table 4.1. In GSP, there is no option for inputting a turbine inlet throat area and the compressor PR must be directly assigned. Therefore the MATLAB model is first run to determine the PR before entering the result into the *Design* function of GSP. GSP will then scale a specified sample compressor map to the design point PR, efficiency and corrected mass flow. This compressor map is also exported from GSP and used in the MATLAB model. Unfortunately, only the default map data may be outputted and the scaling must be rewritten in MATLAB. To compare the off-design performance between both models, the Fuel-Air Ratio (FAR) is varied between 0.016 and 0.024. Important outputs are compared for both models in Figure 4.7 to Figure 4.12. The error in the MATLAB model is defined as the ratio of the absolute difference between the MATLAB and GSP values to the MATLAB-calculated value.

As is shown, the error in the model is <0.5% with respect to the compressor mass flow, pressure ratio and efficiency. A low error in these parameters is expected as the same compressor map is used in both models. The TIT has an error ranging between 2-4% with the GSP-determined value always higher than the value determined by the MATLAB model. It is expected that the TIT would be higher in the MATLAB model as it assumes complete combustion whereas the combustion process in GSP is modelled using the equations for chemical equilibrium which take into account the composition change of the flue gas throughout the process. A possible cause for this error could be the difference in flue gas properties between both models. As mentioned, the composition of the flue gas from reacting Jet-A1 with air is taken from RefProp whereas GSP has its own built-in property data.

The error range for both the EGT and net work are 0-1% and 4-10% respectively. The error in the EGT is expected to be low as the PR across the turbine in both models is approximately the same. The larger error in the net work is due to the nature of the equations used in its calculation. Since the compressor and turbine work are computed from the product of their respective mass flow and enthalpy changes, any error in the inlet and/or outlet temperatures between both models will be magnified in the work calculation. As the compressor PR, mass flow and efficiency are almost identical between both models, the error in the compressor work calculation is negligible meaning any error in the net work is mainly due to the turbine work calculation. Since the turbine work is computed from the TIT and EGT, the error in this calculation will be the result of a combination of error in both of these temperatures.

Table 4.1: Design point parameters for the validation of the thermodynamic model.

Parameter	Unit	Value
T_{01}	K	288.15
P_{01}	bar	1.01
$\dot{m}_c$	kg/s	2.00
PR_c	-	9.16
FAR	-	0.02
A_t	mm^2	2000
η_c	%	84.00
η_t	%	88.00

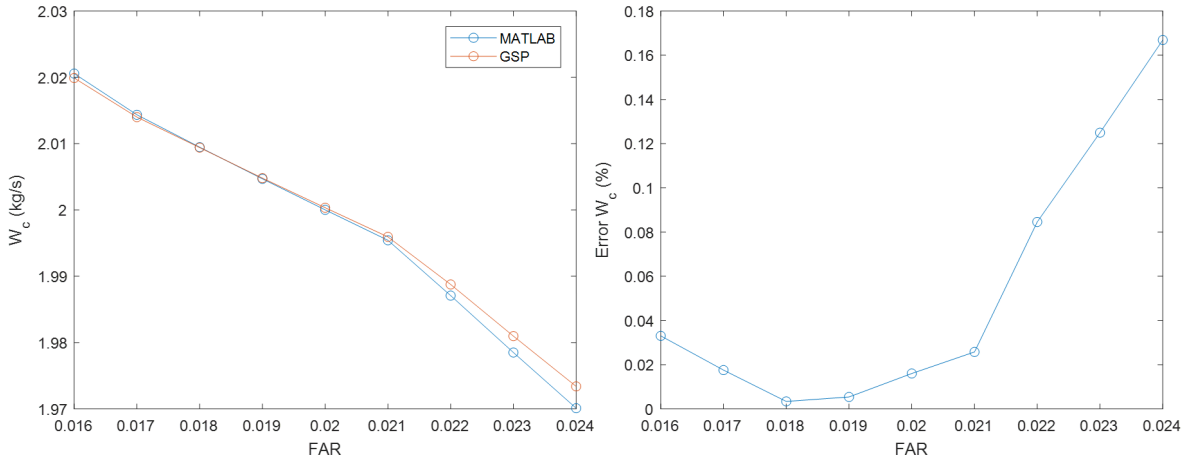

Figure 4.7: Comparison in corrected compressor mass flow between the MATLAB and GSP models.

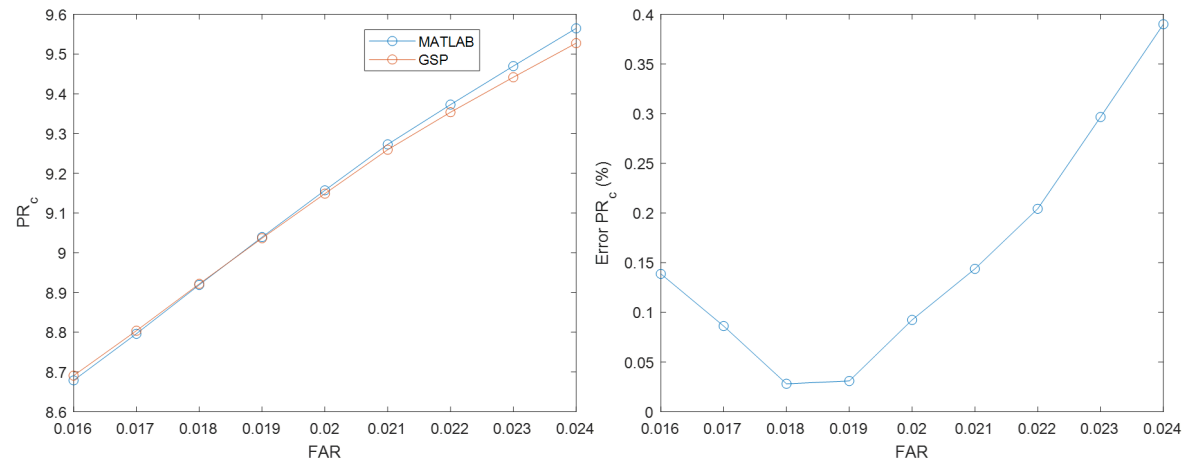

Figure 4.8: Comparison in compressor PR between the MATLAB and GSP models.

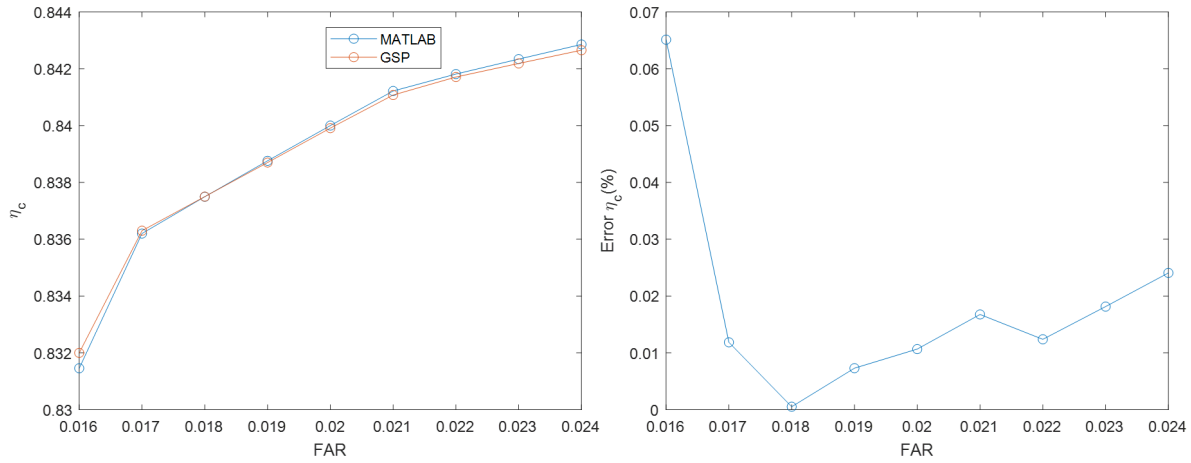

Figure 4.9: Comparison in compressor isentropic efficiency between the MATLAB and GSP models.

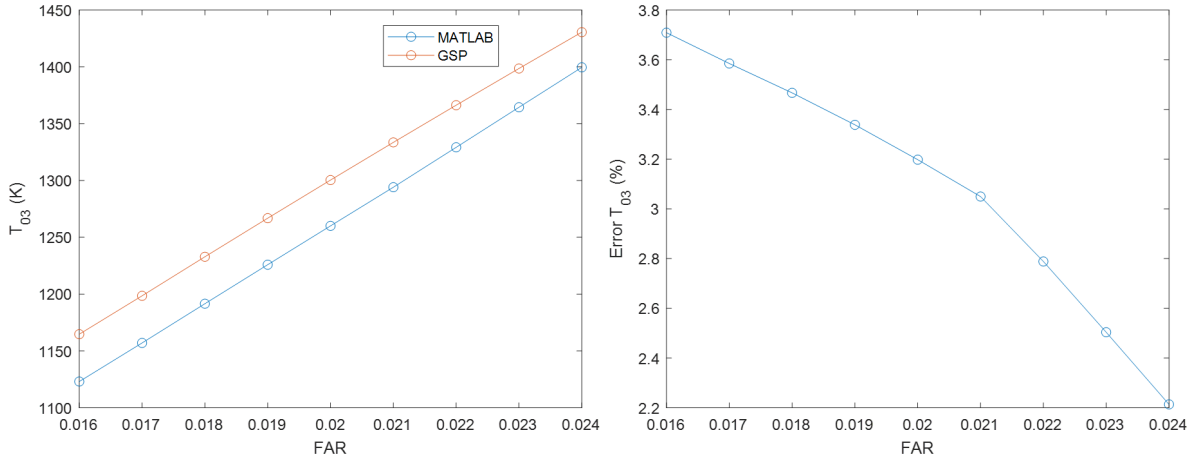

Figure 4.10: Comparison in TIT between the MATLAB and GSP models.

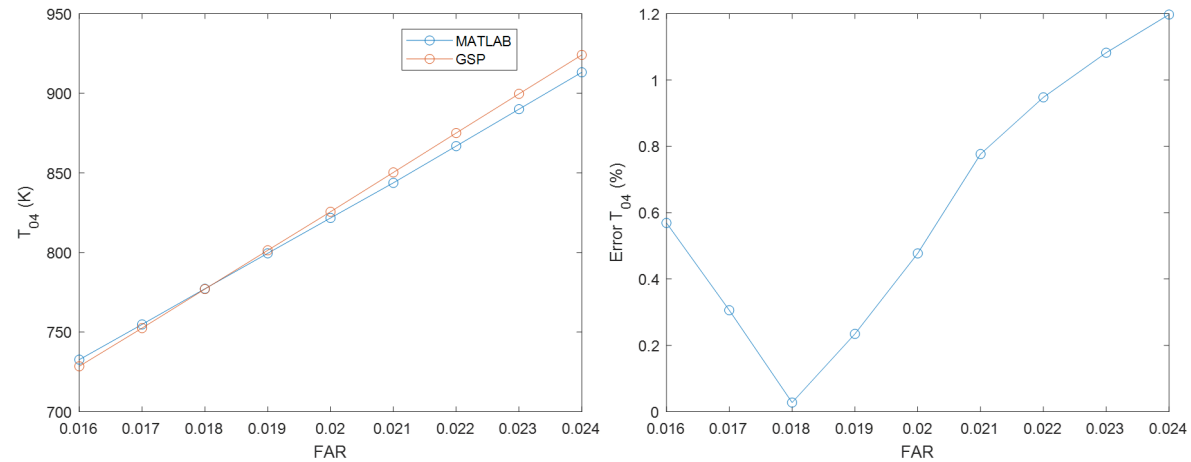

Figure 4.11: Comparison in EGT between the MATLAB and GSP models.

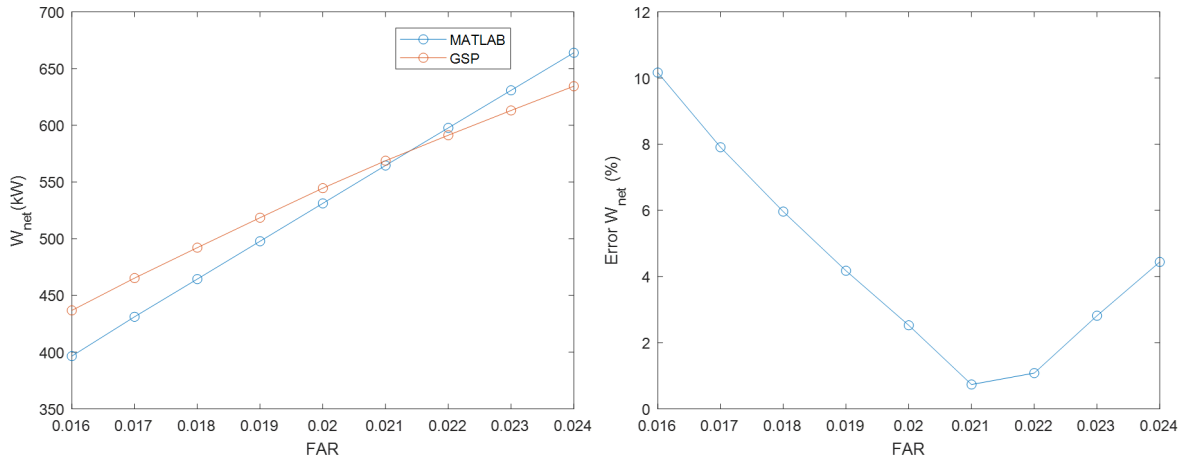

Figure 4.12: Comparison in net shaft work between the MATLAB and GSP models.

5 Thermodynamic Model of the Honeywell 331-500

The Honeywell 331-500, the APU for the Boeing 777, is shown below in Figure 5.1. The power section of this APU has a two stage centrifugal compressor, a reverse flow annular combustion chamber and a three stage axial turbine. On a common shaft, the turbine drives a single stage centrifugal load compressor and an accessory gearbox. The gearbox drives the electrical generator as well as oil and fuel pumps. Cooling air is bled from the compressor outlet for cooling of the combustion chamber and the first stage of the turbine. A simplified diagram of the internals of the machine is shown below in Figure 5.2.

As previously mentioned, the gas turbine model from section 4 represents the power section of a typical APU. That model must now be modified to represent the specifics of the 331-500 including the load compressor and generator. Additionally, several unknowns such as the real component efficiencies of the machine must be determined. This modified model, with its unknowns, is referred to as the Black Box Model (BBM). This section will outline the new calculation process for the BBM as well as the resulting design point performance parameters of the 331-500.

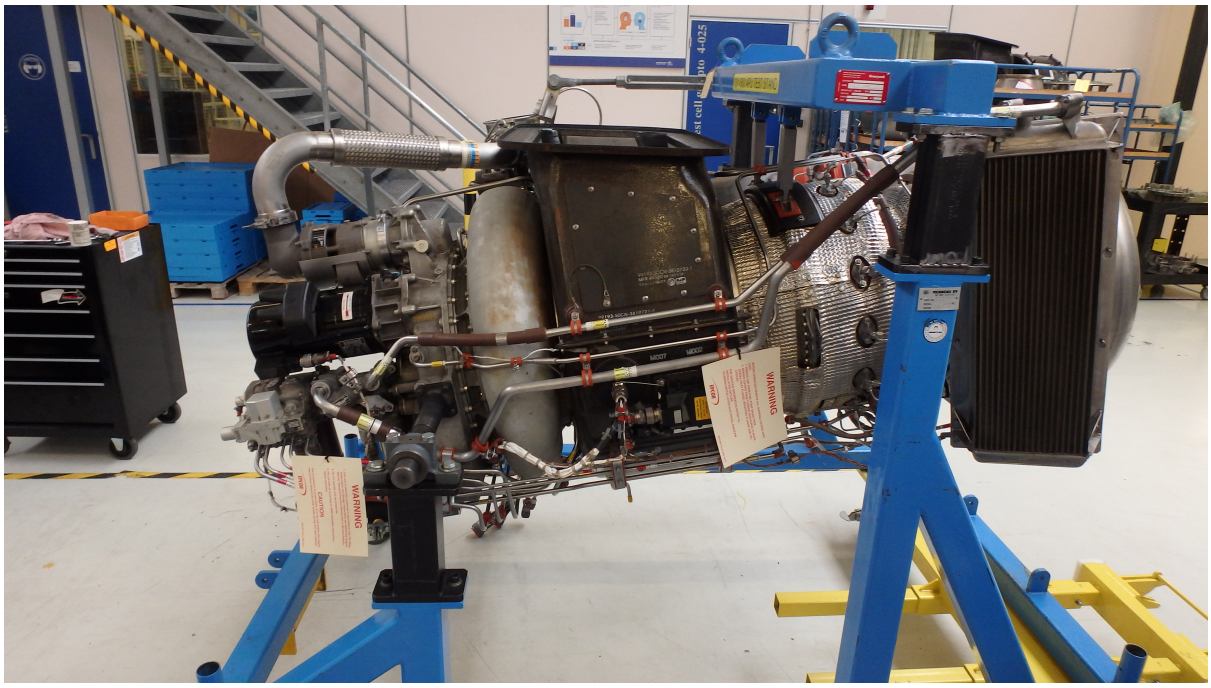

Figure 5.1: The Honeywell 331-500 APU in a stand at the shop floor of EPCOR B.V.

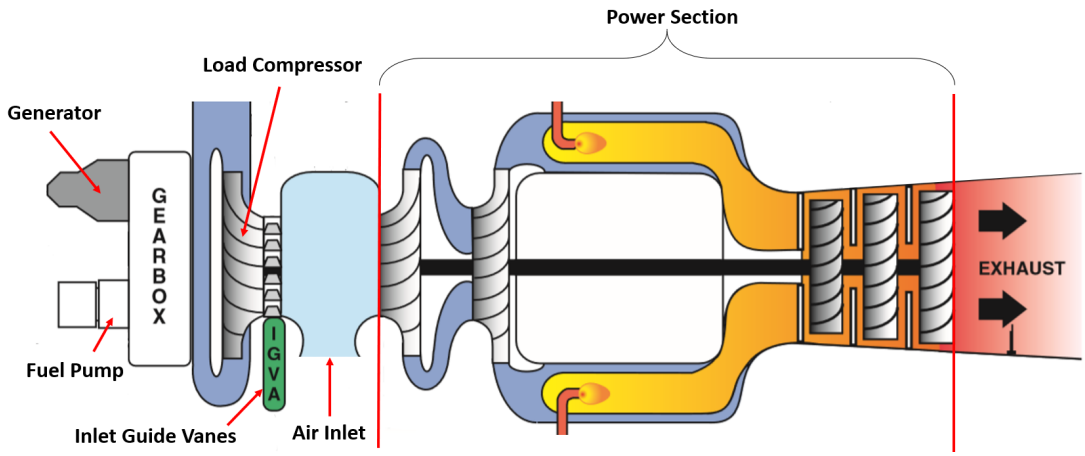

Figure 5.2: Diagram of basic components of the Honeywell 331-500 APU [15].

5.1 331-500 Schematic and Unknown Parameters

The schematic for the thermodynamic model of the 331-500 is shown below in Figure 5.3. The load compressor takes air from the same inlet as the power section compressor and compresses it to ambient conditions at *State 1* to conditions at *State b*. As with the gas turbine model in section 4.1, the shaft mechanical efficiency is assumed to be 100% meaning the gearbox is not included in the model. The generator is simply modelled as a mechanical load on the shaft. Test cell data is used to calculate the design point of the machine but, due to a limited number of measurements, there are multiple unknowns present. These include the compressor mass flow and PR, combustion chamber and turbine cooling flows, and the compressor and turbine efficiencies. The methods for determining these unknowns are outlined below.

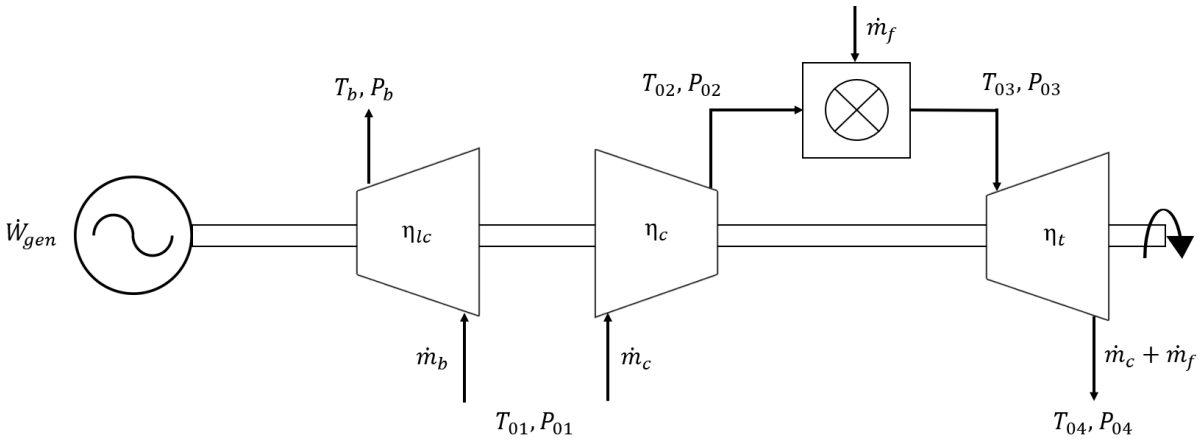

Figure 5.3: Schematic of the Honeywell 331-500 APU.

5.1.1 Compressor Mass Flow and Pressure Ratio

The compressor mass flow is estimated by taking an energy balance over the power section of the machine as defined in (13) and Figure 5.4 below. This energy balance assumes that the total work supplied by the turbine is equal to the sum of the load compressor, compressor and generator loads. In other words, it is assumed that there is a net-zero work balance on the shaft. Similarly, mechanical work for driving the fuel and oil pumps is considered negligible.

To determine the PR of the machine, the turbine throat is measured. As mentioned previously, the throat area is the summation of the minimum area between each stator vane, or NGV. The first stage NGV assembly of the 331-500 turbine, consisting of 20 nozzle segments that are joined together, is shown below in Figure 5.5. A 3-D scan of one of the nozzle segments is completed and the throat area computed through the use of the CATIA computer-aided design program. As shown in Figure 5.6, the surface of each nozzle is curved thereby making it difficult to calculate the throat area. With an estimated error of ±5%, the value of the throat area was determined to be approximately 4000 mm^2.

$$\dot{m}_c = \frac{\dot{Q}_{cc} - \dot{W}_{lc} - \dot{W}_{gen} - \dot{m}_f h_{04}}{h_{04} - h_{01}} \tag{13}$$

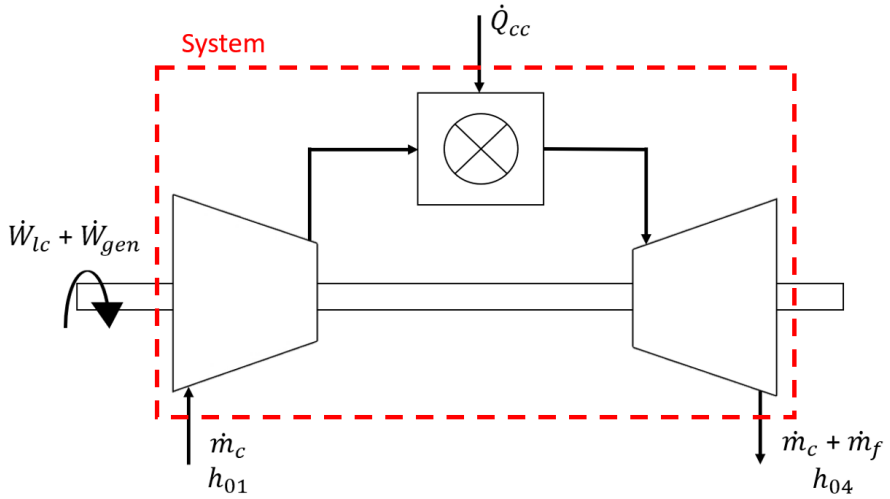

Figure 5.4: Definition of the system around the APU power section from which an energy balance is taken for estimating the compressor mass flow.

Figure 5.5: Assembled first stage NGV of the Honeywell 331-500 APU.

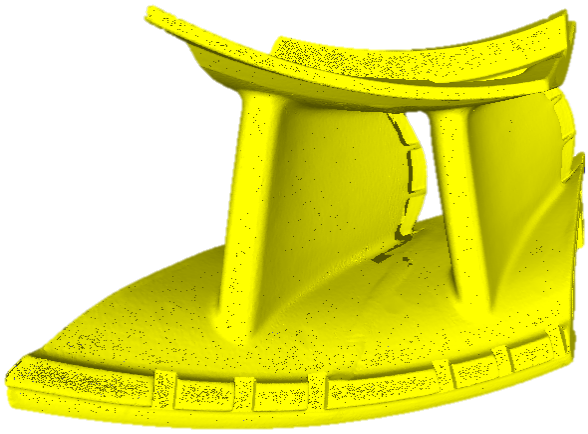

Figure 5.6: 3-D scan of a single nozzle segment from the first stage NGV of the Honeywell 331-500.

5.1.2 Component Efficiencies and Remaining Unknowns

Modelling of the first stage cooling flow was attempted but, due to the EGT being highly sensitive to its value, it was decided not to include it in this study. As was outlined previously, the gradient descent algorithm will become highly unstable if variables are used which are very sensitive to one or more of the cost function terms. Regarding the compressor efficiency, it is not possible to calculate it with the limited test cell data and instead a value is assumed. The effect of this will be discussed later in section 6.4. Lastly, the turbine efficiency is determined using the gradient descent algorithm.

5.2 Fitting the Black Box Model to the Test Cell Data

The calculation process for the fitting of the BBM to the test cell data is shown below in Figure 5.7. To calculate the turbine efficiency, the gradient descent algorithm determines a value that will minimise the error between the measured and calculated EGT. This error in the EGT is represented in the cost function which is defined in (14) below. As the energy balance in (13) is used to estimate the compressor mass flow, a net-zero shaft work balance is enforced and there is no need to include an extra term in the cost function to minimise any error as it will already be negligible.

$$J = \left(1 - \frac{T_{04}}{EGT}\right)^2 \tag{14}$$

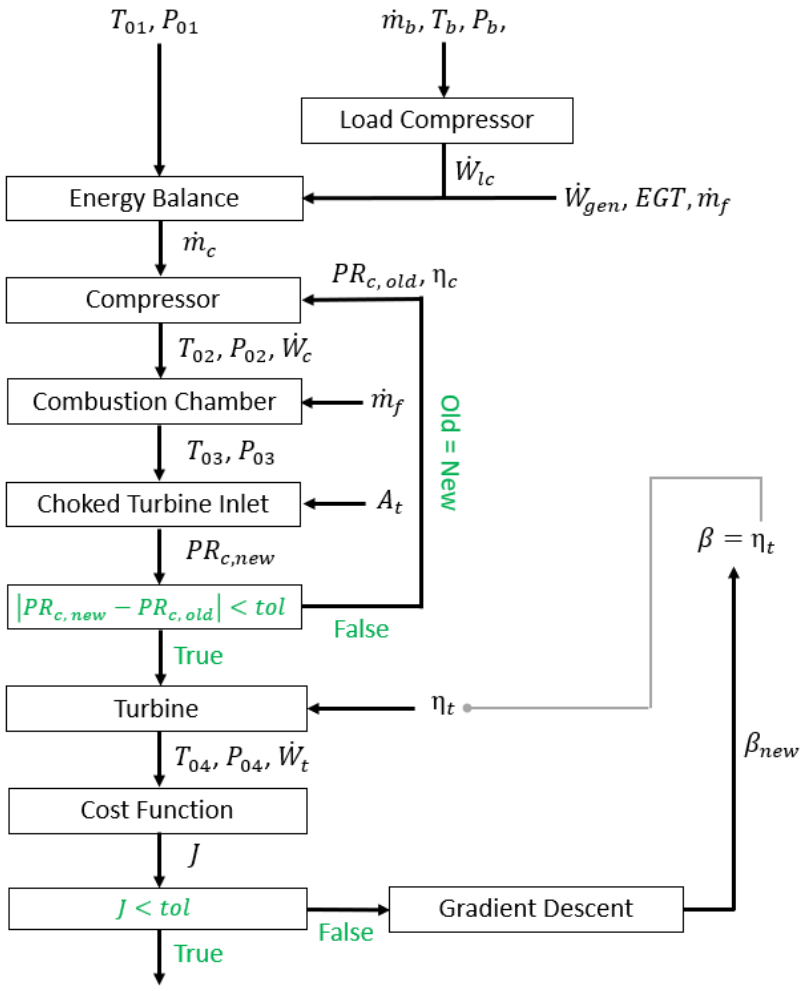

Figure 5.7: Calculation process for fitting the BBM to the on-design operation of the 331-500. The turbine efficiency is adapted until the error between the calculated and measured EGT is minimised.

5.3 Design Point Results

The design point of the 331-500 is considered to be at MES operating conditions. At this condition, the machine supplies 180 HP (134 kW) of mechanical work to the generator and approximately 2.6 kg/s of bleed air at 4.2 bar. The compressor efficiency is assumed to be 75% at an ambient temperature and pressure of approximately 290K and 1.01 bar respectively. As the load compressor outlet temperature and pressure are measured, the load compressor efficiency may be calculated. The eight measurements that are recorded from each test cell run and used in the model are:

1. Ambient temperature
2. Ambient pressure
3. Fuel flow
4. Load compressor air flow
5. Load compressor outlet temperature
6. Load compressor outlet pressure
7. Generator mechanical load
8. EGT

MES data from a total of fourteen APUs is used to characterise the design point performance of the 331-500. Mean results and the Coefficient of Variation (COV), defined as the standard deviation divided by the mean, are tabulated below in Table 5.1. The measured parameters with the most variance are the fuel flow, EGT, ambient temperature, load compressor PR and load compressor mass flow. As the compressor mass flow is determined from an energy balance comprising a variety of these parameters, it also shows a significant level of variance. A value of 75% was chosen for the compressor efficiency to ensure that the subsequent fitting of the BBM would result in a turbine efficiency that is slightly larger than that of the compressor. As will be discussed later in a sensitivity analysis of the model in 6.4, increasing the compressor efficiency results in a lower turbine efficiency and vice versa. In most gas turbines, the turbine efficiency is slightly larger than that of the compressor therefore, a compressor efficiency of 75% was chosen which resulted in a turbine efficiency of approximately 76%.

The magnitude of the residual error between both the measured and calculated EGT, along with that of the shaft work balance, is plotted in Figure 5.8. For all fourteen APUs, the error is negligible.

Table 5.1: Mean, maximum and minimum performance parameters from fourteen Honeywell 331-500 test cell runs when operating at the MES power condition.

Parameter	Unit	Max	Min	Mean	COV (%)
T_{01}	K	297.93	281.59	290.00	1.82
P_{01}	bar	1.03	0.98	1.01	1.18
$\dot{m}_c$	kg/s	5.10	4.69	4.88	2.61
PR_c	-	11.45	10.67	11.10	2.00
$\dot{m}_f$	kg/s	0.089	0.082	0.085	2.53
$\dot{m}_b$	kg/s	2.78	2.49	2.61	2.62
PR_{lc}	-	4.38	4.10	4.21	1.84
$\dot{W}_{gen}$	kW	136.69	131.01	134.00	1.15
T_{03}	K	1257.79	1210.04	1238.65	1.26
EGT	K	862.59	818.15	841.96	1.70
η_{lc}	%	79.00	76.11	77.61	1.04
η_c	%	75.00	75.00	75.00	0.00
η_t	%	77.57	75.08	76.22	0.77

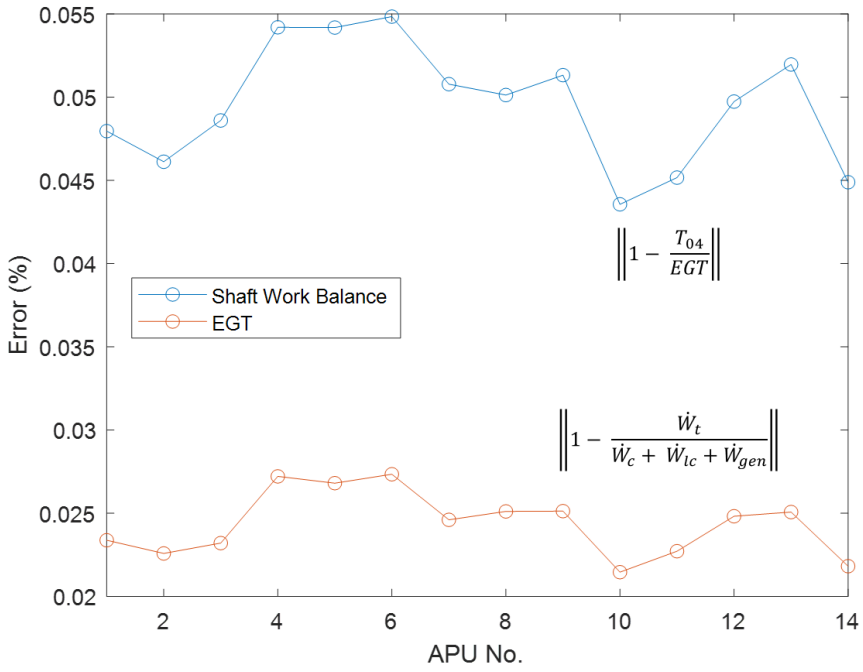

Figure 5.8: Residual error between both the measured and calculated EGT as well as that of the net-zero shaft power balance for the fourteen Honeywell 331-500 test runs at MES power condition.

6 Deterioration Modelling of the Honeywell 331-500

Once the BBM has been fitted to the test cell data of the 331-500, a thermodynamic model that is representative of the performance of the APU during design point operation is now available for use. To avoid confusion, this model is referred to as the 331-500 Thermodynamic Model (500TM) for the remainder of this report. The next step is to further develop the 500TM such that it is capable of representing the off-design, or on-wing, performance of the machine. Since it has been assumed that the turbine remains choked and the combustion chamber performance is unchanged for off-design operation, the only requirement is to provide a compressor map for the off-design operation of the compressor. Once completed, the 500TM is then capable of analysing deterioration data.

In analysing the deterioration of the 331-500, it was decided to use the turbine efficiency as the single variable for GPA. As discussed in section 2.2, the failure mechanisms leading to T1 blade failure are a result of the deterioration in the condition of the machine's turbine. This deterioration will lead to a reduction in the performance of the turbine which is physically quantified as its efficiency. Adaptive modelling is used to adjust the turbine efficiency until the EGT of the BBM matches that which is measured on-wing. It was considered to also include the compressor efficiency and/or turbine throat area as adaptive variables however insufficient on-wing measurements prevent this.

Before analysing the real 331-500 APU on-wing data, it is desirable to first artificially generate and analyse deterioration data. This allows the sensitivity of the adaptive modelling process to various input parameters, including the compressor efficiency and turbine throat area, to be tested. The process for doing this, along with the subsequent analysis is discussed in the following subsections.

6.1 Off-design Operation of the Honeywell 331-500

To simulate the off-design operation of the 331-500, the process is similar to what was done with the off-design operation of the gas turbine model in section 4.5.2. A sample compressor map from GSP is scaled to the design point of both compressors to vary their efficiency, mass flow and PR with ambient conditions. The design point conditions are taken as the mean

value of the parameters from Table 5.1 that were determined from the test cell analysis of the machine.

The maps are shown in Figures 6.1 and 6.2. Black and blue lines denote the corrected speed curves and efficiency contours respectively while marked in red is the design point of the machine as determined from the MES test cell analysis. The mass flow is corrected to standard sea level conditions with an ambient temperature and pressure of 288.15 K and 1.013 bar respectively.

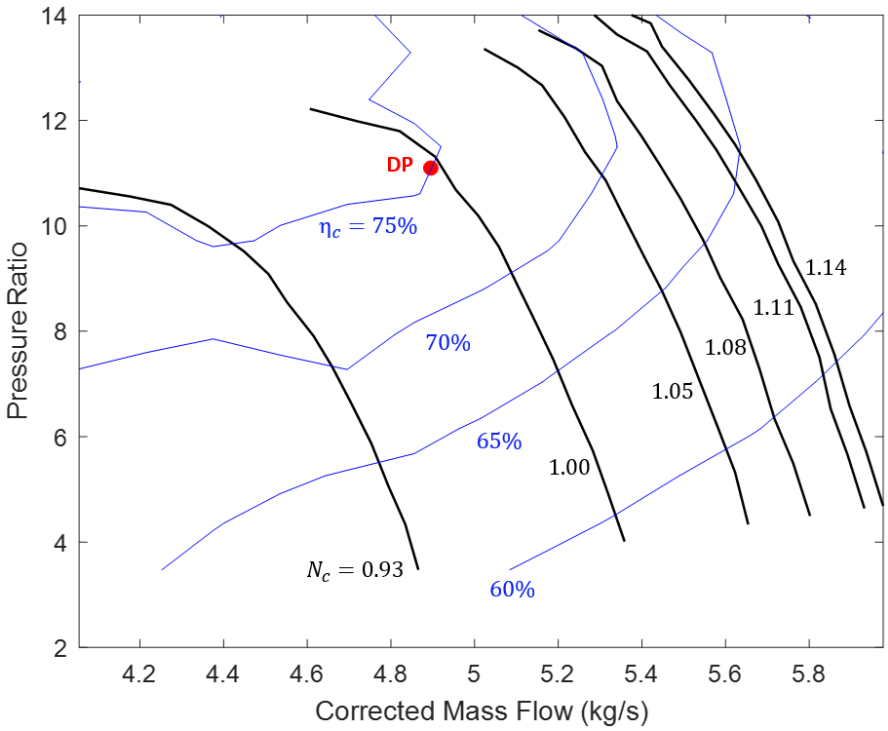

Figure 6.1: Assumed compressor map for the compressor of the Honeywell 331-500 APU as scaled from the *smallhpc* map from GSP.

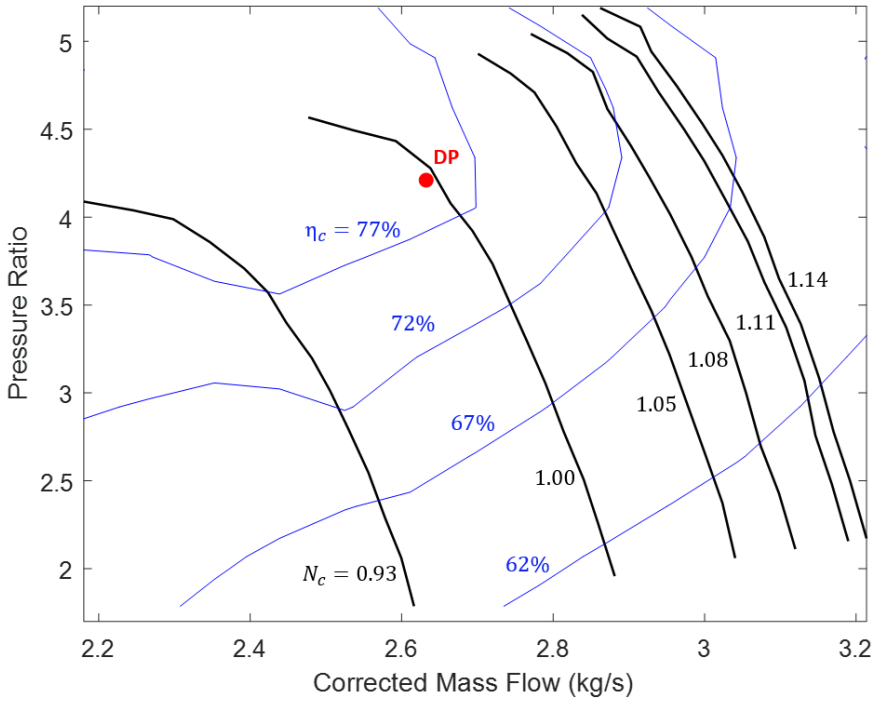

Figure 6.2: Assumed compressor map for the load compressor of the Honeywell 331-500 APU as scaled from the *smallhpc* map from GSP.

6.2 Generating Artificial Deterioration Data

To generate deterioration data, the 500TM, which at this stage is capable of off-design operation, is modified such that it reflects the characteristic behaviour of a deteriorating APU. This new model, which may be used to generate performance data that is representative of an unhealthy on-wing 331-500, will be referred to as the White Box Model (WBM) for the remainder of this report. The generated performance data from the WBM may then be used as an input to the 500TM which will then calculate the deteriorating turbine efficiency through adaptive modelling.

The process of using the WBM to generate deterioration data is shown below in Figure 6.3. To mimic the behaviour of a 331-500 in operation, the fuel flow varies such as to ensure that the work supplied by the turbine is always equal to the total load on the shaft. For example, if the turbine efficiency is artificially lowered to simulate deterioration, the fuel flow will increase to raise the TIT and ensure the turbine meets the required load. One such way of achieving this is to again make use of the gradient descent algorithm. Rather than varying the turbine efficiency to reduce the error in the calculated and measured EGT, as was done in fitting the BBM to the test cell data, gradient descent may be used to continuously vary the fuel flow

such that a net-zero work balance on the shaft is maintained. This error is quantified in a cost function as defined in (15) below. By varying the fuel flow to minimise this function, the desired effect of generating performance data that is characteristic of a 331-500 with a deteriorating turbine is achieved.

$$J = \left(1 - \frac{\dot{W}_t}{\dot{W}_c + \dot{W}_{lc} + \dot{W}_{gen}}\right)^2 \tag{15}$$

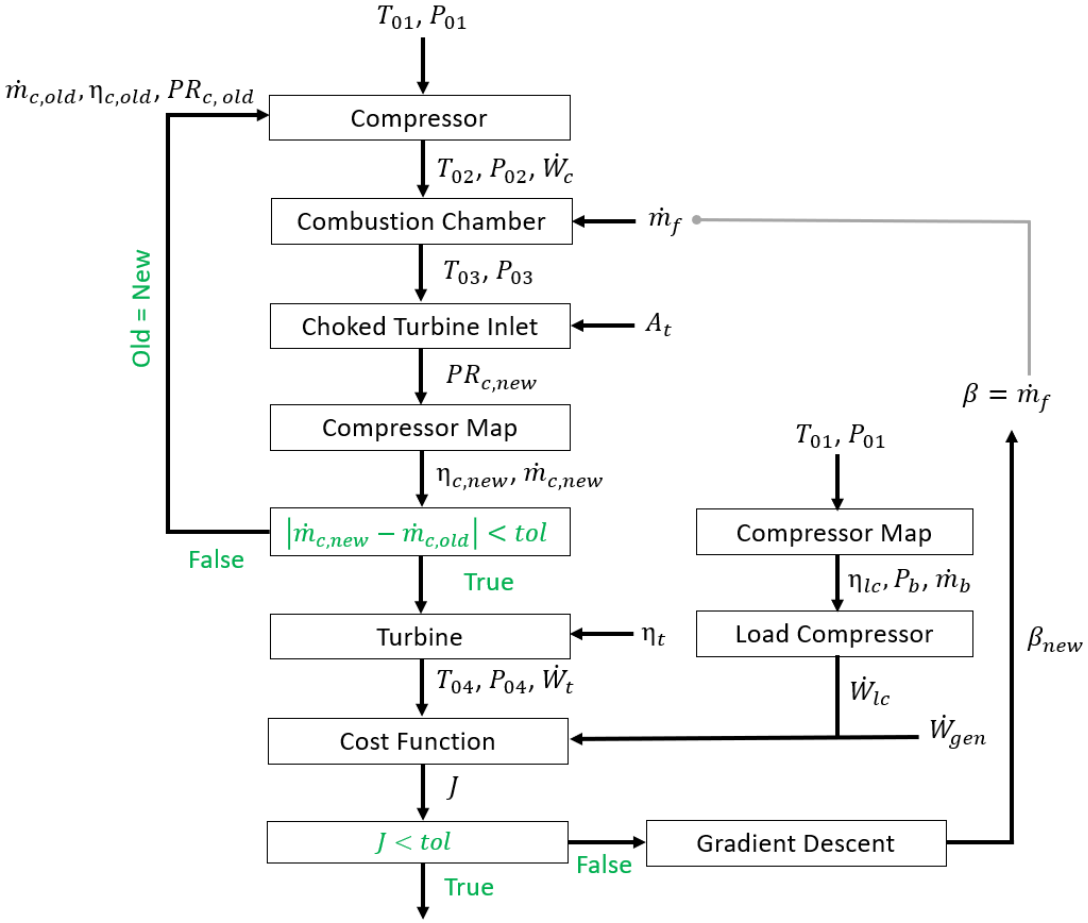

Figure 6.3: Calculation process for generating deterioration data using the WBM. The fuel flow is adjusted until a net-zero work balance on the shaft is achieved.

6.3 Adapting the Turbine Efficiency to the Deterioration Data

The process of adapting the turbine efficiency to minimise the error between the 500TM and the generated performance data is shown below in Figure 6.4. As a compressor map is now used to determine the compressor mass flow, rather than the energy balance equation,

a net-zero work balance on the shaft should be enforced to ensure the model is behaving as a real 331-500 in operation. As was done in the WBM cost function above, a term that represents the error between the turbine work and total load on the shaft is added to the cost function of the 500TM. By minimising the cost function, defined in (16) below, the gradient descent algorithm will minimise both the error between the measured and calculated EGT and the error in the shaft work balance.

$$J = \left(1 - \frac{T_{04}}{EGT}\right)^2 + \left(1 - \frac{\dot{W}_t}{\dot{W}_c + \dot{W}_{lc} + \dot{W}_{gen}}\right)^2 \tag{16}$$

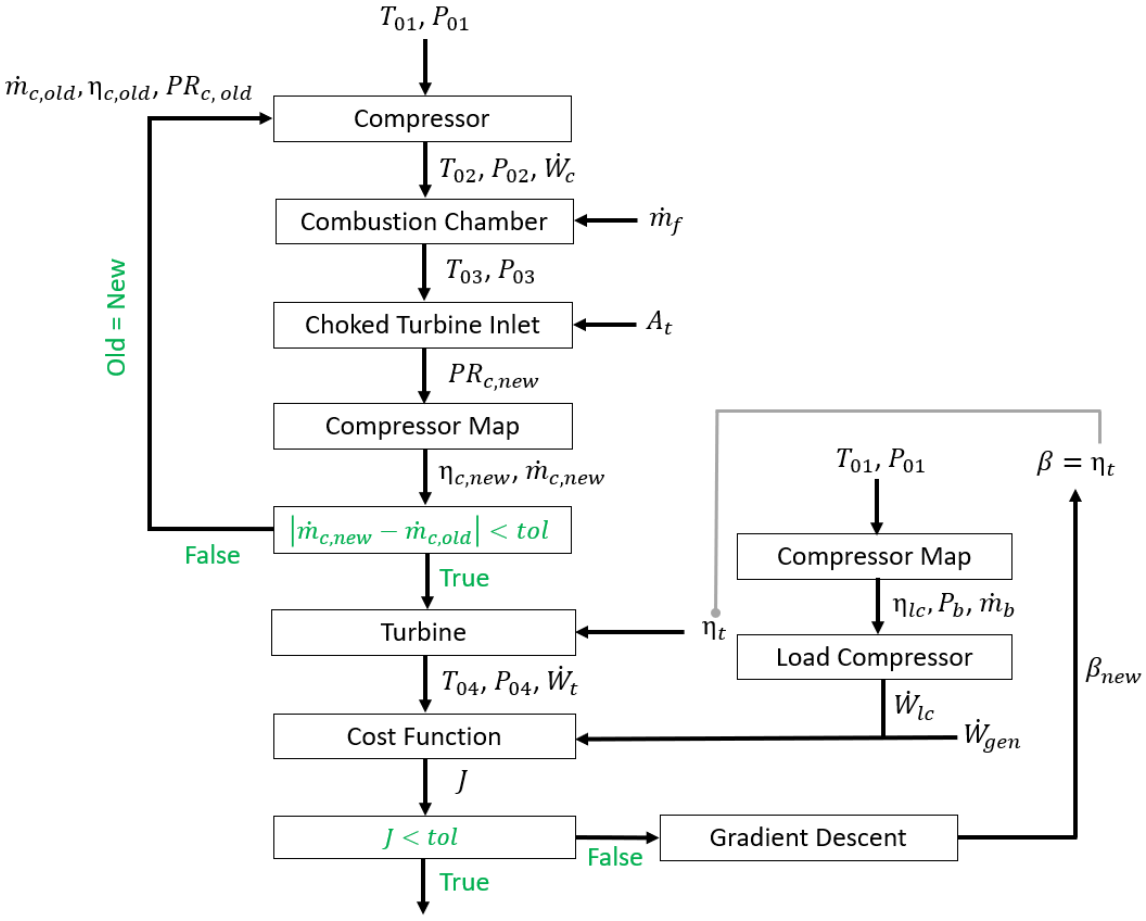

Figure 6.4: Calculation process for adapting the turbine efficiency to minimise the error between the 500TM and the generated performance data.

6.4 Sensitivity Analysis on Model Inputs

Now that a model is available to generate deterioration data for the 331-500, it may be used to conduct a sensitivity analysis on the adaptive modelling process of the 500TM. In generating the deterioration data, the turbine efficiency is varied arbitrarily from its healthy value of approximately 76% to a value of 72%. This decrease is done over a course of 3000 discrete data points with each point representing a MES cycle. As shown in Figure 6.5, the ambient temperature is varied sinusoidally between 278-298 K to further enforce off-design behaviour of the compressor. If there is no input noise in the model, or error in the compressor efficiency and turbine throat area, the adaptive modelling process will compute the turbine efficiency exactly. This is shown in Figure 6.6 below along with the gradient descent's increase of the fuel flow to counter the reduction in turbine efficiency and maintain a net-zero work balance on the shaft. The effect of sensor noise in the input data on the adaptive modelling process, as well as the effect of any error in the compressor efficiency or throat area, is discussed in the following subsections.

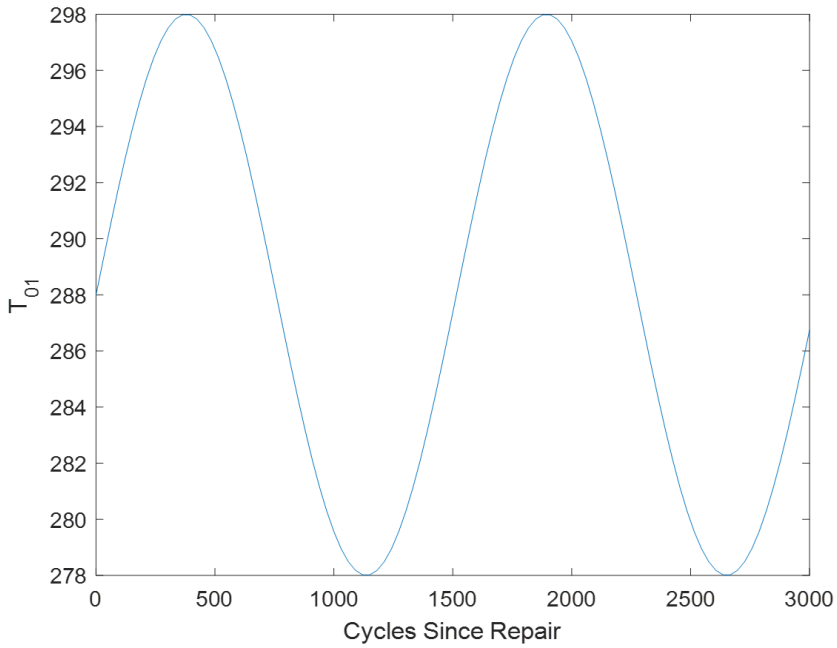

Figure 6.5: Variance of the ambient temperature between 298K and 278K for the generated deterioration data.

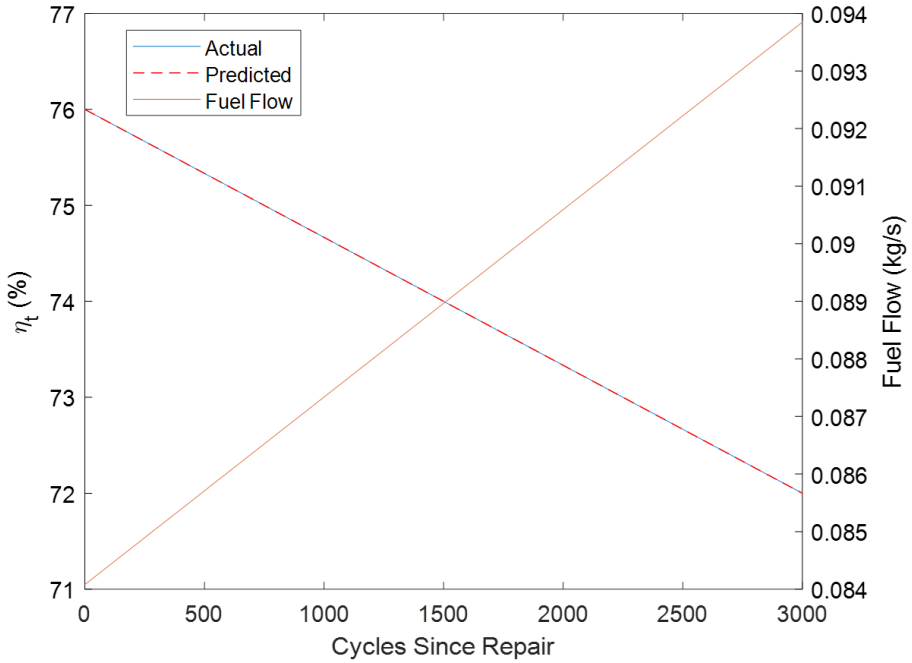

Figure 6.6: Actual (WBM) and predicted (500TM) turbine efficiency using the gradient descent algorithm with no input noise and exact compressor efficiency and turbine throat area.

6.4.1 Compressor Efficiency

Assuming a constant efficiency for off-design analysis, such as the value for the design efficiency, will lead to fluctuations in the predicted turbine efficiency. These fluctuations will correspond to the fluctuating ambient conditions. Additionally, any error in the constant value chosen for the compressor efficiency will shift the predicted turbine efficiency away from its actual value. A lower-than-actual compressor efficiency will result in a higher-than-actual turbine efficiency, and vice versa.

In the generated data, the design point compressor efficiency is 75% and its value is varied with off-design operation using a compressor map while the adaptive modelling of the 500TM is done with constant efficiencies of 70%, 75% and 80%. The resulting effect is shown in Figure 6.7 below. As expected, the fluctuations in turbine efficiency are present and an incorrect compressor efficiency causes the predicted value to shift away from its actual value. However, the trend in turbine deterioration is the same across all cases.

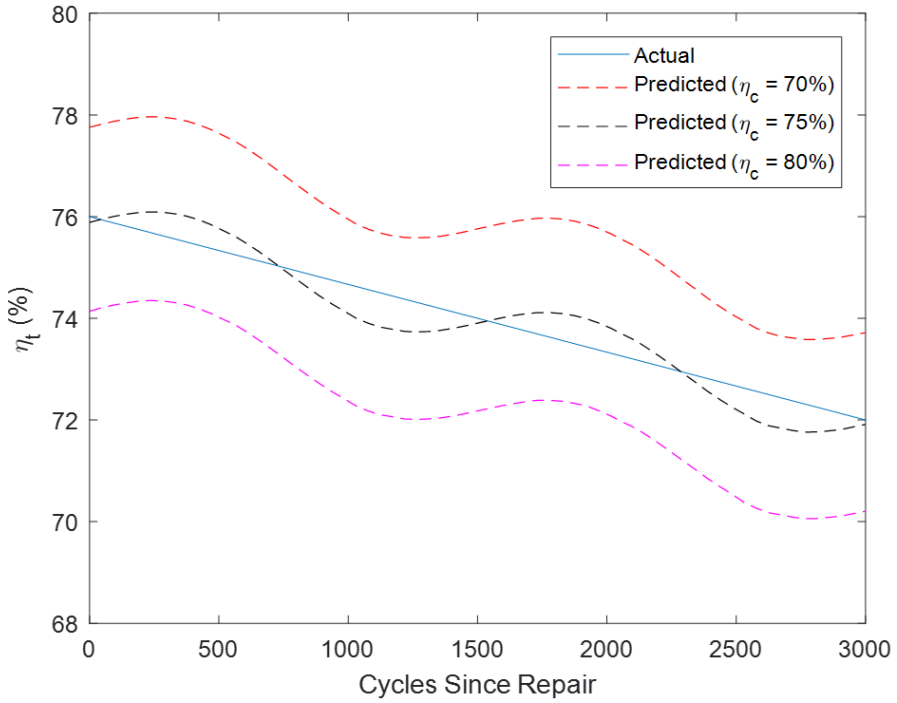

Figure 6.7: Actual (WBM) and predicted (500TM) turbine efficiency using the gradient descent algorithm when various constant compressor efficiencies are assumed for the 500TM. The actual WBM data has a design point efficiency of 75% and varies via a compressor map.

6.4.2 Turbine Throat Area

As with the compressor efficiency, the effect of an error in the turbine throat area calculation is shown below in Figure 6.8. The actual value for the performance data is 4000 mm^2 while values of ±10% are also analysed. A lower-than-actual throat area results in a lower-than-actual turbine efficiency and vice versa. Again, the trend in deterioration is similar across all cases.

As the turbine deteriorates, the first stage NGV will lose material. This loss in material will lead to a reduction in the turbine inlet pressure, as defined in the choked turbine inlet equation, thereby causing an increase in compressor mass flow and a reduction in turbine performance. To counter this loss in PR, the controller on the APU will increase the fuel flow to further raise the TIT thereby accelerating turbine deterioration. Since the 500TM assumes a constant throat area of 4000 mm^2, this will lead to an error in the turbine efficiency prediction. To investigate the effect, the WBM was modified such that the turbine throat area linearly increases by 25%, from 4000 mm^2 to 5000 mm^2, over the course of the turbine deterioration. As shown in Figure 6.9, there is a significant error between the predicted and

actual turbine efficiency. By assuming a constant throat area, the deterioration in the NGV will lead to an under-prediction of the NGV. At the final data point, a 25% error in the throat area leads to a 6% error in the turbine efficiency prediction.

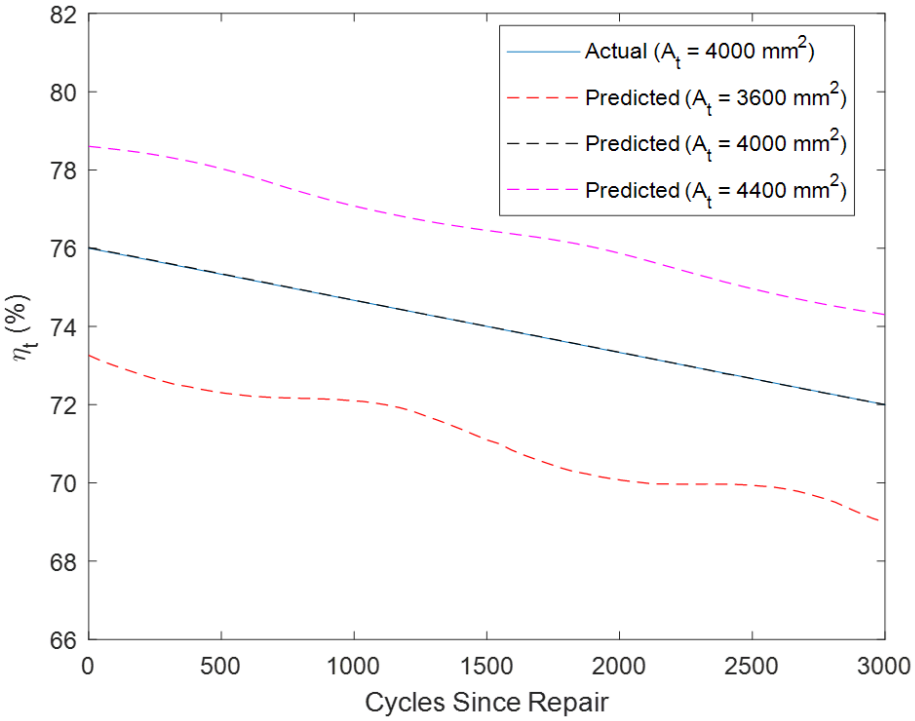

Figure 6.8: Actual (WBM) and predicted (500TM) turbine efficiency using the gradient descent algorithm when various constant throat areas are assumed for the 500TM.

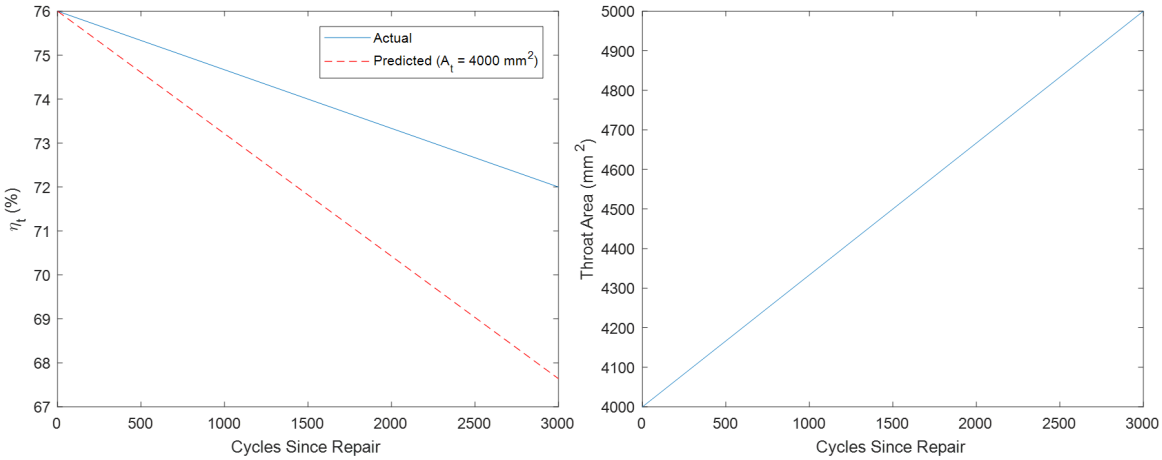

Figure 6.9: Actual (WBM) and predicted (500TM) turbine efficiency using the gradient descent algorithm when a constant throat area is assumed in the 500TM yet it is increasing in the WBM due to deterioration.

6.4.3 Input Parameters

With the remaining six input parameters for the thermodynamic model, artificial noise of ±2% is added to each and the individual effect on the turbine efficiency prediction is determined. The effect of the combination of noise from all six parameters is also determined. Based on a discussion with Mr. Kaj Rook, an APU engineer at EPCOR, the on-wing sensors for measuring the performance of the 331-500 are expected to have an error of ±1% however ±2% is used to provide a margin of safety. Results are shown in Figures 6.10 to 6.13.

It is evident that the most sensitive parameters to the adaptive modelling process are the ambient temperature and the EGT with a resultant error range in the turbine efficiency of ±1.03% and ±0.74% respectively. This is to be expected as the ambient temperature has a large effect on the performance of a gas turbine which is represented numerically through its use in computing the efficiency, mass flow and PR of both compressors as well as in the load calculation of both of these components. The EGT is directly used as one of the terms in the cost function as well as affecting the load output of the turbine hence it will also have a major effect on determining the adapted turbine efficiency.

The generator load makes up approximately 5% of the total load on the shaft therefore it has a marginal effect on the turbine efficiency calculation. On the other hand, the load compressor contributes to approximately 20% of the total load therefore the outlet (bleed) pressure will have a larger impact.

The results of this sensitivity analysis suggest that the major contributors to any noise that is present in the results of the on-wing analysis will be the ambient temperature and EGT measurements.

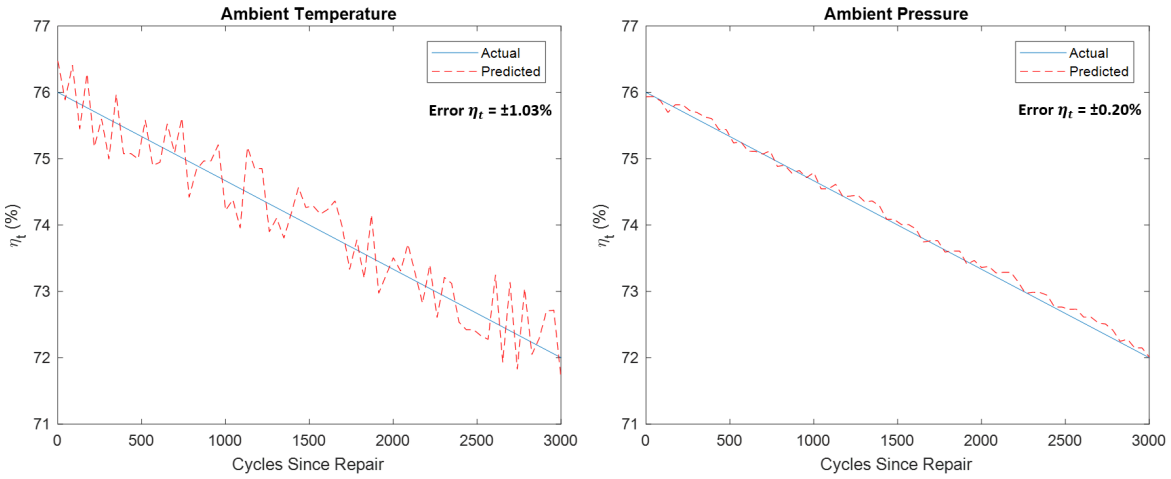

Figure 6.10: Actual (WBM) and predicted (500TM) turbine efficiency using the gradient descent algorithm when artificial noise of ±2% is added to ambient temperature and ambient pressure input.

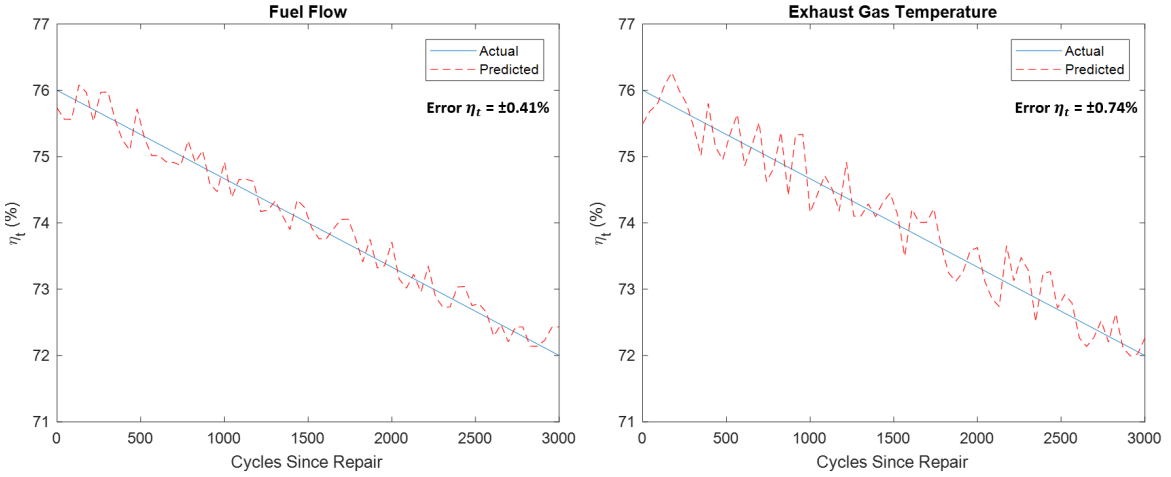

Figure 6.11: Actual (WBM) and predicted (500TM) turbine efficiency using the gradient descent algorithm when artificial noise of ±2% is added to fuel flow and EGT input.

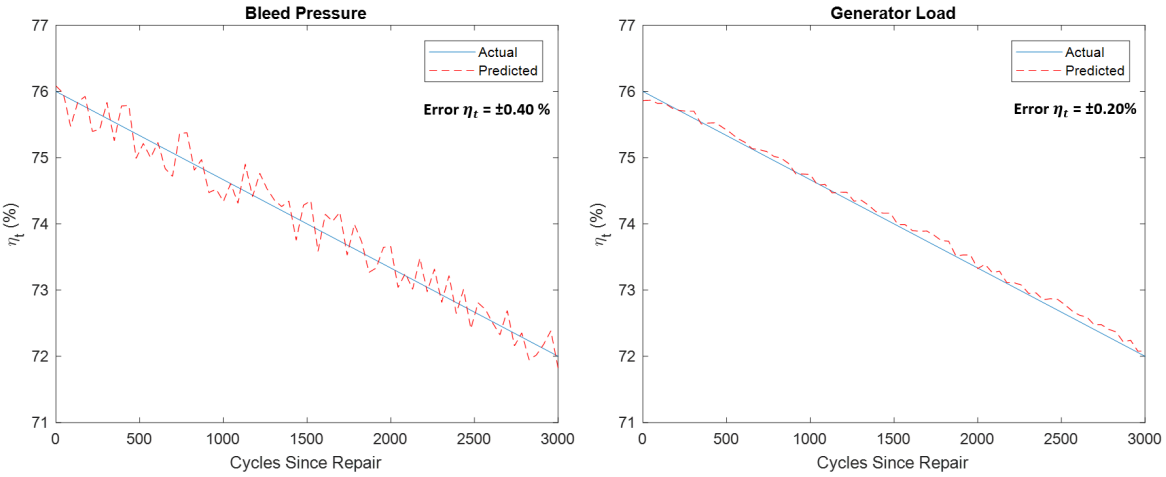

Figure 6.12: Actual (WBM) and predicted (500TM) turbine efficiency using the gradient descent algorithm when artificial noise of ±2% is added to bleed pressure and generator load input.

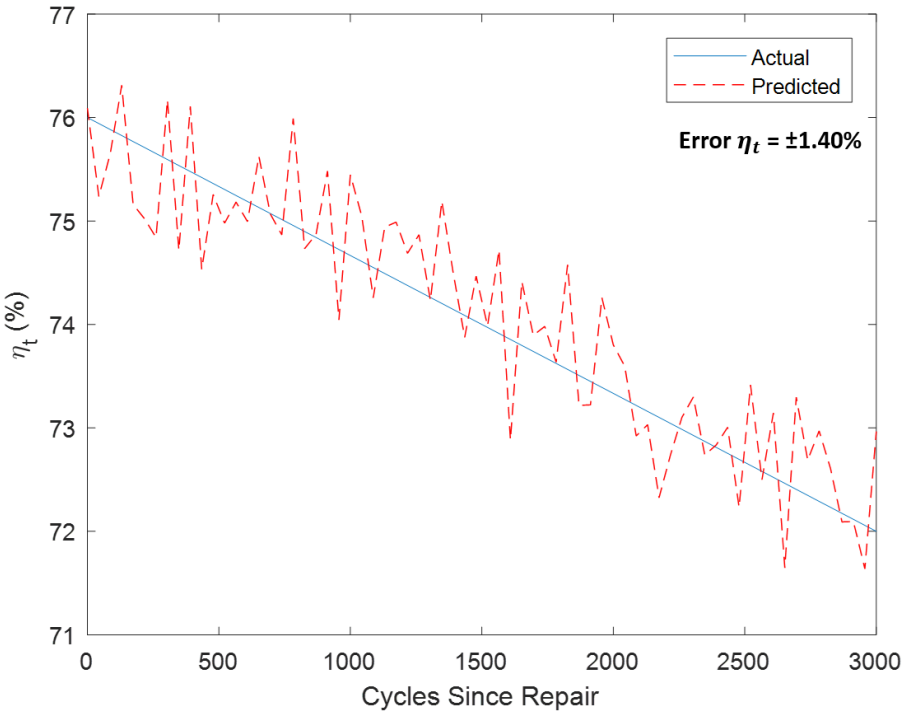

Figure 6.13: Actual (WBM) and predicted (500TM) turbine efficiency using the gradient descent algorithm when artificial noise of ±2% is added to all six input parameters.

7 Analysis of Historical On-wing Data

Once the adaptive modelling process has been tested on the generated deterioration data, it may now be used to conduct GPA on the real performance data of on-wing APUs. As mentioned, the hypothesis of this study is to investigate whether or not GPA can be used as an effective measure to predict first stage turbine blade failure of the 331-500. But, to effectively predict the future failure of an APU, historical failure and deterioration data must first be analysed so that identifiers, in the form of trends in the output data, can be determined and then utilised to monitor APUs in operation.

In the analysis of the historical data, inputs in the form of on-wing sensor measurements are fed into the 500TM before the turbine efficiency is adapted to reduce the error between the model and reality. It was originally planned that the calculation process of the model would be identical to that used in the analysis of the WBM-generated data (Figure 6.4) however, due to the non-physical behaviour of the model when using the compressor map to estimate the compressor mass flow, the process had to be changed. This is described in section 7.3 below. Before that, limitations in the amount of available data including the number of APUs and on-wing parameters are discussed.

7.1 Number of APUs and the Timescale of the Data

It is advantageous to analyse historical failure data over the entire life cycle of an APU i.e. from its repair to its failure. Having the full life cycle performance data for a 331-500, which can include up to 10000 MES cycles, allows the entire deterioration history of the machine's turbine to be analysed which makes it more easy to identify any trends.

Of the twenty-three APUs that have sufferred T1 blade failures since EPCOR began its MRO services on APUs, historical data for analysis is available for only four. Of these four APUs, the maximum number of MES cycles before failure of which data is available is 1979. As this data is insufficient for forming the entire deterioration history of the turbine, performance data at other conditions is also required. These include the performance of healthy APUs and the performance of APUs that have undergone significant deterioration but are not yet at risk of T1 blade failure. Again, due to the limited number of data, only a handful of APUs fit these conditions. These are summarised below in Table 7.1 along with the total number of MES cycles available for each data set. The work order is also included as a reference for the disassembly photos.

To capture the healthy performance of the 331-500, data from five APUs directly after their repair is analysed. For the deteriorated performance, data from six APUs in the lead-up to a removal due to extended run time, known as high time, is analysed. This results in a total of fifteen APUs which are used for the analysis of historical data in this study.

Table 7.1: Number of APUs with available historical performance data in the lead-up to T1 blade failure, high time removal, or directly after repair.

APU No.	Work Order	Data Set	Data Range	No. MES Cycles
1308	102379	T1 Blade Failure	25/03/14 - 07/01/18	1979
1602	102323	T1 Blade Failure	26/03/14 - 27/08/17	1903
1552	102208	T1 Blade Failure	23/03/14 - 17/06/17	1384
1608	102312	T1 Blade Failure	25/03/14 - 10/10/17	1888
1590	101711	High Time Removal	27/03/14 - 15/08/18	1884
1465	102258	High Time Removal	26/03/14 - 12/08/18	1685
1466	102374	High Time Removal	27/03/14 - 17/12/17	1676
1835	102295	High Time Removal	27/03/14 - 17/08/17	1399
1925	102377	High Time Removal	25/03/14 - 21/01/18	1851
1710	102412	High Time Removal	25/03/14 - 18/02/18	1940
1664	101166	Post-repair	16/05/14 - 15/08/18	2083
1642	101585	Post-repair	29/10/15 - 14/08/18	1289
1801	101654	Post-repair	07/11/15 - 14/08/18	1487
1390	101363	Post-repair	09/01/15 - 07/08/18	1530
1509	101183	Post-repair	05/07/14 - 14/08/18	1453

Comparing the performance of different APUs at different conditions, rather than analysing the entire life cycle performance of each APU that has undergone T1 blade failure, will have its limitations. As outlined in equation (4), GPA is designed to relate the performance of a healthy, reference engine to its corresponding unhealthy data by adapting the conditional parameters of the machine. The subsequent delta in the conditional parameter is the deterioration of that component. Since each APU will have different, initial conditions, such as turbine and compressor efficiencies, this delta may be used as a more accurate method for comparing the deterioration of multiple machines. However, the initial turbine efficiency of each of the four T1 blade failures and six high time removals is not known therefore this delta may not be computed. Instead, the results of turbine efficiency in section 8 plot only the absolute

turbine efficiency over the course of the data.

7.2 Number of On-wing Measurements

The on-wing MES measurements used in the 500TM model are listed below. Although not used as an input in the thermodynamic model, another parameter of importance is the TIT that is estimated using the APU controller (APUC). As outlined later, this may be used to compare to the TIT that is predicted by the model.

1. Ambient temperature
2. Ambient Pressure
3. Fuel Flow
4. Load compressor outlet pressure
5. Generator electrical load
6. EGT

Unlike in the test cell, the load compressor outlet temperature and mass flow are not measured on-wing yet both are required for determining the mechanical load of the load compressor. To account for this, a scaled compressor map is used to determine the component's efficiency which, with the known PR, is used to calculate the outlet temperature of the machine. As for the mass flow of the load compressor, a 331-500 test manual supplied by Honeywell states that the component should supply a discharge corrected air flow of 104-108 lb/min (0.786-0.816 kg/s) during MES [16]. The discharge corrected air flow W is defined in (17) below and, from the MES test cell results, a mean value of 106 lb/min was determined. By assuming that the corrected flow is also 106 lb/min for every on-wing MES cycle, the real load compressor mass flow may then be determined.

$$W = \frac{\dot{m}\sqrt{\frac{T_o}{288.15}}}{\frac{P_o}{1.01325}} \tag{17}$$

Another limitation in the availability of on-wing measurements is that the generator electrical load, and not the mechanical load, is measured on-wing. To determine the mechanical load, the component's power factor and mechanical efficiency are required. In the test manual, multiple generator electrical loads are listed with their corresponding shaft mechanical loads thereby allowing a relation between the efficiency and loading to be determined. But, the turbine efficiency is relatively unaffected by the generator load therefore it was decided to

use an average mechanical efficiency of 87.8% for the component. The power factor of the generator is listed as 1.0 in the manual.

7.3 Determining the On-wing Compressor Mass Flow

During the test cell analysis, the compressor mass flow was estimated using a power section energy balance as defined in (13). The objective of this analysis was to use the mean mass flow, PR and efficiency as the design point conditions to which the compressor map from GSP would be scaled to. Then, during the on-wing analysis, it was aimed to solely use the compressor map to determine the mass flow rather than relying on the energy balance equation which was expected to be sensitive to on-wing sensor noise.

However, when analysing the on-wing performance data using the compressor map, the results were largely non-physical. For all of the APUs that were analysed, the turbine efficiency was very noisy. Furthermore, the turbine efficiency was increasing in some of the high time removal data. When the analysis was repeated with the energy balance used to estimate the compressor mass flow, the results were physical and far smoother. For example, Figures 7.1 and 7.2 below show the deterioration in turbine efficiency for APUs 1308 and 1608, two of the T1 blade failures, as well as 1466 and 1925, two of the high time removals. When the compressor mass flow is estimated using the compressor map, the behaviour is far noisier than that of the energy balance. Furthermore, the efficiency is increasing in the lead-up to removal in APUs 1466 and 1925.

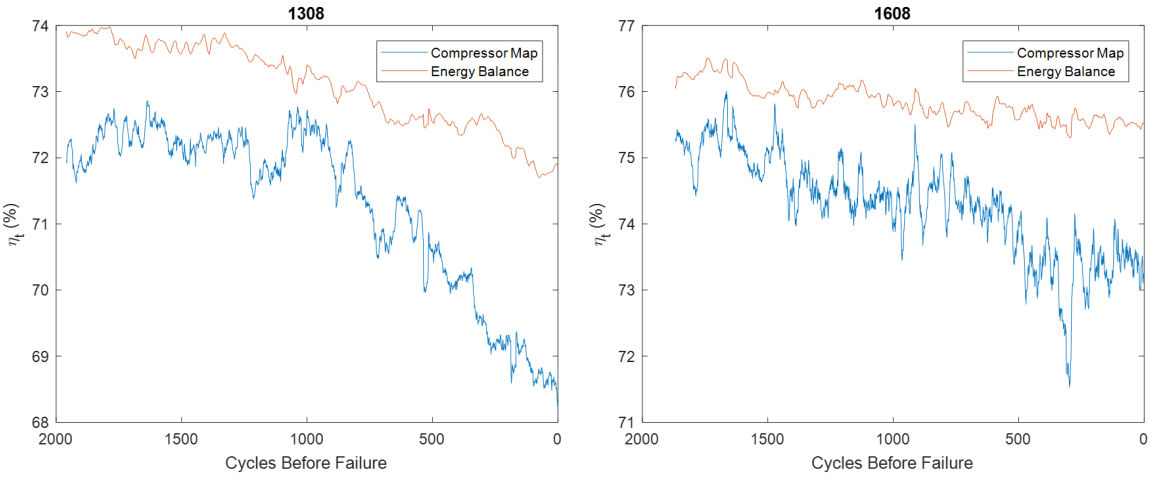

Figure 7.1: Comparison in the turbine efficiency prediction when either the compressor map or power section energy balance is used to estimate the compressor mass flow for APUs 1308 and 1608.

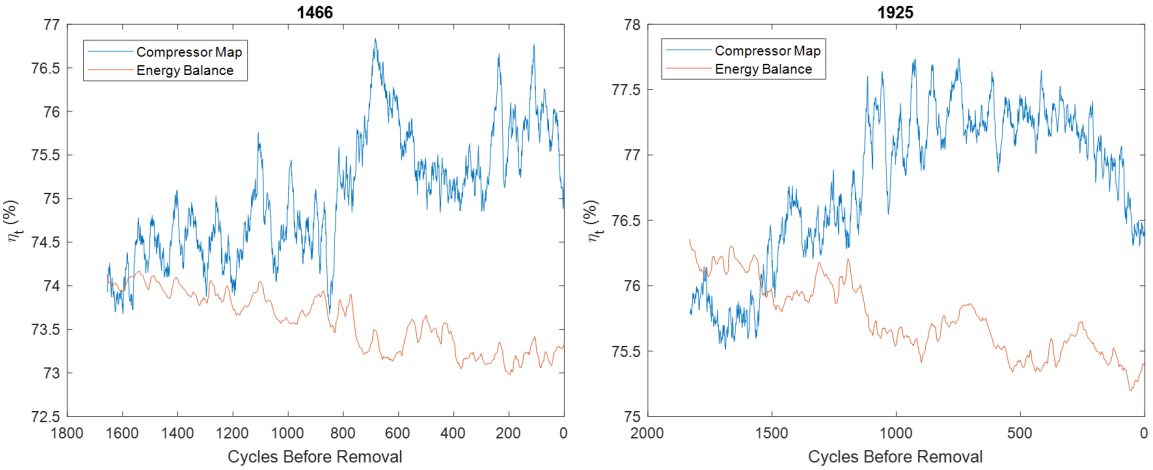

Figure 7.2: Comparison in the turbine efficiency prediction when either the compressor map or power section energy balance is used to estimate the compressor mass flow for APUs 1466 and 1925.

From further investigation, it appears that the reason for this non-physical behaviour is due to the mismatch between both estimated compressor mass flows. As shown in Figure 7.3 below, differences in the values of the mass flow between both the compressor map and energy balance are present in all four of these APUs. Initially, both estimated mass flows match reasonably well yet, in the lead-up to either failure or removal, both estimations begin to deviate from each other. For APUs 1466 and 1925, the energy balance estimates a mass flow that is lower than that of the compressor map while the opposite is true for the two T1 blade failures.

In the two high time removals, the energy balance mass flow is decreasing whereas the compressor map value tends to increase or remain relatively flat. This decrease is to be expected as the compressor will most likely experience fouling thereby leading to a reduction in the energy balance mass flow. However, this is not true of the two T1 blade failures which show an increasing mass flow in both compressor map and energy balance estimations. As discussed in the sensitivity analysis in section 6.4, an increase in the turbine inlet throat area due to deterioration will lead to an increase in the compressor mass flow therefore any fouling effects will be difficult to observe in the the T1 blade failure performance data.

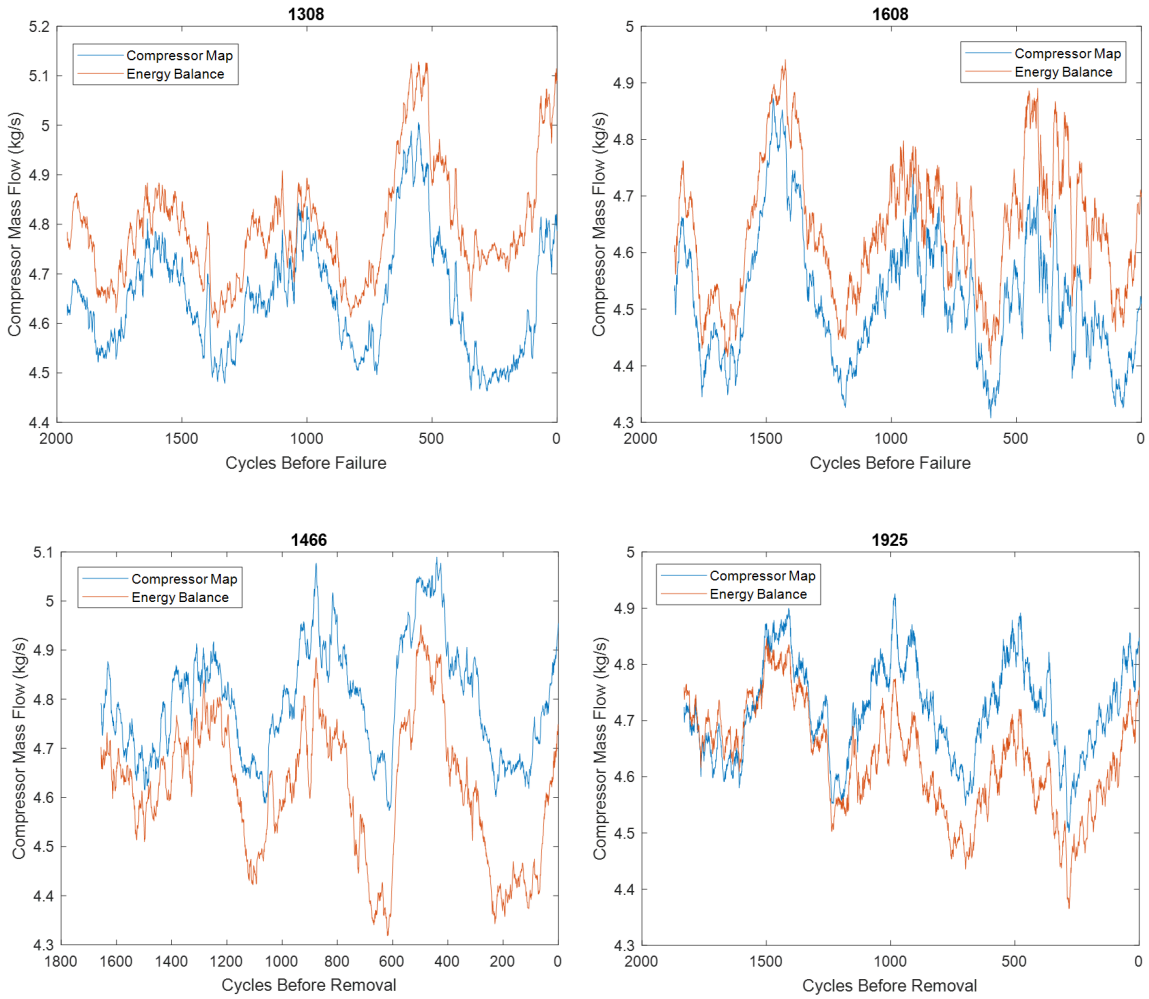

Figure 7.3: Comparison in the compressor mass flow when either the compressor map or power section energy balance is used to estimate its value.

Since the gradient descent algorithm is attempting to minimise both the error between the measured and calculated EGT, as well as maintaining a net-zero shaft work balance, any error between both mass flow estimations is problematic. Looking at Figure 7.4, it is evident that the algorithm is unable to maintain a net-zero work balance on the APU shaft when the compressor map is used to estimate the compressor mass flow. Initially, the error is relatively low in all cases yet begins to increase in the lead-up to either failure or removal. As expected, the point at which the increase in error takes place is at the same point as which the both mass flow estimates begin to deviate. Since the algorithm is also attempting to minimise the second term in the cost function defined in (16), which represents the error between the measured and calculated EGT, it will not be able to do so when the compressor map is used to estimate the mass flow. This is shown in Figure 7.5. On the other hand, since the power

section energy balance automatically enforces a net-zero work balance on the shaft, the EGT may be minimised with ease.

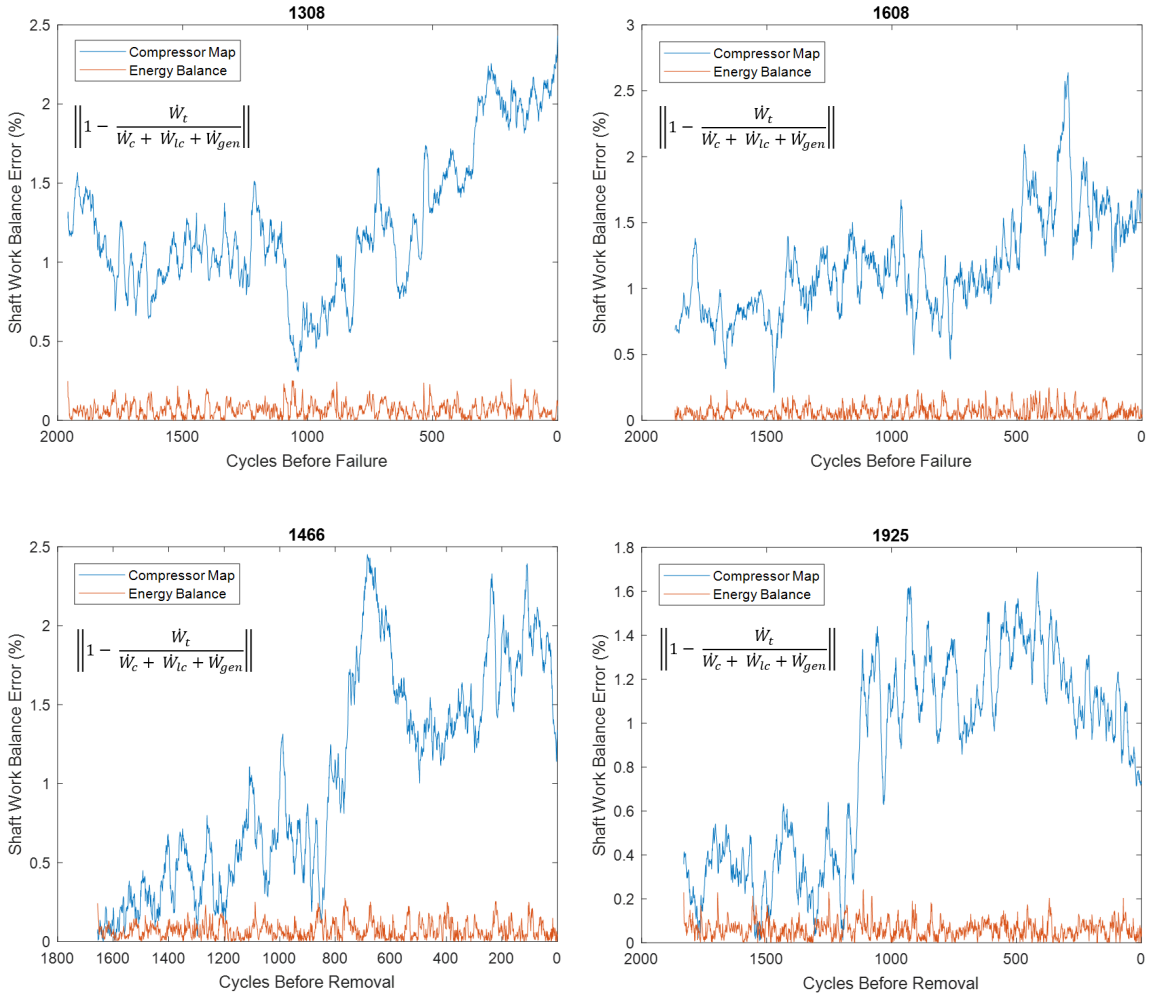

Figure 7.4: Comparison in the error in the net-zero work balance on the shaft when either the compressor map or power section energy balance is used to estimate the compressor mass flow.

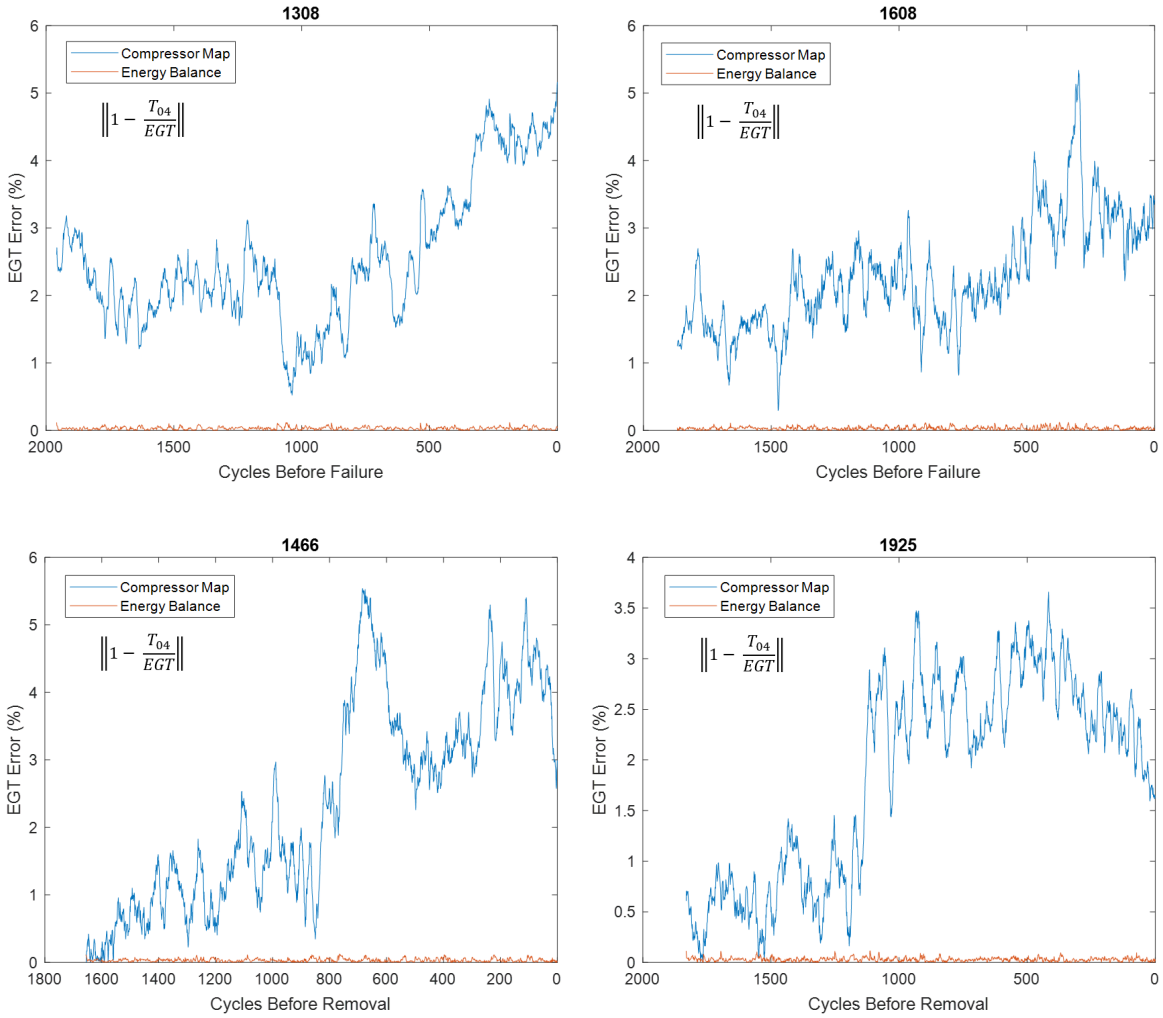

Figure 7.5: Comparison in the error between the measured and calculated EGT when either the compressor map or power section energy balance is used to estimate the compressor mass flow.

This exact behaviour is observed in all of the remaining APUs. In all six of the high time removals, there is a reduction in the mass flow that is determined by the energy balance which leads to a deviation from the compressor map estimation. This deviation is potentially a result of compressor fouling. In the T1 blade failures, both mass flow estimations either increase or stay flat which may be a result of a deteriorating first stage NGV. In either scenario, this deviation results in the gradient descent algorithm being unable to minimise the error in the measured and calculated EGT while also maintaining a net-zero work balance on the shaft. This leads to a non-physical prediction of the turbine efficiency along with significant noise. Therefore, it was decided to continue using the energy balance to estimate the compressor mass flow during on-wing analysis while the compressor map is used to determine only the component's efficiency. The updated calculation process for adapting the turbine efficiency

of the 500TM to the on-wing deterioration data is shown below in Figure 7.6.

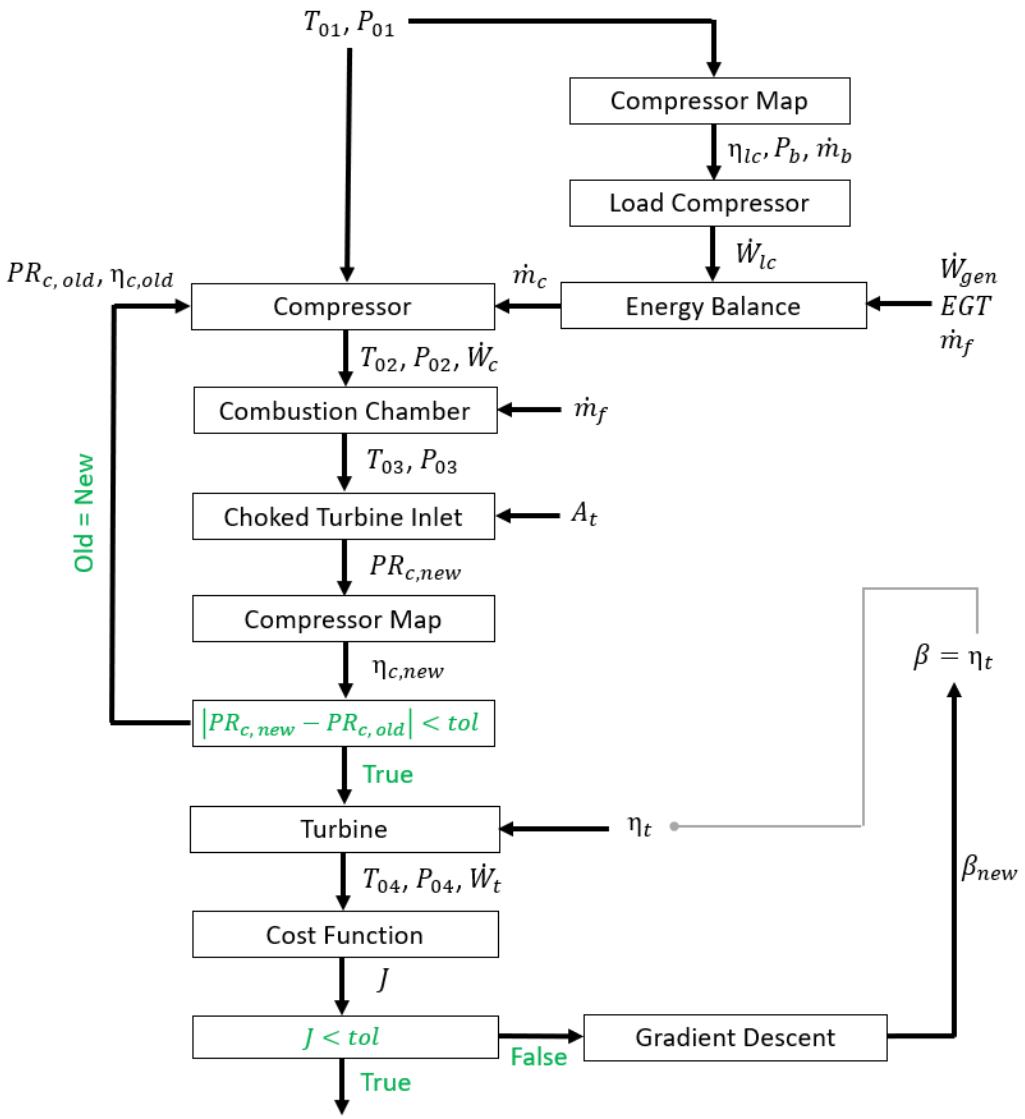

Figure 7.6: Calculation process for adapting the turbine efficiency of the BBM to the 331-500 deterioration data when the power section energy balance is used to estimate the compressor mass flow.

8 Results

The results from the analysis of the performance data of all fifteen APUs are detailed below. As outlined in Table 7.1, these comprise four T1 blade failures, six high time removals and the post-repair performance of another five APUs. In an attempt to smooth the noise of the data, each of the seven inputs are read into the BBM as a twenty-cycle moving average. After testing several numbers for the moving average, twenty was chosen as it was an acceptable balance between removing noise while not smoothing out any visible trends in the deterioration. At the end of this section, a summary of the analysis is included.

8.1 First Stage Turbine Blade Failure Data

The deterioration in the turbine efficiency of the four T1 blade failure APUs, with each APU denoted by its serial number, is plotted in Figure 8.1 below. Directly after, the EGT and fuel flow data of each APU are plotted in Figure 8.2.

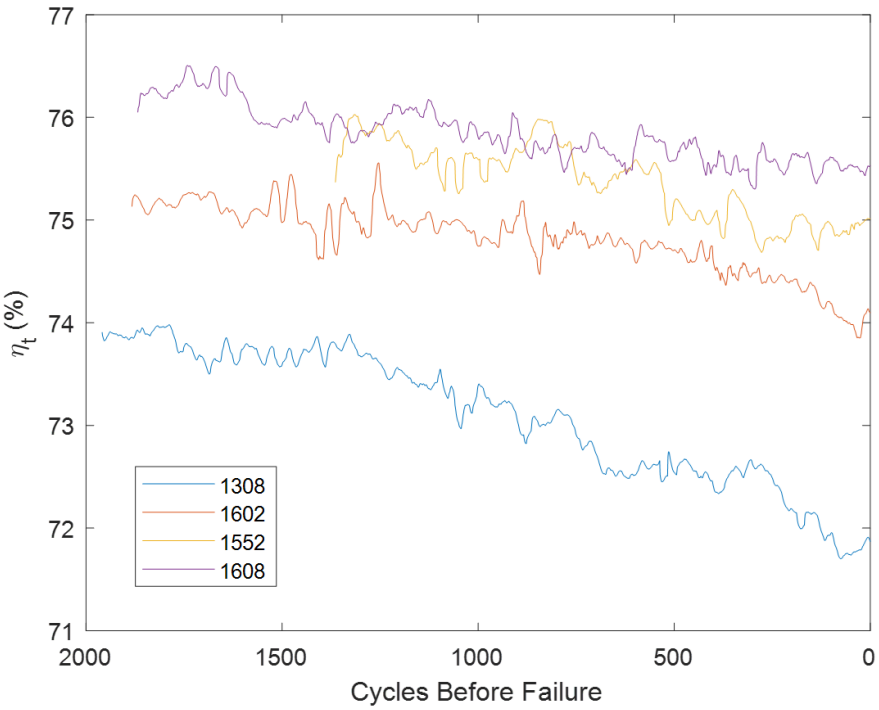

Figure 8.1: Deterioration in turbine efficiency for four 331-500 APUs in the lead-up to failure.

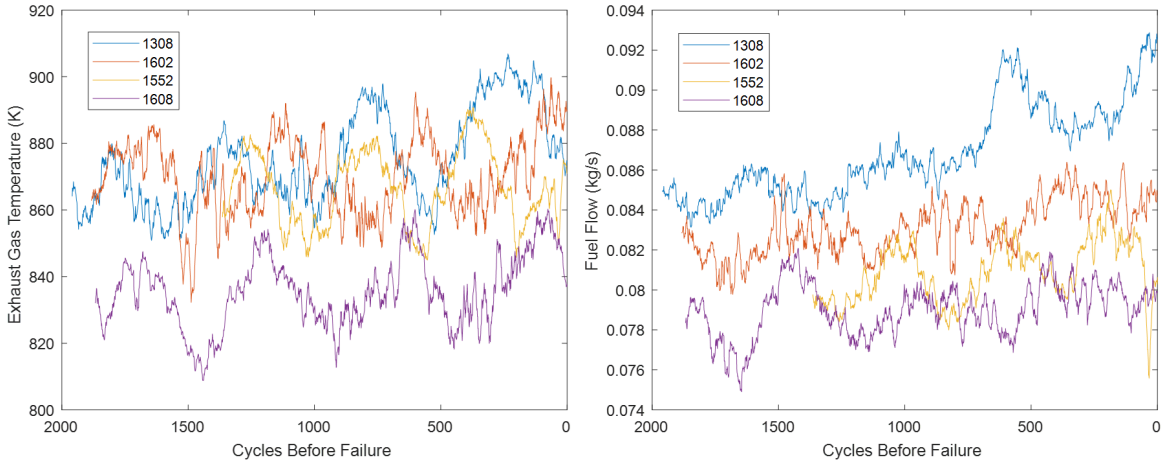

Figure 8.2: Measured EGT and fuel flow data for the four 331-500 APUs in the lead-up to T1 blade failure.

As expected, the turbine efficiency is deteriorating in all four APUs. However, in APUs 1308, 1602, and 1552, the turbine efficiency begins to rapidly deteriorate in the lead-up to failure. In these three APUs, the slope first appears constant and then, ranging between 800-1300 cycles before failure, it becomes increasingly negative which suggests that the performance of the turbine tends to drop off before failure. Contrastingly, this behaviour is not observed in APU 1608 which maintains a relatively constant deterioration rate.

By observing the EGT and fuel flow data, it can seen that it is more difficult to identify any clear trends. Sensor noise and periodic fluctuations, which are due to seasonal ambient conditions, are present. However, it is clear that both the EGT and fuel flow are increasing in the lead-up to failure. This behaviour is expected since any deterioration in turbine performance will result in an increase in fuel flow, hence EGT, to counter the loss in performance and meet the required shaft load. The APU with the lowest turbine efficiency, 1308, is also the APU with the highest fuel flow and EGT. The opposite is true for APU 1608 which has the highest efficiency and lowest values of fuel flow and EGT.

The TIT of the 331-500 is estimated using a controller on the machine (TIT_{apuc}). It is also of interest to compare its value to the TIT that is calculated by the model (T_{03}). This is shown in Figure 8.3. As expected, APU 1308 experiences the largest TIT while 1608 the lowest which is what is expected for the turbines with the lowest and highest efficiencies respectively. The thermodynamic model determines the TIT using an energy balance over the combustion chamber whereas, as listed in the Honeywell training manual, the controller determines the

TIT based only on temperature and pressure sensor measurements with no mention of the fuel flow or generator load [15]. Despite this, the behaviour of both the model and controller estimations are very similar with the shapes of both curves almost identical for each of the APUs below.

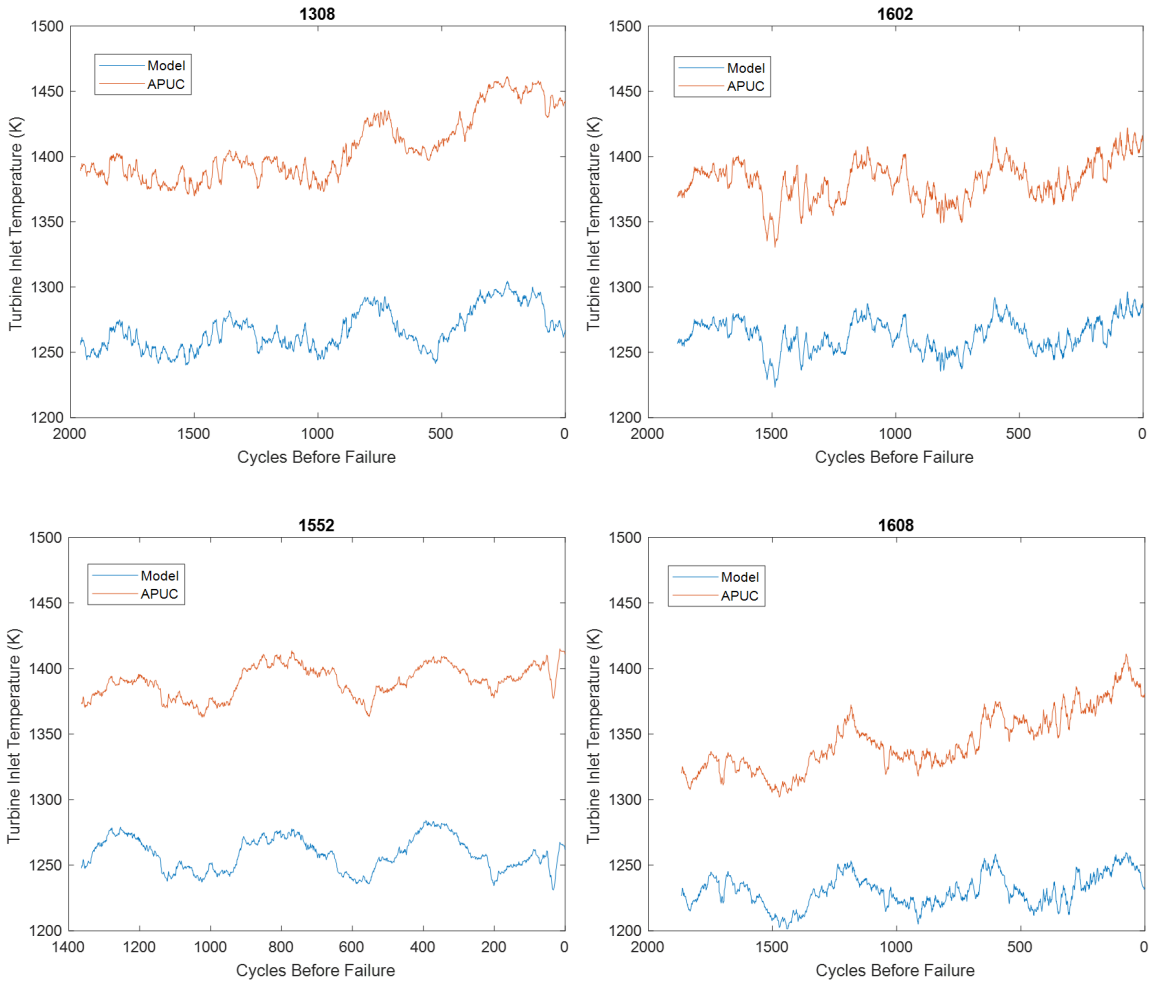

Figure 8.3: Comparison between model- and controller-calculated TIT data for APUs 1308, 1602 1552 and 1608 in the lead-up to T1 blade failure.

Although the shapes of both TIT calculations are very similar, there is a significant delta between both TIT calculations which may be due to a variety of reasons. As many assumptions are made in the building of the 500TM, including both compressor efficiencies and flue gas properties, a mismatch between both TIT calculations is expected. But, it appears that this delta tends to increase as T1 failure approaches. In Figure 8.4 below, the ratio of the controller- to the model-calculated TIT is plotted for all four APUs. With the exception of APU 1602, the ratio tends to increase rapidly in the lead-up to failure. APU 1308, again the APU with both

the lowest value of and most significant drop off in turbine efficiency, has the largest ratio with a value of 1.14, or 14% difference in both TIT estimations, at failure.

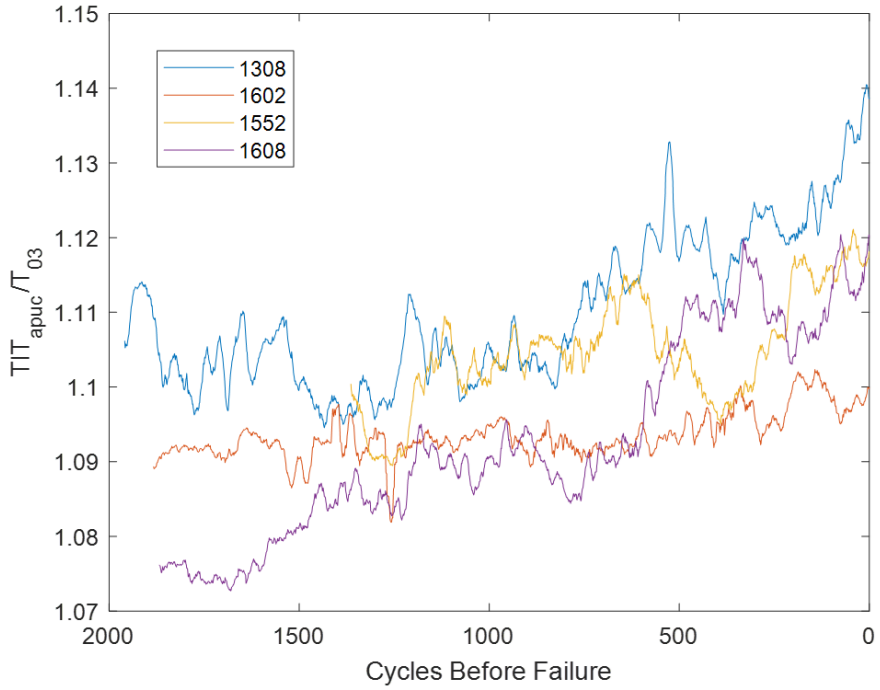

Figure 8.4: Ratio of controller- to model-calculated TIT for the four 331-500 APUs in the lead-up to T1 blade failure.

The cause(s) of the sharp increase in the difference between both TIT measurements in the lead-up to failure is unclear. It is possible that, as the first stage NGV deteriorates, the deviation from the typical turbine performance of the machine will lead to an error in the controller calculation of the TIT. Since the controller most probably determines the TIT based on a relation between the sensor measurements mentioned above, this relation would have been programmed by Honeywell as based on data from healthy 331-500s in operation. As the turbine deteriorates, its performance will also deviate from this typical healthy behaviour thereby weakening any correlation between the sensor measurements and the TIT. A more detailed correlation analysis of the controller and the sensor inputs is conducted in section 8.4.

The loss of NGV material may also be a cause of the sharp decrease in the gradient of the turbine efficiency in the lead-up to failure. As highlighted in Figure 6.9 from the sensitivity analysis, an increase in the turbine inlet throat area will lead to a reduction in PR and a corresponding increase in fuel flow. By assuming a constant throat area of 4000 mm^2, this increase

in throat area will lead to a under-prediction in the turbine efficiency and it may be a cause of the observed behaviour in the gradient. In Figure 8.5 below, the extent of deterioration of the first stage NGV after T1 blade failure is shown.

As mentioned when discussing the failure mechanisms of T1 blade failure in section 2.2, any loss in material in the NGV will result in a reduction in turbine performance and a corresponding increase in fuel flow and TIT. Eventually, a blade will release from the first stage rotor leading to extensive damage.

Figure 8.5: Deterioration in the first stage NGV after T1 blade failure for APUs 1602 (left) and 1552 (right).

Figure 8.6: Deterioration in the first stage NGV after T1 blade failure for APUs 1608 (left) and 1308 (right).

8.2 High Time Removal Data

For five out of the six high time removals, the turbine efficiency and TIT ratio are plotted in the lead-up to removal in Figures 8.7 and 8.8 respectively.

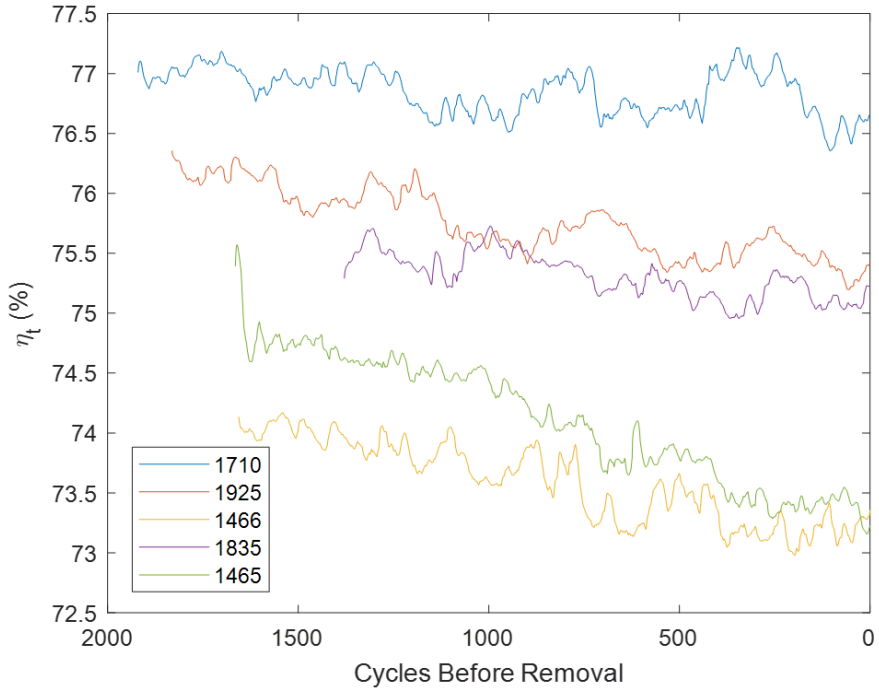

Figure 8.7: Deterioration in turbine efficiency for five 331-500 APUs in the lead-up to removal due to high time.

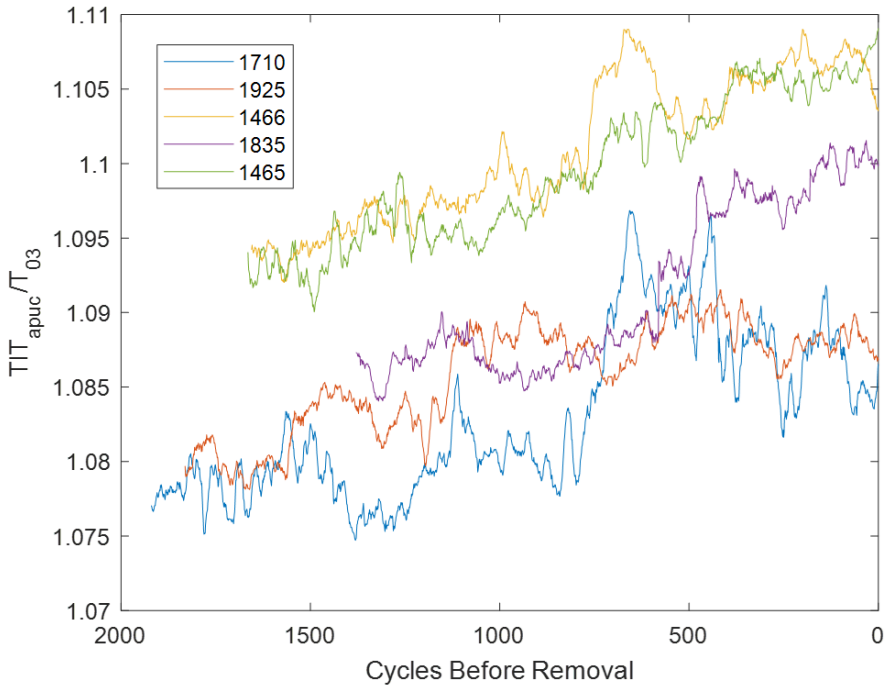

Figure 8.8: Ratio of controller- to model-calculated TIT for five 331-500 APUs in the lead-up to removal due to high time.

The turbine efficiency curves for APUs 1465 and 1466 have the steepest gradient and tend to decrease more rapidly in the final 1000 cycles before removal while the other three APUs have a relatively constant gradient. As expected, the ratio of the controller- to model-calculated TIT is also the largest for these two machines. APU 1710 has the least-steep gradient in its turbine efficiency curve and also has a lower value of the TIT ratio which suggests its condition is better than the other four APUs.

To assess the condition of each APU at removal, disassembly photos of each machine's first stage NGV are observed. These are shown in Figures 8.9 to 8.13 below. Despite some cracking and corrosion, APU 1710 appears to have the best condition with its first stage NGV still relatively intact. APU 1925, the one with the second best condition, shows a significant loss of material in some of its vanes yet the leading edges of all vanes are still intact. This is not the case for the three remaining APUs, particularly 1466 and 1465, which show extensive loss of material with some of the cracks running through entire vanes.

Figure 8.9: Deterioration in the first stage NGV of APU 1710 after removal due to high time.

Figure 8.10: Deterioration in the first stage NGV of APU 1925 after removal due to high time.

Figure 8.11: Deterioration in the first stage NGV of APU 1835 after removal due to high time.

Figure 8.12: Deterioration in the first stage NGV of APU 1465 after removal due to high time

Figure 8.13: Deterioration in the first stage NGV of APU 1466 after removal due to high time.

Comparing these photos to the graphs of turbine efficiency and TIT ratio, it is apparent that there is a relationship between the condition of the first stage NGV, the gradient in turbine efficiency and ratio of the controller- to model-calculated TIT for every MES cycle of a 331-500. A steeper gradient and higher TIT ratio suggests that the turbine is more deteriorated than a machine with a flatter gradient and lower ratio. APUs 1465 and 1466 show the steepest gradients in efficiency and the largest TIT ratio while also showing extensive deterioration. The gradient in the turbine efficiency of APUs 1835 and 1925 are relatively similar while the TIT ratio of 1835 is larger which may explain why its NGV is more deteriorated. In contrast, APU 1710 has the flattest gradient, lowest TIT ratio and the best condition.

Lastly, to show the effect of a repair on the turbine efficiency and TIT ratio, the performance data from the sixth and final high time removal in the lead-up to removal and directly after the subsequent repair is analysed. Results are plotted in Figures 8.14 and 8.15 below.

As expected, the turbine efficiency will increase directly after repair. Similarly, the TIT ratio will decrease as the differences between the model and APUC become smaller as the turbine is now operating as expected without any material loss in the first stage NGV. After repair, the TIT ratio continues to drop before stabilising at a value below that of a deteriorated machine. A similar effect is observed in the turbine efficiency and is also present in the results of the five post-repair APUs in the following subsection.

It is also noteworthy that the TIT ratio is very large in the lead-up to the removal with an almost 16% difference in both calculations of TIT at removal. Similarly, although difficult to observe with the limited data points, the gradient in the turbine efficiency is also largely

negative. Both of these observations suggest that the turbine is very deteriorated. Looking at the disassembly photos of the first stage NGV in Figure 8.16, this component has indeed undergone severe deterioration with much of the first stage NGV material missing. Again, this suggests that there is a relationship between the TIT ratio and the gradient of the turbine efficiency. This will be discussed in more detail in the summary at the end of this section.

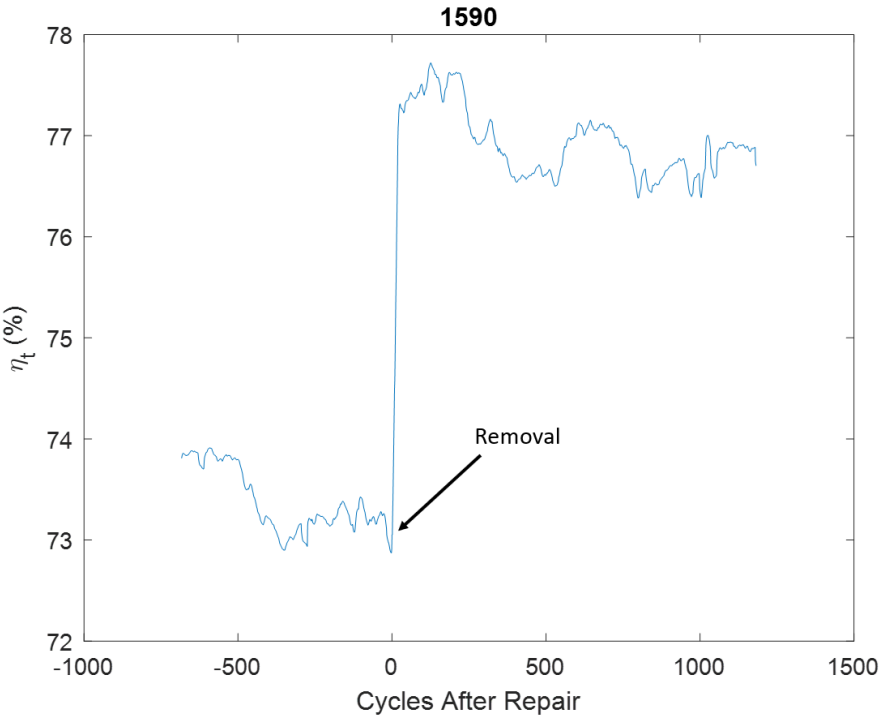

Figure 8.14: Deterioration in turbine efficiency for APU 1590 in the lead-up to removal and directly after repair.

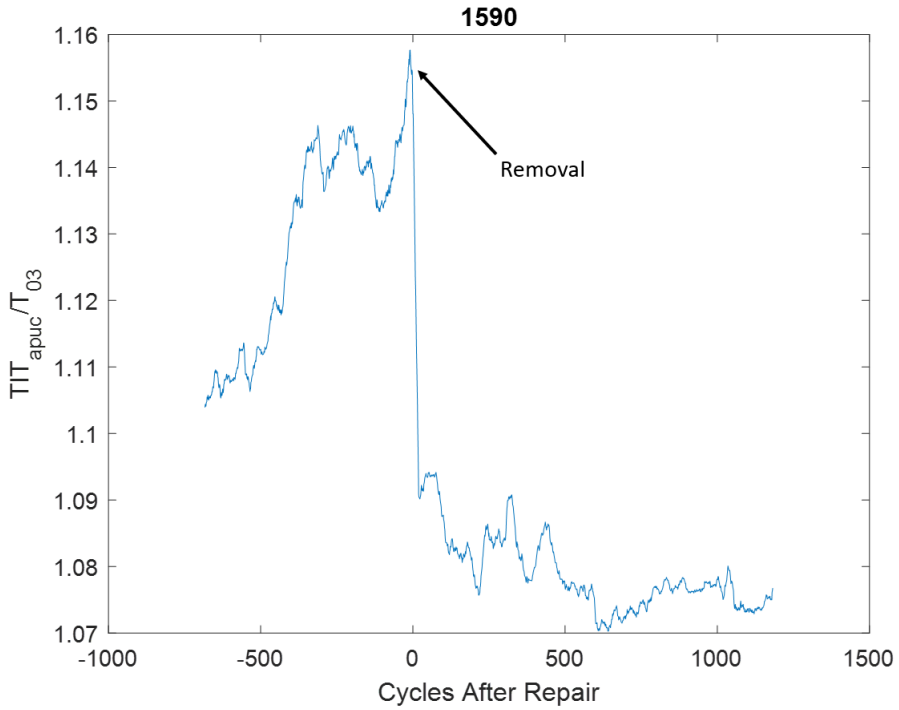

Figure 8.15: Ratio of controller- to model-calculated TIT for APU 1590 in the lead-up to removal and directly after repair.

Figure 8.16: Deterioration in the first stage NGV of APU 1590 after removal due to high time.

8.3 Post-repair Data

In Figures 8.17 and 8.18 below, the turbine efficiency and TIT ratio is plotted for five APUs directly after repair. For the first 300-500 MES cycles, the efficiency tends to decrease rapidly before stabilising and remaining relatively constant. A similar behaviour is observed in Figure 8.18 where the TIT ratio for each APU, with the exception of 1642, tends to decreases rapidly

from a relatively large value. One possible reason for this is the wear-in of the machine. As with any gas turbine, performance directly after manufacture or repair will be affected by wear/rub-in of components such as the seals [8]. Since this behaviour is not accounted for in the model, non-physical behaviour will occur until the machine begins to operate as expected. After this, the gradient of the turbine efficiency begins to flatten which is what is expected for the performance of a healthy APU. Similarly, the value of the TIT ratio for every APU is below that of the deteriorated machines that were analysed previously.

However, once the gradient has flattened, there is a significant variance in the value of the turbine efficiency for each APU. As calculated from the test cell analysis, an average healthy turbine efficiency is expected to be approximately 76%. At the final data point, the efficiency of these post-repair APUs ranges between 78.5% and 74.8%. As discussed in section 6.4.1, the choice of compressor efficiency for the model will have an effect on the turbine efficiency. Additionally, installation and build effects will also impact on this level of variance [8].

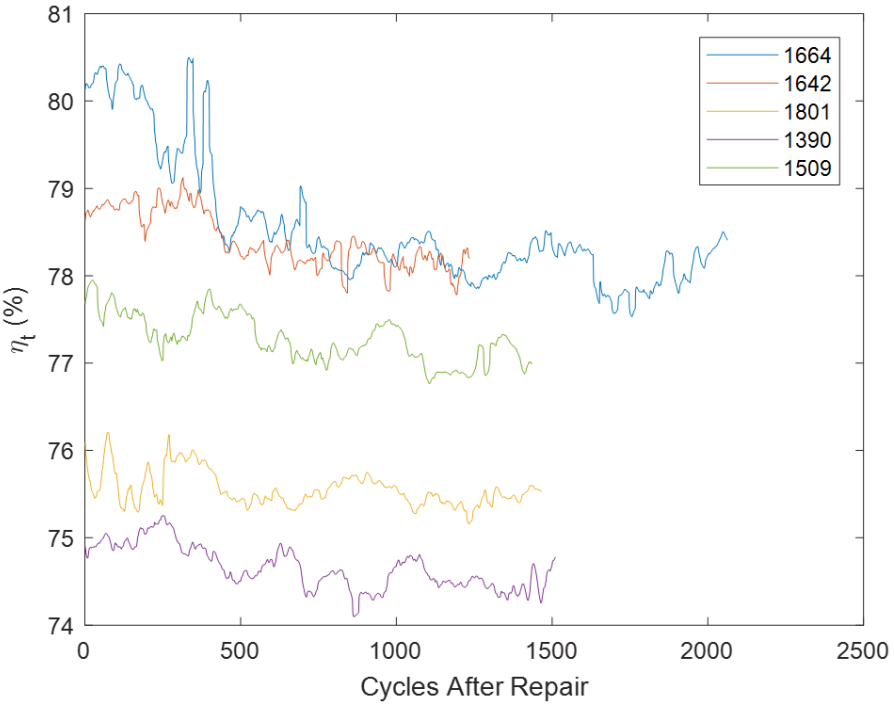

Figure 8.17: Deterioration in turbine efficiency for five 331-500 APUs directly after repair

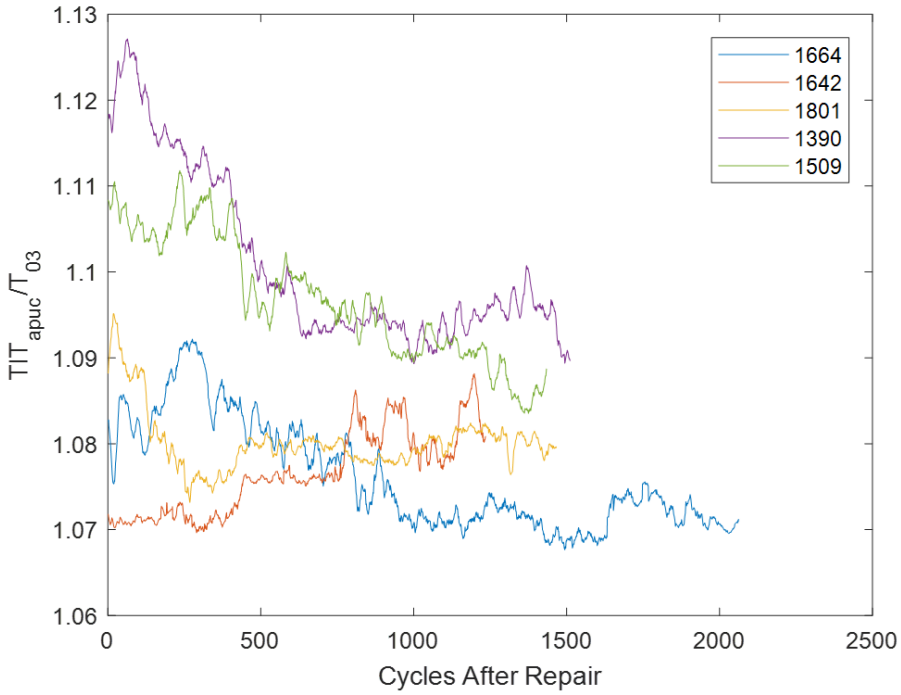

Figure 8.18: Ratio of controller- to model-calculated TIT for five 331-500 APUs directly after repair.

8.4 TIT and Sensor Data Correlation

In the Honeywell training manual for the 331-500, it lists that the APUC determines the TIT based only on sensor measurements of the EGT, load compressor outlet pressure, and ambient temperature and pressure with no mention of the fuel flow or generator load. This suggests that the controller estimates the TIT based on a preprogrammed relation between itself and the input variables. To investigate this, a correlation coefficient (R) for each input variable is calculated. This is done for all four T1 blade failures and the first five high time removals that were analysed above. To investigate the effect of the heavily deteriorated T1 blade failure data on the correlation, the coefficients are calculated when the high time removal and T1 blade failure data are analysed on their own as well as when both data sets are included together for analysis. The results of the mean correlation coefficient are shown in Table 8.1 below.

Table 8.1: Range of determined correlation coefficients between each APUC input variable and the controller-calculated TIT for the T1 blade failure and high time removal data sets.

Input Variable	$\overline{R}$ (T1)	$\overline{R}$ (High Time)	$\overline{R}$ (T1 & High Time)
EGT	0.843	0.957	0.906
Ambient Temperature	0.630	0.673	0.654
Ambient Pressure	-0.369	-0.117	-0.229
Bleed Pressure	-0.537	-0.487	-0.509

The EGT and ambient temperature are most strongly correlated to the controller-calculated TIT while the load compressor pressure has almost no correlation. For the EGT and ambient temperature, the T1 blade failure data has a lower level of correlation than the high time removals which suggests that the heavy deterioration of the turbine results in an error in the APUC calculation. This is not surprising since a rapid increase in the ratio of both the controller- and model-calculated TIT was observed in the T1 failure data above indicating a deviation between the model and controller which is most likely due to deterioration.

To determine a relation between the ambient temperature, EGT and TIT, a non-linear equation of the form defined in (18) is fitted to the data with coefficients provided in Table 8.2. To further investigate the effect of the T1 blade failure on the correlation, this is completed for both the T1 blade failure and high time removal data together as well as the high time removal data on its own. When analysing only the high time removals, the resulting root mean squared error and correlation between the equation and the data is 3% and 0.996 respectively. When including the T1 blade failures in the data, the error and correlation worsens to 10% and 0.906 respectively. Including the ambient and load compressor outlet pressures in the equation adds further complexity yet does not reduce the error or improve the correlation.

$$TIT_{apuc} = b_0 + b_1\left(T_{04}\right)^{b_2} + b_3\left(T_{01}\right)^{b_4} \tag{18}$$

Table 8.2: Coefficients for the non-linear equation relating the measured EGT and ambient temperature to the controller-calculated TIT.

Parameter	High Time	T1 & High Time
b_0	-462.23	-751.65
b_1	1.0772	1.0724
b_2	1.0417	1.0491
b_3	3865	5743
b_4	-0.3287	-0.3395

To illustrate the effect of the T1 blade failure data on the non-linear fit, a comparison between both the controller-calculated TIT and that of the relation in (18) is plotted in Figure 8.19 below using both sets of coefficients. The TIT is compared for APUs 1308 and 1608, two of the T1 blade failures, and APUs 1465 and 1925, two of the high time removals.

For the two T1 blade failures, the relation is relatively accurate until approximately 600 cycles before failure. After this point, the controller and relation curves begin to deviate from each other. This point is in approximately the same location that the TIT ratio begins to increase for both of these APUs in Figure 8.3. Again, this suggests that the heavy deterioration that the 331-500 experiences in the lead-up to failure results in an observable error in the APUC calculation of the TIT. For the two high time removals, the relation proves to be relatively accurate in calculating the TIT and, if the coefficients for the equation are based only off the high time removal data, the relation matches the controller-calculated TIT almost exactly.

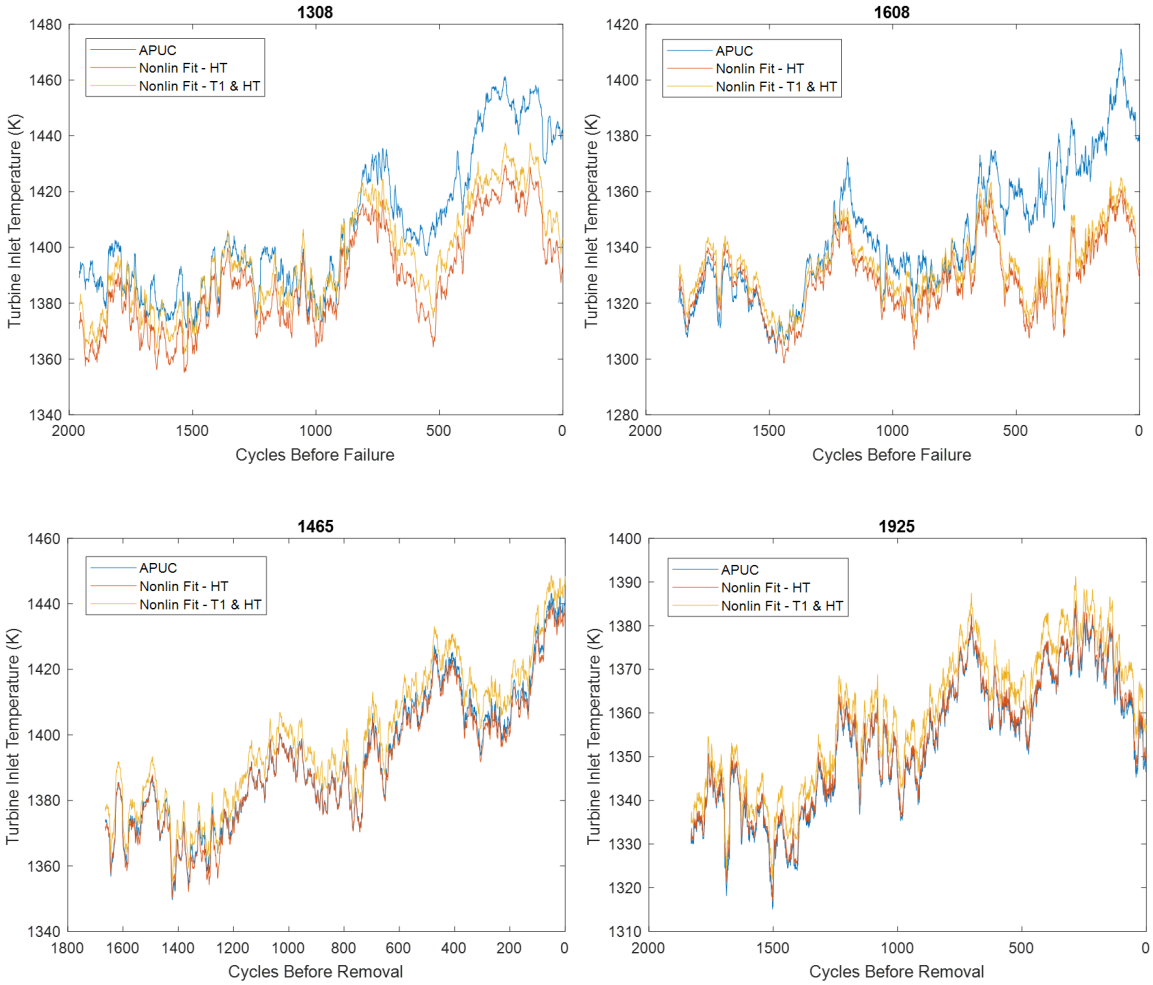

Figure 8.19: Comparison between the controller-calculated TIT and that determined by a non-linear relation for APUs 1308, 1608, 1465 and 1925.

8.5 Summary

From the above results and disassembly photos, it is evident that there is a relationship between the condition of the first stage NGV of a 331-500 and both the gradient in turbine efficiency and ratio of the controller- to model-calculated TIT. A steeper gradient and higher TIT ratio suggests that the turbine is more deteriorated than a machine with a flatter gradient and lower ratio. Sensor measurements, such as the EGT and fuel flow, have identifiable trends but are significantly noisy and fluctuate with ambient conditions. Unlike the turbine efficiency, which is far smoother, this noise makes it difficult to use any of the sensor measurements for failure prediction.

In Table 8.3 below, the gradient of the turbine efficiency ($\frac{d\eta_t}{dC}$) and the ratio of controller- to

model-calculated TIT for each of the fifteen APUs mentioned above are summarised. For logistical reasons, an aircraft operator should be given notice to remove an APU at least 200 cycles before the requested removal date. For that reason, the gradient of the turbine efficiency below is calculated at 200 cycles before failure/removal in the T1 failure/high time removal data and at the last data point in the post-repair data. As the turbine efficiency data contains some noise, the gradient is calculated by fitting a line through the data using a least-squares approach and then calculating the slope. Similarly, as the TIT data for the controller and model is also noisy and tends to fluctuate, the ratio is calculated by taking a mean at 200 cycles before failure. The mean is calculated based on the previous 50 cycles from this data point. Finally, to quantify the condition of the NGV, a value between 0 and 1 is assigned to a variable A_{NGV}. A value of 0 represents a NGV that is completely deteriorated with no material left and a value of 1 represents a healthy NGV with full material. These are not exact representations of the NGV damage but are estimated from the disassembly photos. These results are also presented graphically in Figures 8.20 and 8.21 below.

Table 8.3: Tabulated data on the gradient of the turbine efficiency, ratio of controller- to model-calculated TIT, and condition of the first stage NGV for all fifteen APUs from the study. APU serial numbers highlighted in red, orange and green indicate T1 blade failures, high time removals, and post-repair performance respectively.

APU No.	A_{NGV}	$\frac{d\eta_t}{dC}(10^{-3})$	$\frac{TIT_{APUC}}{T03}$
1308	0.3	-1.10	1.120
1602	0.3	-1.00	1.097
1552	0.3	-1.22	1.110
1608	0.3	-0.35	1.110
1590	0.3	-1.20	1.145
1465	0.6	-1.07	1.105
1466	0.7	-0.59	1.107
1835	0.7	-0.44	1.088
1925	0.8	-0.31	1.087
1710	0.9	-0.15	1.084
1664	1.0	-0.26	1.070
1642	1.0	-0.23	1.084
1801	1.0	-0.04	1.079
1390	1.0	-0.19	1.091
1509	1.0	-0.30	1.086

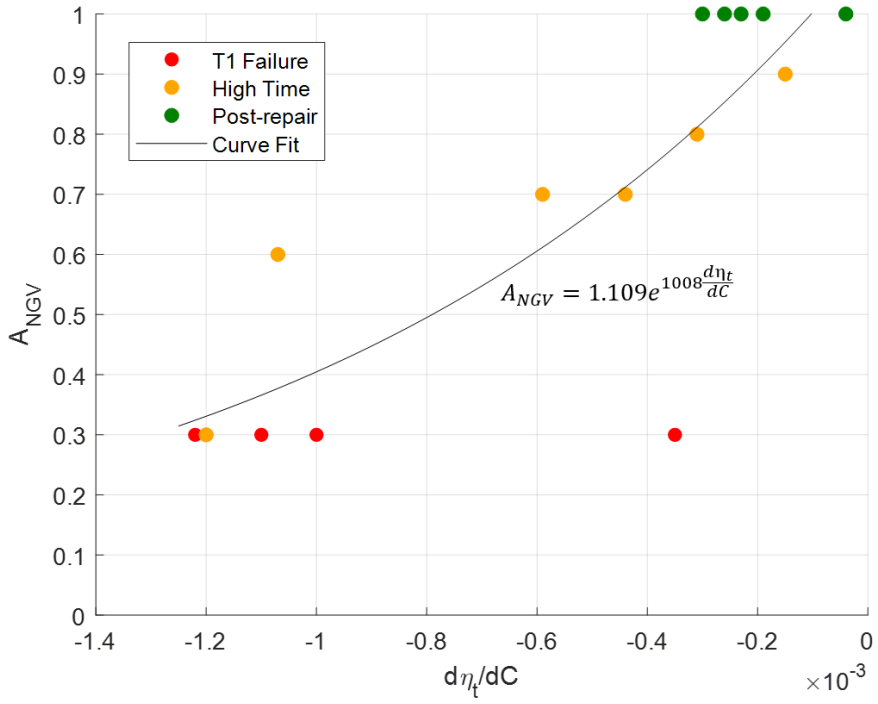

Figure 8.20: Relationship between the area of the first stage NGV and the gradient of the turbine efficiency for the Honeywell 331-500.

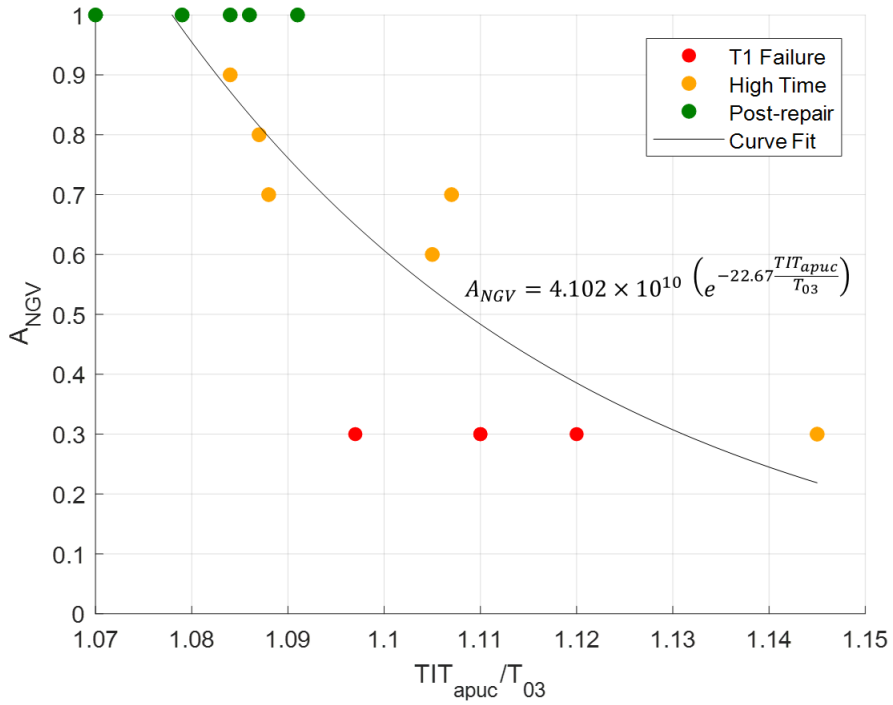

Figure 8.21: Relationship between the area of the first stage NGV and the ratio of controller- to model-calculated TIT for the Honeywell 331-500.

The T1 blade failures, which have a heavily deteriorated NGV and are highlighted in red, tend to have a more negative gradient in efficiency and a larger TIT ratio than the machines with a healthier NGV. However, in certain APUs, a largely negative turbine efficiency gradient is not matched with a large TIT ratio, and vice versa. For example, in APU 1608, the gradient is not as steep as the other T1 failure APUs although its TIT ratio is large at failure. The opposite is true of APU 1602 which has a relatively low value of TIT ratio yet also has a steep turbine efficiency gradient in the lead-up to failure. This suggests that monitoring just one of these parameters is not sufficient to predict a heavily deteriorated NGV and therefore predict a potential T1 blade failure.

Of the six high time removals, which are highlighted in orange, the machines which had a more deteriorated NGV at removal also have a largely negative gradient in turbine efficiency and a large TIT ratio. APU 1465, which had approximately 40% of its NGV remaining at removal, has a gradient which is over seven times larger in magnitude than that of APU 1710 which had a largely intact NGV at approximately 80%. Similarly, all five post-repair APUs, which are highlighted in green and assumed to have approximately all of their NGV material remaining, have relatively small values of turbine efficiency gradient and TIT ratio as compared to the more deteriorated machines.

From this analysis, it is evident that there are useful trends in the historical data which may be used for the monitoring of APUs in operation. The formulation of a rule based on these results is discussed in the following section.

9 Future Failure Prediction of 331-500s in Operation

When discussing the failure mechanisms of T1 blade failure, it was stated that the loss of material in the first stage NGV will lead to a reduction in turbine performance and a subsequent increase in fuel flow and TIT, which will lead to more corrosion of the T1 rotor blades and the eventual release of a blade. It is therefore important to remove a 331-500 from operation once the first stage NGV starts to become significantly damaged, such as the case with APU 1465 which had approximately 60% of the NGV material remaining at repair. It is also important that an APU should not be removed too early, such as with APU 1710, as it may be capable of operating for up to a thousand or more cycles. Therefore, to successfully monitor and predict T1 blade failure on current and future 331-500s in operation, the identified trends from the historical analysis should be used to formulate a rule that signals a removal when the first stage NGV of an APU has **60% or less** material remaining.

Due to the limited availability of historical data, it is not possible to say whether or not a robust rule exists that can determine all future T1 blade failures. However, based on Table 8.3, thresholds can be defined which can signal a heavily deteriorated first stage NGV. Since a relationship between the NGV health and the risk of a T1 blade release is now known, this may be used to aid engineers at EPCOR to decide on whether or not to schedule an APU removal. This process is discussed below.

9.1 Formulation of a Rule for Failure Prediction

From observing the results of both the turbine efficiency gradient and TIT ratio, it appears that the latter is more helpful in identifying a deteriorating NGV. The turbine efficiency gradient appears to drop off in the final 200 cycles before failure leaving a short period of time to schedule a removal whereas the TIT ratio tends to increase towards a range of 1.100-1.145 in the final 600 cycles before failure. However, the gradient is still useful for indicating that the turbine is in an unhealthy state and may be used to compare the condition of the NGV of multiple APUs.

Based on the results in Figure 8.20, a threshold of $\mathbf{-0.8 \times 10^{-3}}$ on the gradient would have predicted three out of the four T1 blade failures within approximately 1300-400 cycles before failure. Additionally, it would have signalled that APUs 1465 and 1590, which had 60% or

less NGV material remaining at removal, should have been removed at an earlier time. Furthermore, APUs 1710, 1925 would not have been removed as their gradient is far less steep and their NGV is in a relatively healthy state. It is advised that the gradient be calculated by fitting a line every 200-300 cycles otherwise, due to noise, the calculation will occasionally return largely negative and positive gradients which are not representative of the actual performance.

When using just this threshold on the gradient. the length of time from the signal for removal to the actual T1 failure is 1300-400 cycles. As this is quite large, a threshold of **1.11** on the TIT ratio should be added to the rule to improve the prediction. When used alone, this threshold would have also missed one of the T1 blade failures but, in combination with the threshold on the gradient, all T1 blade failures would have been predicted between 600-250 cycles before failure. Figure 9.1 shows the definition of both of these thresholds on the two final graphs from the previous section.

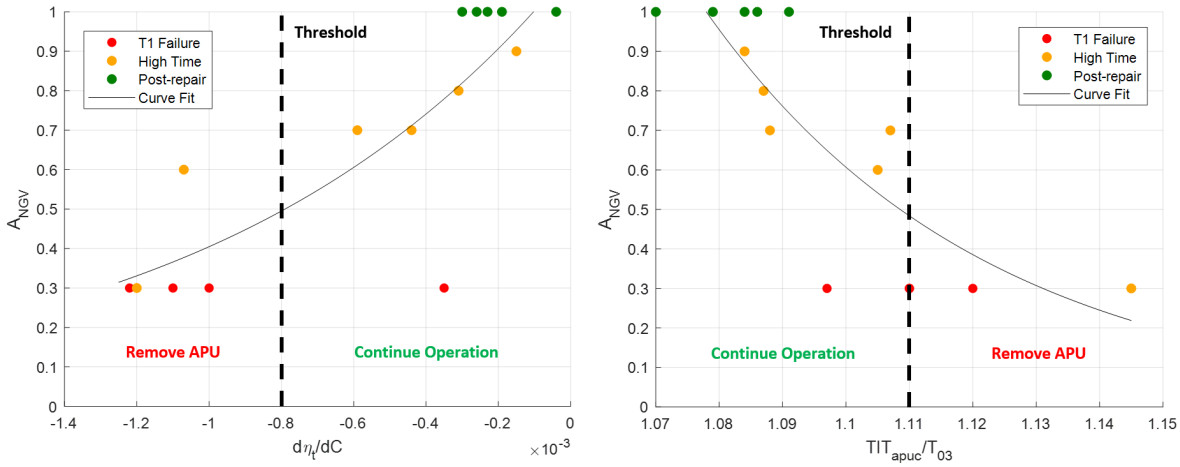

Figure 9.1: Definition of the threshold of -0.8×10^{-3} and 1.11 on the turbine efficiency gradient and TIT ratio to signal a heavily deteriorated turbine of the Honeywell 331-500.

However, this rule has some drawbacks. In the case of APU 1308, the TIT ratio will occasionally pass above the threshold of 1.11 for a short number of cycles before dropping again. As mentioned in the previous section, this may be resolved by calculating the ratio as a mean every 50-100 cycles to further smooth the noise in the TIT data. It should also be stated that, rather than directly removing an APU as soon as this threshold is surpassed, its behaviour should be observed to ensure that the TIT ratio is consistently above 1.11 and has not just breached above it due to noise or simply a faulty sensor or data processing error. Similarly, in the post-repair data, both the turbine efficiency and TIT ratio thresholds would

have signalled that all APUs should be removed in the cycles directly after their repair. As explained previously, the steep gradients and large TIT ratio are most likely due to the wear-in of components leading to a large error in the model. To account for this, any signals from both thresholds should be suppressed for approximately the first 500 cycles after repair.

In summary, the formulated rule is one that functions as a Boolean *OR* (‖) operator where either the turbine efficiency gradient or TIT ratio exceeding a threshold of $\mathbf{-0.8 \times 10^{-3}}$ and **1.11** respectively will signal the removal of a 331-500 from operation. This is represented in Figure 9.2 below as a flowchart. The rule would have predicted all four T1 blade failures between 600-250 cycles before failure as well as signalling that APUs 1590 and 1465, the most deteriorated high time removals, should have been removed at an earlier date. To avoid unnecessary requests for removal during post-repair performance, any signals should be suppressed for approximately the first 500 cycles.

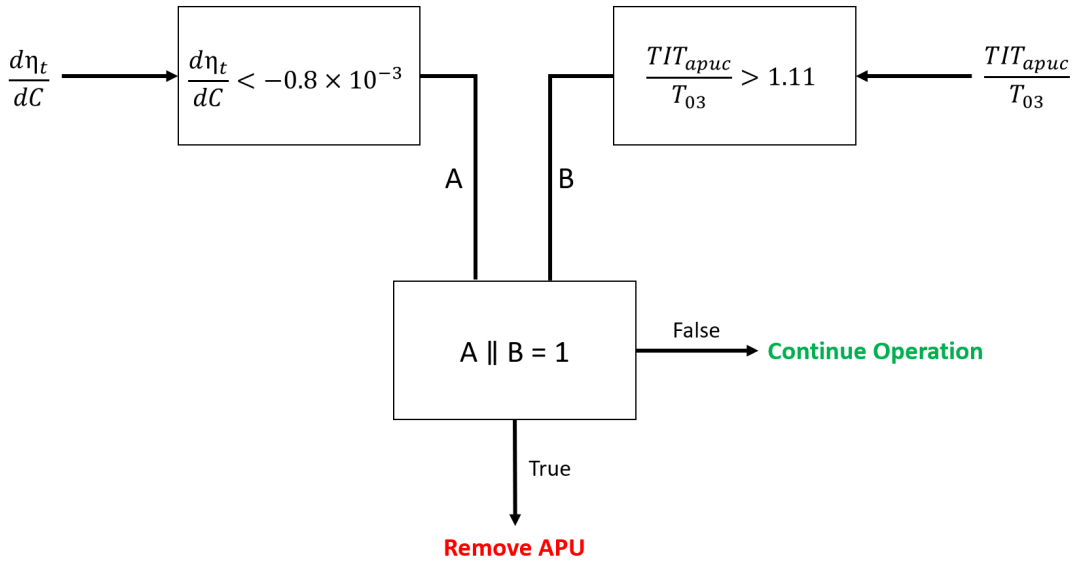

Figure 9.2: Visual representation of a rule functioning as a threshold on the turbine efficiency gradient and TIT ratio to signal the removal of a 331-500.

10 Conclusion

This study has focused on the development of a tool for the condition monitoring and predictive maintenance of the Honeywell 331-500 APU. T1 blade failure was selected as the focus of this study as it is a sudden and severe failure that leads to extensive damage of the hot section of the machine. From investigation, hot corrosion and thermal fatigue have been identified as the failure mechanisms leading to T1 blade failure. As a result of a loss in thermal barrier coating, the material of the first stage NGV of the 331-500 degrades leading to a reduction in turbine performance. This reduction in performance is countered by an increase in fuel flow, hence TIT, by the APUC leading to further corrosion and fatigue crack growth. Additionally, the ingestion of environmental contaminants both accelerates corrosion and obstructs blade cooling passages. A combination of these self-reinforcing effects leads to the eventual release of a first stage blade.

A thermodynamic model of the 331-500 was created and validated using GSP. Test cell data of the 331-500 operating at MES, a high-power load condition, was used to characterise the machine at its design point before analysing on-wing performance. GPA, in the form of adaptive modelling with gradient descent, was the chosen method for the on-wing analysis. Based on the failure mechanisms of T1 blade failure, the turbine efficiency was selected as the adaptive variable for the analysis of historical failure data. As a result of a limited amount of data, the analysis also had to be completed on the performance of 331-500s leading up to a high time removal and also directly after repair. The reason for this is that the performance of both healthy and unhealthy APUs should be analysed to identify any trends in deterioration data that are characteristic of T1 blade failure.

Based on both the analysis and accompanying 331-500 disassembly photos, it was observed that there is a relationship between the condition of the first stage NGV and the gradient in turbine efficiency and the ratio of the controller- to model-predicted TIT. Both a largely negative gradient and large TIT ratio indicate that the NGV is heavily deteriorated and has lost significant material. In all T1 blade failures, the gradient in turbine efficiency rapidly decreased in the lead-up to failure while the TIT ratio rapidly increased suggesting that the deterioration rate of the NGV increases in the lead-up to failure. A sensitivity analysis on the turbine throat area, along with a correlation analysis on the APU controller input, support this finding.

Since the condition of the first stage NGV has been shown to be related to the likelihood of a first stage blade release, this relation may be used as a means of predicting future failure. A rule has been formulated and functions as a Boolean *OR* operator in which a threshold of $\mathbf{-0.8 \times 10^{-3}}$ and **1.11** has been defined for the turbine efficiency gradient and TIT ratio respectively. If either of these thresholds are reached during on-wing 331-500 operation, the APU should be removed for repair. Based on the analysis of historical data, a rule of this form would have predicted all four T1 blade failures within 600-250 cycles before failure as well as signalling the removal of any APUs which had a NGV with 60% or less material remaining.

11 Recommendations for Future Work

Throughout the process of building the thermodynamic model of the Honeywell 331-500 and analysing historical performance data, several sources of error were present. These errors and any recommendations for future work on the predictive maintenance of APUs at EPCOR will be discussed in this section.

11.1 Additional Test Cell Measurements

As mentioned in section 5.1, several unknowns exist when characterising the compressor of the 331-500 at its design point. To estimate the compressor mass flow, a power section energy balance was utilised while the PR is determined based on the assumption of a choked turbine and the measuring of the throat area. The compressor efficiency had also to be assumed.

If the total compressor outlet pressure and temperature could be measured in the test cell, the fitting of the BBM to the test cell data would be far more accurate. An accurate calculation of the mass flow, PR and efficiency under MES conditions would provide a better representation of the compressor and should lead to less spread in the design point results. But, unless an accurate compressor map is available for off-design analysis, the energy balance will have to continue to be used for on-wing analysis. This is problematic as this equation is sensitive to the calculation of the load compressor and generator work as well as the combustion chamber heat addition. Any error in these calculations, including the assumption of constant mechanical and combustion efficiencies, will likely result in a large source of error in the model. The prospect of building a probe that could be inserted into one of the outlet tubes of the 331-500 compressor to determine the outlet conditions was discussed with test cell operators at EPCOR but, due to time constraints and cost, this was not pursued. If GPA is to be used as the main method for the future predictive maintenance of the 331-500, then it is recommended that this be done.

Lastly, when building the 500TM, it was attempted to model the cooling flow but, due to the sensitivity of the gradient descent algorithm to its value, it was removed. Originally, the model was designed such that a fraction of the compressor air flow was subtracted before the combustion process and then mixed with the flue gas during the turbine calculations. However, the EGT and turbine efficiency were highly sensitive to this fraction of air flow and since its value is unknown, it was decided to exclude it from the model. Perhaps information from Honeywell on the cooling flow behaviour can be provided in the future.

11.2 Availability of APUs with Sufficient Data

As mentioned in section 7.1, it is recommended to analyse the entire performance history of each 331-500 APU, from repair to removal, to understand the deterioration behaviour of the machine. Analysing the post-repair, moderate deterioration, and heavy deterioration performance of separate APUs is not ideal. To minimise the error in build effects, particularly in the compressor performance, it is better to use GPA to calculate a delta in the turbine efficiency, from a healthy installation value to a value at failure, rather than calculating the absolute values.

As EPCOR have only launched *Prognos for APU* in late 2017, it will take a number of years to capture the full performance history of 331-500s in operation. Currently, with just four T1 blade failures and a small amount of high time removals, it is not possible to develop a rule that will predict all future T1 blade failures with absolute certainty. But, as time progresses and more data comes available, the accuracy of GPA and other data analysis techniques for failure prediction will improve. Methods such as decision trees or neural networks can be used with adaptive modelling to enhance the classification of failures as based on the calculated deterioration data.

11.3 Effect of Deterioration on The Model

This study focuses primarily on the deterioration of the turbine of the 331-500 and does not account for any worsening in performance of the two compressors and the combustion chamber. As with the blade cooling flow, it was originally aimed to include mechanical and combustion efficiencies in the model but the calculated turbine efficiency is sensitive to their value. This is also true for the pressure loss in the combustion chamber. In an ideal case, a map would be used for the combustion chamber and, as with both compressor maps, calibration factors may be used to modify the maps to account for deterioration. However, this would require more on-wing sensor measurements such as both compressor outlet conditions. In reality, less measurements exist and the deterioration must either be estimated or it be accepted that this will be an additional source of error in the model.

A potential research topic for future work would be to build a model of both compressors of the 331-500 and include deterioration effects. As highlighted in Figure 6.7 during the sensitivity analysis, any error in the compressor efficiency will significantly affect the calculation of the turbine efficiency. If a model of both compressors was created, it could be

coupled with this thermodynamic model of the entire 331-500 to improve the overall accuracy of the turbine health prediction. Both compressor models could also be used to identify any compressor-specific failures such as bearing or seal failures. A similar study could be undertaken on the off-design performance of the combustion chamber as it will also have a large effect on the model.

However, this will require accurate component maps instead of using sample maps from GSP that are scaled to the design point of the real component. As stated in the GSP user manual, the difference between the design point mass flow, PR and efficiency between both the real and sample compressor should be <25% otherwise there will be a significant difference in the Reynolds number of both machines leading to large deviations from the actual performance [17]. The design point PR and mass flow of the 331-500 is approximately 11 and 5 kg/s respectively whereas the *smallhpc* sample map has corresponding values of 6.3 and 5.5 kg/s. That large difference in PR will most likely lead to errors in the model. Again, by making use of further test cell measurements, it may be possible to create a more accurate map of the component for future analysis.

References

[1] C. Markou, G. Cros, A. Cioranu, and E. Yang, *Airline Maintenance Cost Executive Commentary*. International Air Transport Association, 2011.

[2] L. Marinai, L. Probert, and R. Singh, "Prospects for aero gas-turbine diagnostics: a review," *Applied Energy*, 2004.

[3] Intergovernmental Panel on Climate Change, *Climate Change 2014 Synthesis Report*. IPCC, 2014.

[4] W. Bredow, "Encyclopedia of Aircraft - Passenger and Cargo Aircraft," (accessed 26/10/2018). [Online]. Available: http://www.bredow-web.de/Berlin_Tegel/Boeing_737-300_Lufthansa/Tragflache/tragflache.html

[5] Honeywell Aerospace, "Air Transport and Regional Brochures: 131-9A Auxiliary Power Unit," (accessed 26-October-2018). [Online]. Available: https://aerospace.honeywell.com/~/media/UWSAero/common/documents/myaerospacecatalog-documents/ATR_Brochures-documents/131-9A_US.pdf

[6] ——, *331-500 First Stage Turbine Corrosion*. Honeywell Air Transport Operators Conference, 2012.

[7] L. Urban, "Gas path analysis applied to turbine engine condition monitoring," *AIAA*, vol. 10, no. 7, pp. 72–1082, 1972.

[8] M. Verbist, "Gas path analysis for enhanced aero-engine condition monitoring and maintenance," Ph.D. dissertation, Delft University of Technology, 2017. [Online]. Available: dx.doi.org/10.4233/uuid:e1079009-84c2-482d-afe4-e1f9fde0d137

[9] A. Stamatis, K. Mathioudakis, and K. Papailiou, "Adaptive simulation of gas turbine performance," *ASME*, vol. 89-GT-205, 1989.

[10] W. P. J. Visser and M. Broomhead, "GSP, a generic object-oriented gas turbine simulation environment," *ASME*, vol. 2000-GT-0002, 2000.

[11] D. L. Doel, "Interpretation of weighted-least-squares gas path analysis results," *ASME*, vol. 2002-GT-30025., 2002.

[12] W. P. J. Visser, O. Kogenhop, and M. Oostveen, "A generic approach for gas turbine adaptive modelling," *Journal of Engineering for Gas Turbines and Power*, 2004.

[13] A. K. Shukla and O. Singh, "Effect of compressor inlet temperature and relative humidity on gas turbine cycle performance," *International Journal of Scientific Engineering Research*, vol. 5, 2014.

[14] S. L. Dixon and C. A. Hall, *Fluid Mechanics and Thermodynamics of Turbomachinery*, 7th ed. Elsevier Incorporated, 2010.

[15] Honeywell Aerospace, *331-500 Line Maintenance Manual*, 2018.

[16] ——, *Honeywell 331-500[B] Engine Manual*, 2016.

[17] GSP Development Team, *GSP 11 User Manual*. National Aerospace Laboratory, 2013.